論文 / 著書情報
Article / Book Information

題目(和文)	ポリイミドメモリ材料の開発
Title(English)	Development of polyimide memory
著者(和文)	黒澤忠法
Author(English)	Tadanori Kurosawa
出典(和文)	学位:博士(工学), 学位授与機関:東京工業大学, 報告番号:甲第9077号, 授与年月日:2013年3月26日, 学位の種別:課程博士, 審査員:上田 充
Citation(English)	Degree:Doctor (Engineering), Conferring organization: Tokyo Institute of Technology, Report number:甲第9077号, Conferred date:2013/3/26, Degree Type:Course doctor, Examiner:
学位種別(和文)	博士論文
Type(English)	Doctoral Thesis

Ph.D. Dissertation

Development of Polyimide Memory

ポリイミドメモリ材料の開発

2012

Tadanori Kurosawa

11D07047

Department of Organic and Polymeric Materials

Graduate School of Science and Engineering

Tokyo Institute of Technology

Chapter 1. General Introduction

1-1. Electronic memory device

During the past few decades, remarkable growth in the information society has enabled us to deal with enormous amount of data. Hand in hand with this society advancement, the demands for extremely large capacity and yet small size memory device are increasing. To meet these requirements, striking developments in the field of electronics based on semiconductors have been achieved during the past few decades.[1]

A memory device is a basic component of electronic equipment which stores data temporary or permanently. As shown in Figure 1-1, memories can be classified into two types, which are volatile memory and non-volatile memory.[2] A volatile memory is a type of memory which cannot hold the stored data without the external electronic power supply, that is, the written data will disappear after turning off the power. On the other hand, a non-volatile memory can sustain the stored data without the power supply, that is, the written data will not disappear unless or even after an additional procedure is carried out. For instance, dynamic random access memory (DRAM) and static random access memory (SRAM), both used in nowadays computers, are volatile memories. On the other hand, write once read many (WORM) type memories represented as compact

disc (CD), digital versatile disc (DVD), and Blue-ray Disc are non-volatile. FLASH type memories such as universal serial bus (USB) flash drive, secure digital (SD) memory card, and solid state drive (SSD) are also non-volatile.

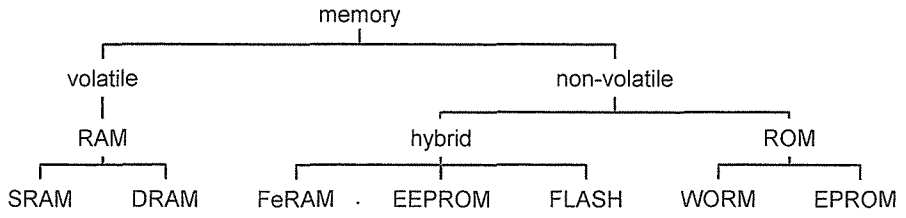

Figure 1-1. Classification of memories.

In terms of storing data, a memory device needs two distinct (bistable) electronic states which can be assigned as "0" and "1" or "OFF" and "ON". Figure 1-2 shows the typical structure of a current DRAM memory device. Inside a memory device, there is an element which can create the two distinct electronic states in each intersection of electrical wires (word line and bit line) laid in a gridlike fashion. Therefore, the memory device stores data by using the patterns of "0" and "1" created by this element. Inside this element, there is a fine electric circuit which is composed of a complementary metal oxide semiconductor (CMOS) transistor and a capacitor (C). In this electronic circuit, "0" and "1" correspond to the discharged and charged state of the C. The properties such as volatility (volatile or non-volatile) of these semiconducting memories can be controlled by changing the electric circuit of the element. For instance, tailoring the C to a floating gate metal oxide semiconductor (FGMOS) transistor will change the memory property form the volatile DRAM to the non-volatile FLASH type memory.

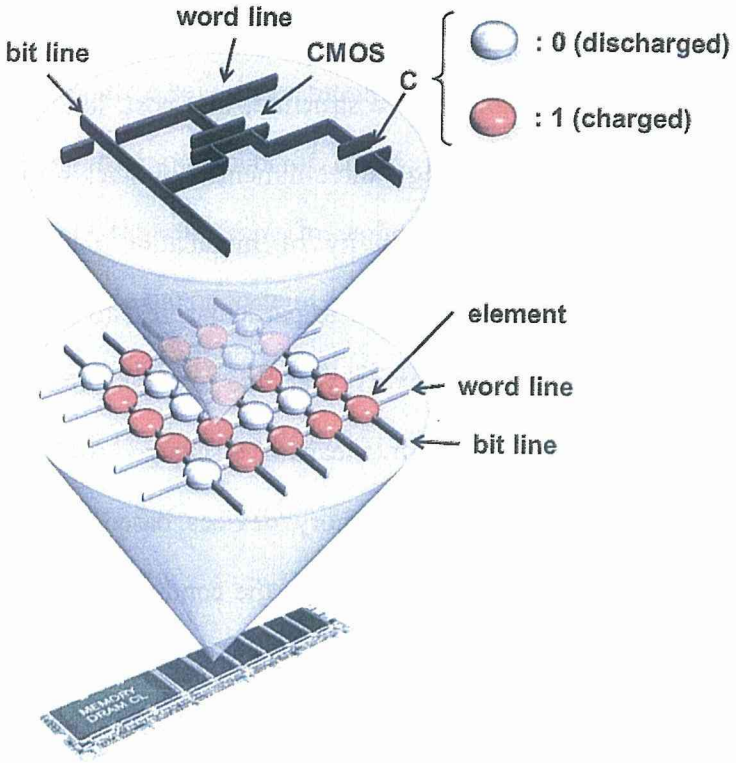

Figure 1-2. Typical structure of DRAM.

During the past few decades, the capacity of current semiconducting memory devices has drastically increased and their size has dramatically decreased.[1] The combination of increasing the capacity and scaling down the size has been achieved by scaling down the electronic circuit of element by conventional lithography technologies. However, these techniques are facing issues to be addressed, such as physical limitation of the resolution of the lithography patterns, high process cost, *etc.*, which are threatening the continuous scaling of current semiconductors to maintain Moore's law.[1] Therefore, studies of alternative materials for such current devices are of great significance.

1-2. Polymer memory

In recent years, increasing attentions have been paid to applications in memory

devices based on polymeric materials.[1-2] They have been developed and studied for several advantages, like flexible device structure, low cost, long range processability (due to possible solution processing), three-dimensional stacking capability for high density data storage, and the possibility of modulating their properties through molecular design and chemical synthesis. In particular, resistive type memory devices have attracted significant interests every year due to their simple structure.[2] Unlike current memory devices storing data by means of discharged (0) and charged (1) states in electronic circuits, resistive type memory devices based on polymeric materials operate in a completely different way, utilizing the conductivity response of the active layer to the applied voltage, in which the low and high conductivity states are assigned to "0" and "1", respectively. This means that the polymer layer can be a memory element, which in the current memory device generally consists of a minute and complicated electric circuit. Thus, the device structure can be simplified and fabricated in three steps, as shown in Figure 1-3. First, the bottom electrode is placed on the substrate. Secondly, the active layer is cast. Finally, the top electrode is placed on the active layer. Also, a three-dimensional stacking device, which is difficult to construct using conventional techniques, can be fabricated by replicating these process.

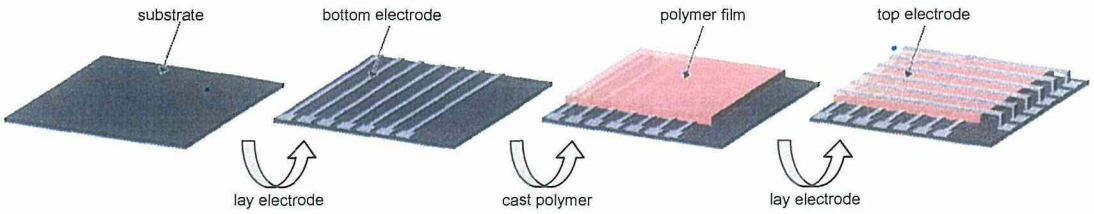

Figure 1-3. A schematic diagram of the fabrication process for a polymer memory device.

Over the years, a large number of polymeric materials, including functional polyimides (PIs), conjugated polymers,[3-7] polymers with specific pendant groups,[8-12]

polymer-graphene complexes,[13-16] polymer/fullerene blends,[17-18] and polymers blended with nanoparticles,[19-21] *etc.*, have been reported to show bistable electrical switching properties. These reported polymers of blend systems are basically comprised of electron donor (D) and electron (A). This is because the D and A units facilitate the carrier transport or provide the opportunity to generate charge transfer (CT) state which both are crucial for creating the two distinct electronic states such as low and high conductivity states.[2]

1-3. Polyimide memory

Considering the fabrication process requirements, among all the polymer systems, PI is thought to be one of the most suitable candidates for memory materials due to its outstanding thermal stability, chemical resistance, and mechanical strength.[22] However, because of its high chemical resistance, PI exhibits a low solubility in the common organic solvents. Therefore, in general, thermal imidization is carried out by heating the soluble precursor poly(amic acid) (PAA) film to obtain a PI film. By this method, intermolecular imidization is promoted and also the packing behavior highly depends on the film-forming method. Both phenomena might significantly change the nature electrical performance of the polymer which makes it difficult to clarify the relationship between the polymer structure and the resulting property.[23] Hence, the design of a soluble PI, while maintaining a high thermal stability, mechanical strength and exhibiting good memory properties, is highly required to omit this heating process.

During recent years, large numbers of PIs showing various kinds of memory properties, from volatile memory properties (DRAM and SRAM) to non-volatile memory properties (FLASH and WORM type), have been reported.[24-32] The control

through these memory properties has been achieved, to some extent, by tuning the chemical structure of the D or A moieties. Therefore, understanding the relationship between the chemical structure and memory properties is a subject of utmost importance in the development of polymer memory materials.

1-3-1. Volatile DRAM and SRAM properties

In 2006, Kang *et al.* reported the first soluble PI (TP6F-PI) consisting of triphenylamine (TPA) and phthalimide units as the D and A moieties, respectively, showing bistable electrical switching properties (Figure 1-4).[24]

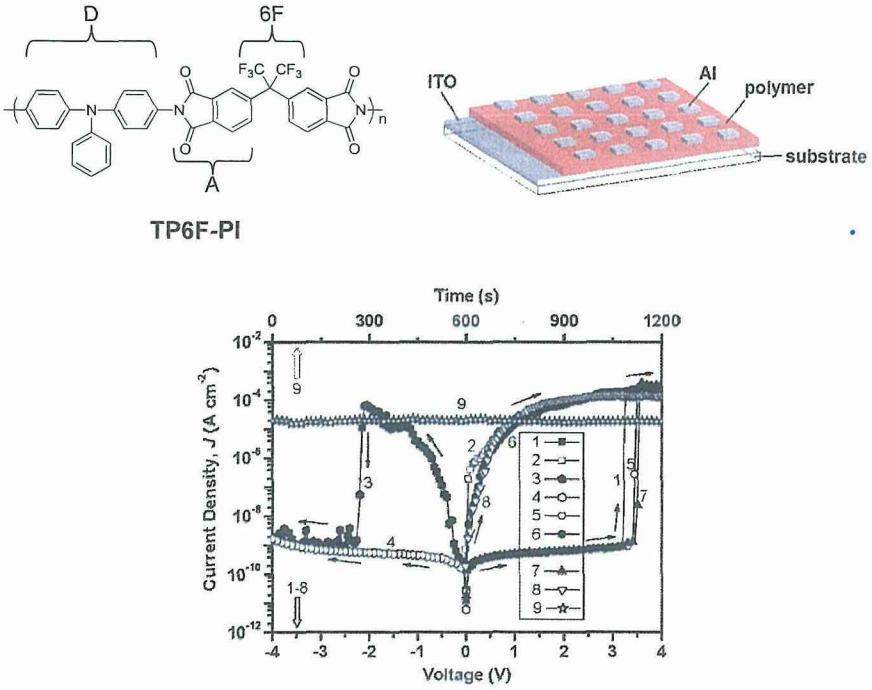

Figure 1-4. The chemical structure of TP6F-PI and typical *J-V* curve measured by the typical polymer memory device shown in the right side. Reprinted with permission from ref. 24. Copyright 2006, American Chemical Society.[24]

The memory property was evaluated by the current density-voltage (*J-V*) curve of an indium tin oxide (ITO)/polymer/Al sandwich device, which is a typical structure of

polymer memory devices (right side in Figure 1-4), measured by a semiconductor analyzer, as shown in the bottom part of Figure 1-4. In the 1st sweep from 0 to 4 V, the current density is low in the range of 10^{-9}–10^{-8} Acm^{-2} until 3.0 V due to the insulating nature of TP6F-PI. However, a sharp increase is observed at around 3.5 V and then the current density is in the range of 10^{-4}–10^{-3} Acm^{-2}, indicating a switching behavior form the low conductivity (OFF) state to the high conductivity (ON) state. The electric transition from the OFF state to the ON state corresponds to the "writing" process of the current memory device. During the subsequent sweep from 0 to 5 V (2nd sweep), the ON state can be maintained at any voltage value, which means that the distinct conductivity states (OFF and ON) can be read at a low voltage value (*e.g.*, below 2 V). In the 3rd voltage sweep from 0 to -5 V, the device remains in the ON state until -2 V. When the applied voltage becomes more negative, a sudden drop in the current density is observed and the device returns to the OFF state. This transition from the ON state to the OFF state serves as an "erasing" process for the current memory device. In the subsequient 4th sweep, the device remains in the OFF state at any voltage value from 0 to -4 V. As can been seen in the 5th and 6th sweeps, the ON state can be recovered by rerunning the positive sweep, indicating that the device is rewritable. However, by turning off the power for 1 min, the switched ON state returns to the initial OFF state without any erasing process (see the 7th sweep), which means that the device cannot sustain the ON state without the power supply and behaves as a volatile memory. The volatile ON state can be reprogrammed by applying a positive voltage over 3 V again and can be sustained by a refreshing voltage pulse of 1 V in every 5 s (plot #9). Combining the writing, reading, erasing, rewriting, and refreshing ability shown above, the memory property of the TP6F-PI is determined to be a volatile DRAM. One

important feature of TP6F-PI is that this PI showed a high solubility in various common organic solvents, which makes it possible to obtain a PI film without the thermal conversion of the precursor PAA as mentioned above. The hexafluoroisopropylidene (6F) group plays an important role in increasing the solubility of the PIs due to its bulkiness and low surface energy. Thus, the 4,4'-(hexafluoroisopropylidene)diphthalimide (6FDI) unit has been widely used for the preparation of PI memory. [25-32]

In 2009, Kang and co-workers also reported a functional PI (PYTPA-PI) for application as a polymer memory material (Figure 1-5).[25] PYTPA-PI consists of TPA-substituted diphenylpyridine and 6FDI as the D and A moieties, respectively.

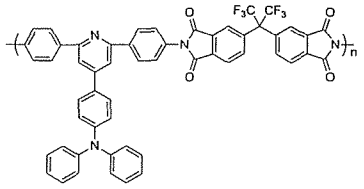

PYTPA-PI

Figure 1-5. The chemical structure of PYTPA-PI.

The memory property of PYTPA-PI characterized by the *J-V* curve of an ITO/PYTPA-PI/Al sandwich device is as followed (Figure 1-6). In the 1st voltage sweep from 0 to 5 V, an abrupt increase in the current density, corresponding to the "writing" process, is observed at around 2.7 V. During the following sweeps (3rd–12th sweeps), similar switching behavior to TP6F-PI, such as transition from the ON state to the OFF state ("erasing" process), volatile behavior, and rewritable behavior is observed. Such behaviors determine the memory characteristic of PYTPA-PI to be a volatile DRAM. Interestingly, when the applied voltage becomes more negative to -2.3 V after the 3rd sweep, the OFF state again switched to the ON state (see the 3rd sweep at Figure 1-6b).

This indicates that the device can be written bi-directionally and control of the negative sweep range, that is 0 to -2 V, can avoid the rewriting behavior.

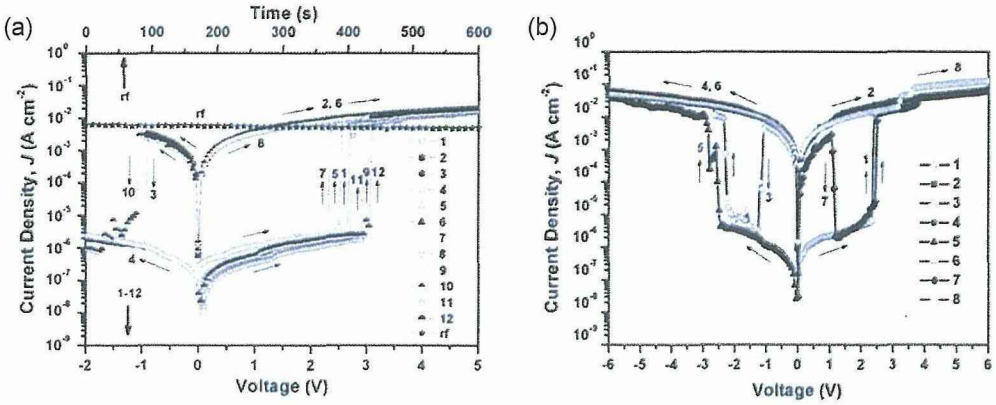

Figure 1-6. (a) The *J-V* curve of an ITO/PYTPA-PI/Al sandwich device and (b) *J-V* curve of the same device showing bi-directional electrical switching behavior. Reprinted with permission from ref. 25. Copyright 2009, American Institute of Physics.[25]

The same group also reported memory properties using functional PI (P(BPPO)-PI) consisting of 2,5-bis(4-phenoxy-phenyl)-1,3,4-oxadiazole (BPPO) and 6FDI as the D and A moieties, respectively (Figure 1-7).[26] In spite of the fact that an oxadiazole unit is usually adopted as the A moiety, the BPPO unit can act as a D moiety due to its lower electron affinity than the phthalimide.

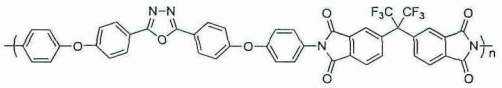

P(BPPO)-PI

Figure 1-7. The chemical structure of P(BPP)-PI.

The memory properties characterized from the *J-V* curve (Figure 1-8) of an ITO/P(BPPO)-PI/Al sandwich device are described below. During the 1st positive sweep from 0 to 4 V, a switching behavior from the OFF state to the ON state, corresponding to a "writing" process, is observed at around 2.3 V, and the induced ON state can be

maintained during the subsequent 2nd sweep. Different to the PYTPA-PI, the ON state cannot be reset to the initial OFF state by sweeping the voltage in the reverse direction (3rd sweep), which means that P(BPPO)-PI is not erasable. Another difference between PYTPA-PI and P(BPPO)-PI is that the ON state of P(BPPO)-PI can be maintained for about 4 min after turning off the power supply. However, the ON state eventually returns to the initial OFF state, which means that the ON state is "remanent", yet volatile. After the ON state has relaxed to the initial OFF state, it can be reswitched to the ON state by reapplying a negative voltage (the 4th sweep), and can be remained during the subsequent negative voltage sweep (5th sweep). Also, the ON state can be sustained by refreshing voltage pulse of -1 V of 1ms duration in every 5 s (the rf plots). Combining these results (the rewritable, refreshable, and also the "remanent", yet volatile nature), P(BPPO)-PI can be considered as a SRAM, which can enable a low power consumption in real applications.

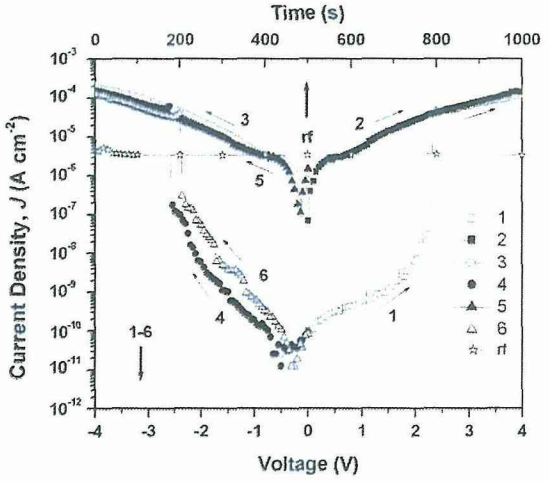

Figure 1-8. The *J-V* curve of ITO/P(BPPO)-PI/Al sandwich device. Reprinted with permission from ref. 26. Copyright 2009, American Chemical Society.[26]

Besides, like P(BPPO)-PI, various kinds of functional PIs containing the D structure

apart from the TPA derivatives were also found to exhibit DRAM or SRAM characteristics (Figure 1-9). These D structures include dibenzothiophene (PI(2,8-APDBT-6FDA) and PI(3,7-APDBT-6FDA)),[27] carbazole (6FDA/DAC),[28] and triphenylethylene (PI-6FDA).[29]

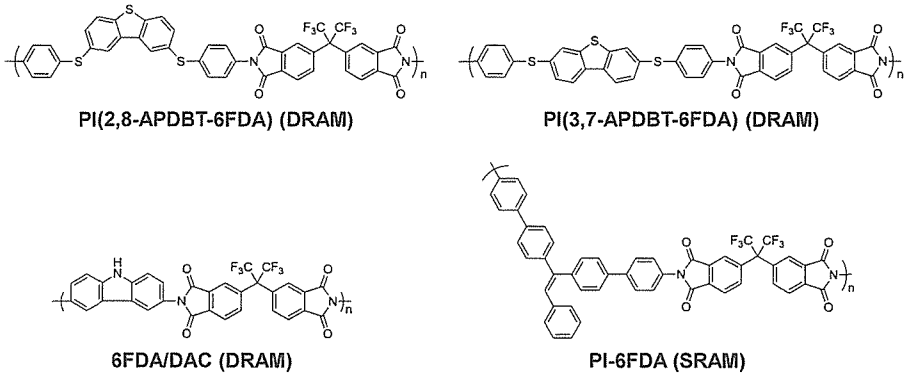

Figure 1-9. Chemical structures of the PIs showing volatile DRAM and SRAM properties.

1-3-2. Non-volatile FLASH and WORM properties

Compared to the volatile DRAM and SRAM behaviors, PIs showing non-volatile FLASH or WORM properties have mostly been developed quite recently. Also, unlike the volatile DRAM and SRAM, there are quite few reports about PIs showing non-volatile FLASH and WORM type memory characteristics.

In 2009, Ueda's group reported memory-exhibiting functional PIs (APTT-6FDA and 3SDA-6FDA) comprised of thianthrene or phenylenethioether derivatives as the D moiety and 6FDI as the A moiety for application as a non-volatile memory (Figure 1-10).[30]

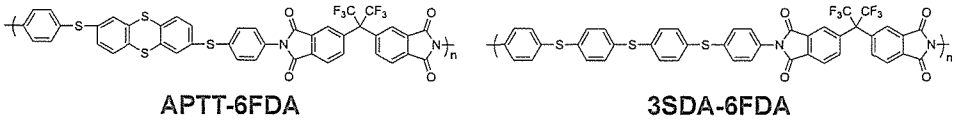

Figure 1-10. Chemical structures of APTT-6FDA and 3SDA-6FDA.

Both PIs showed similar memory characteristics (Figure 1-11). Taking APTT-6FDA for example (Figure 1-11a), an abrupt increase in the current around 1.5 V is observed during the 1st voltage sweep corresponding to the "writing" process. The device remains in a high conductivity (ON) state during the subsequent 2nd sweep and also after turning off the power for more than 10 min, indicating non-volatile behavior. As the voltage is swept in the negative direction, a sudden decrease in the current around -3.2 V, corresponding to the "erasing" process, is observed (3rd sweep) and the device remains in this low conductivity (OFF) state during the subsequent 4th sweep. The ON and OFF states can be reproduced by reapplying the switching threshold voltages (5th to 8th sweeps). Integrating the switching phenomena of the device and its volatility, the device based on APTT-6FDA can be used as a non-volatile FLASH type memory.

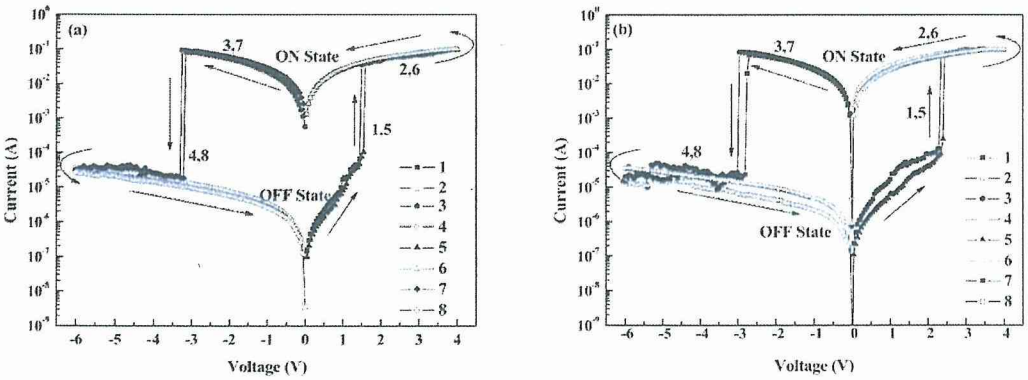

Figure 1-11. Current-voltage (*I-V*) curves of (a) APTT-6FDA and (b) 3SDA-6FDA. Reprinted with permission from ref. 30. Copyright 2009, American Chemical Society.[30]

In 2010, Kang and co-workers also reported functional PIs (AZTA-PIa and OXTA-PIa) for non-volatile memory aplications (Figure 1-12).[31-32] The D structures of AZTA-PIa and OXTA-PIa consist of TPA-substituted diphenyltriazole and TPA-substituted phenyloxadiazole, respectively, while the A structure is set to 6FDI. Like PYTPA-PI,[25] the 1,2,4-triazole of AZTA-PIa and 1,3,4-oxadiazole of OXTA-PIa

were introduced to enhance the CT process between the D and A moieties and affect the memory properties.

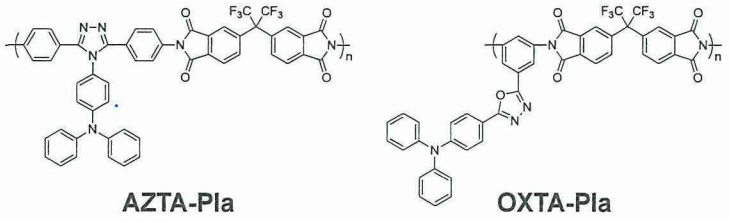

AZTA-PIa **OXTA-PIa**

Figure 1-12. Chemical structures of AZTA-PIa and OXTA-PIa.

The memory effect of the ITO/AZTA-PIa and OXTA-PIa/Al device demonstrated by the *J-V* curve (Figure 1-13) is described below. During the initial voltage sweep, a "writing" process is observed around -2.5 and -1.5 V for AZTA-PIa and OXTA-PIa, respectively. The ON state can be maintained during the subsequent 2nd sweep and also after turning off the electrical power supply, which indicates non-volatile behavior. Moreover, unlike APTT-6FDA and 3SDA-6FDA, the device cannot return to the initial OFF state even by applying the reverse voltage (3rd sweep). The non-erasable non-volatile switching behavior leads to the fact that the memory propertied of AZTA-PIa and OXTA-PIa can be determined as the WORM type.

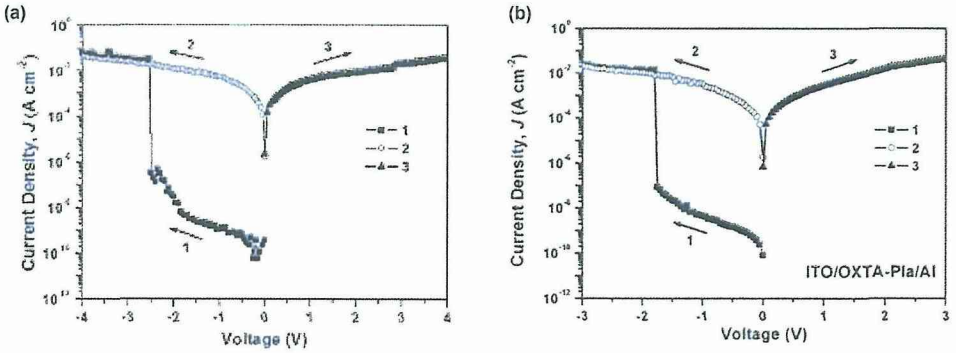

Figure 1-13. *J-V* curves of (a) AZTA-PIa and (b) OXTA-PIa. Reprinted with permission from ref. 31 and 32. Copyright 2010, Wiley,[31] American Chemical Society.[32]

1-3-3. Mechanism and control of volatility

The mechanism underlying the switching phenomena of the functional PIs discussed above is considered to be dominated by the field induced CT theory, in which charges are transferred from the D moiety to A moiety under electrical bias, forming a highly conductive CT state. To further understand this mechanism, the electronic states of the basic unit (BU) are often simulated by density functional theory (DFT) calculations. Figure 1-14 shows the typical simulation results of the molecular orbital corresponding to each energy level of the BU of TP6F-PI using DFT calculations and the plausible electronic transitions under an electric field.[24]

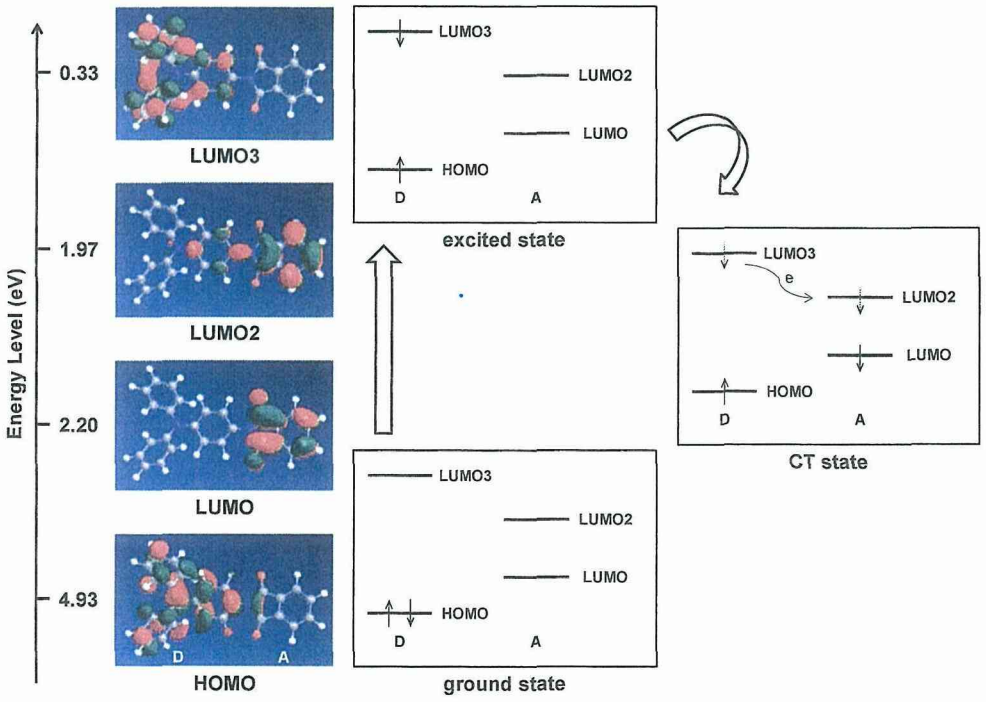

Figure 1-14. Calculated molecular orbitals, the corresponding energy levels of the BU, and plausible electronic transition.

As can be seen, the electron locating on the highest occupied molecular orbital (HOMO) (TPA unit) is locally excited to the 3rd lowest unoccupied molecular orbital (LUMO3)

by applying an electric field higher than the threshold voltage. After the excitation, the electron is gradually transferred to LUMO2 and to LUMO, generating a CT state. This excitation can occur due to the overlapping of molecular orbitals around the TPA moiety at the HOMO to LUMO3. Also, a transition can directly occur from the HOMO to LUMO2 or to the LUMO. During this process, holes are generated at the HOMO, which produces an open channel for the charge carriers to migrate through. Therefore, a sharp increase occurs in the current density around the threshold voltage, indicating the electrical switching from the OFF state to the ON state.

Taking the above mechanism into account, it is obvious that the stability of the CT state upon removal of the external electric power is the determining factor of the volatility. If the CT state is unstable under such a circumstance, the resulting memory characteristic would be a volatile one and *vice versa*. For the case of PIs showing DRAM properties, such as PYTPA-PI, due to the unstable CT state, the CT state immediately dissociates *via* the back CT or a recombination process of the separated charges after removing the power supply. Such dissociation can be delayed or prevented by several factors presented blow.

(a) Conformational change. The dissociation of the CT states of the PIs exhibiting SRAM properties is delayed to some extent, resulting in a "remanent" behavior. Kang's group advocated that such a delay is from the mutation of the dihedral angle between the D and A moieties induced by the external electric field.[26] It is known that when an electric field is applied to the ring-containing organic molecule, the torsional angle between the two aromatic rings will be increased.[33-35] Figure 1-15 shows the simulated BU molecular geometry of the relaxed and excited states of P(BPPO)-PI. During the excitation, the estimated dihedral angle between the phthalimide plane and the phenoxy

plane (θ_1), and the dihedral angle between the phenoxy plane and the oxadiazole plane (θ_2) increases from 40.1° and 67.1° to 54.6° and 72.7°, respectively. This result indicates that the torsional angles of the polymer chain can be increased by applying an electric field. The increased dihedral angle generates an energy barrier that delays the back CT and produces a "remanent" behavior after removal of the power supply.

Properties	Ground State	Excited State
Dipole Moment	2.82 Debye	3.06 Debye
ESP Surface	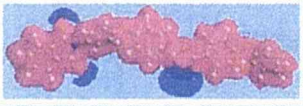	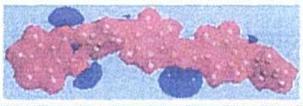
Optimized Geometry	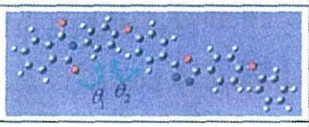	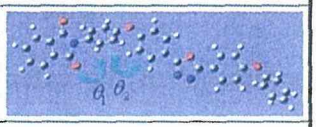
Dihedral Angle	$\theta_1 = 40.1°$, $\theta_2 = 67.1°$	$\theta_1 = 54.6°$, $\theta_2 = 72.7°$

Figure 1-15. Optimized geometries of P(BPPO)-PI and dihedral angles between the component aromatic moieties at the ground state and excited state. Reprinted with permission from ref. 26. Copyright 2009, American Chemical Society.[26]

Extending this concept to a higher extent, the development of a non-volatile memory has been achieved. For example, for AZTA-PIa, the calculated dihedral angle between the phthalimide plane and neighboring benzene ring increases from 42.9° to 60.3° during the excitation (Figure 1-16).[31] This increase in the dihedral angle is much greater than that for TP6F-PI (42.1° to 43.9°)[24] or P(BPPO)-PI (40.1° to 54.6°),[26] which confirms that the energy barrier for the back CT of AZTA-PIa is much higher than that of TP6F-PI or P(BPPO)-PI and explains the non-volatile WORM type behavior.

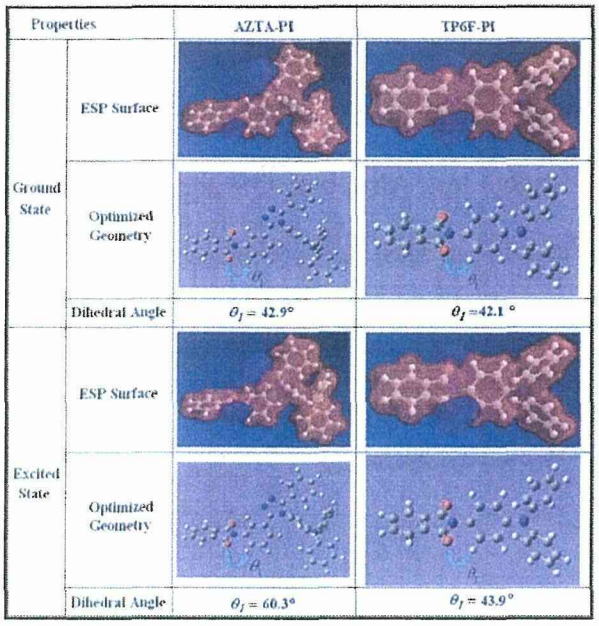

Figure 1-16. Optimized geometries of the BUs of AZTA-PIa and TP6F-PI and the dihedral angles between the component aromatic moieties at the groud state and excited state. Reprinted with permission from ref. 31. Copyright 2010, Wiley.[31]

(b) Dipole moment. Despite the fact that no twisted conformations were observed in the APTT-6FDA and 3SDA-6FDA,[30] these two PIs showed typical non-volatile FLASH type memory behavior. This mismatch in conformation and memory characteristic was explained from another viewpoint of the dipole moment. The calculated dipole moment values of the BU of APTT-6FDA (5.83 D) and 3SDA-6FDA (6.00 D) are much higher than that of TP6F-PI,[24] PYTPA-PI,[25] and P(BPPO)-PI[26] (2.06, 2.55, and 3.06 D, respectively). In this report, it can be seen that the higher the dipole moment, the more stable the CT state.

1-3-4. Other features

The evaluation of memory properties requires not only the *J–V* or *I–V* curve measurement but also endurance, retention stress, and write–read–erase–read (WRER) cycle tests. For instance, the retention times and stress tests of both the

ON and OFF states of P(BPPO)-PI are shown in Figure 1-17a.[26] Under a constant stress of -1 V, no obvious degradation in both ON and OFF states is observed for at least 5 h during the readout test. Also, both ON and OFF states were stable during the stimulus effect test for at least 10^8 continuous read pulses of -1 V (Figure 1-17b).[26]

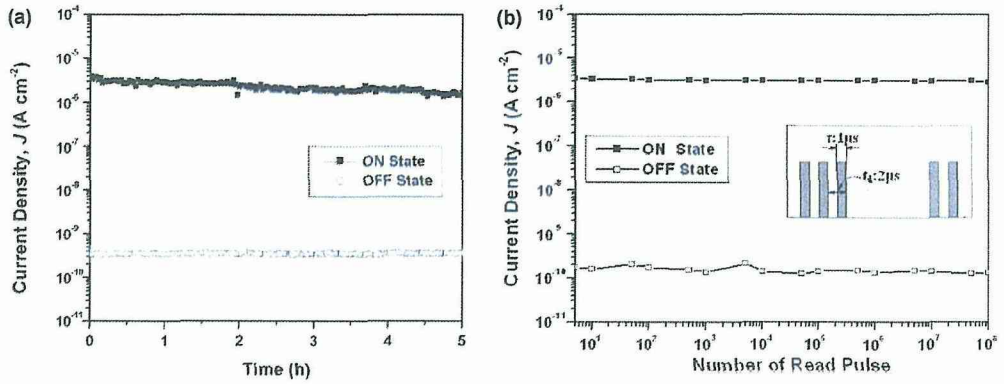

Figure 1-17. (a) Retention times under a continuous readout voltage and (b) the stimulus effect of read pulses on the ON and OFF states of the P(BPPO)-PI. Reprinted with permission from ref. 26. Copyright 2009, American Chemical Society.[26]

The WRER cycle test is required mostly in the case of FLASH type memory. Figure 1-18 shows the typical WRER cycle test of 3SDA-6FDA.[30] The write, read, erase, and reread voltages were set as 3.0, 1.0, -4.0, and -1.0 V, respectively. As can be seen, almost no degradation in both ON and OFF states is observed, indicating a high switching reproducibility. Similar to P(BPPO)-PI and 3SDA-6FDA, almost all the reported PIs showed high endurance to the constant voltage stress, continuous voltage pulse, and WRER cycles so far. Usually in organic and polymeric electronics, the oxidation and reduction processes during long term operation cause changes or, even worse, destroying the original memory properties of the active materials.[1] However, the above results clearly demonstrate that PIs possess high stability to the oxidation or

reduction process and are suitable for long term operation. Moreover, it is possible to enhance such stability by encapsulating these active materials for practical use.

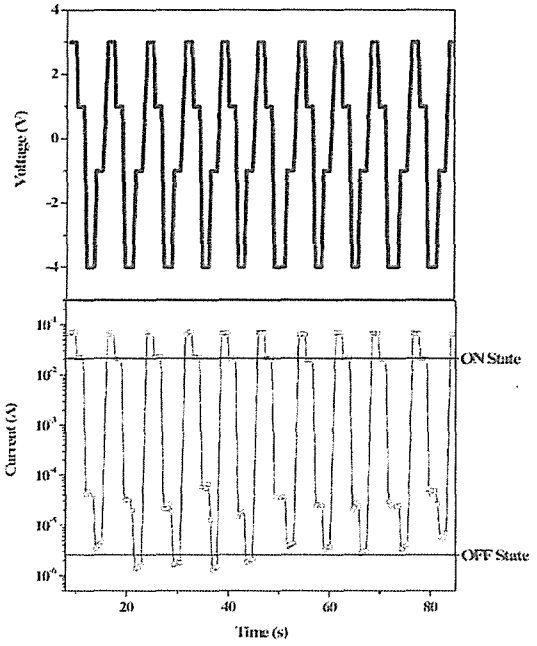

Figure 1-18. The applied voltage sequence and the typical current response to WRER cycles of 3SDA-6FDA. Reprinted with permission from ref. 30. Copyright 2009, American Chemical Society.[30]

1-4. Purpose of this work

Since the very beginning of the development of PI memory, almost all types of memory characteristics from volatile DRAM and SRAM to non-volatile FLASH and WORM types have been reported. These enthusiastic studies have given rise to the possibility of modulating the memory properties through design and chemical synthesis based on certain concepts. However, although the effects of the chemical structures on the resulting properties, such as conformational effects and dipole moment effects, have been elucidate to some extent, the relationship between the chemical structure and the resulting memory characteristic still remains unclear. For instance, despite the structural

similarity of PYTPA-PI and AXTA-PIa, the resulting memory behaviors are completely different. Therefore, fundamental studies for understanding the effects of chemical structures on the resulting memory properties are strongly required. Also, aiming a specific memory property through structural design of the functional PI based on these studies has never been achieved and is a subject of utmost importance.

Focusing on the mechanism underlying the switching behavior, which is field induced CT, the purpose of this work is to elucidate the relation discussed above and construct a concrete design concept to aim a specific memory property through chemical synthesis of functional PI. In this dissertation, the development of functional PIs for the application to memory materials is described in the following six chapters.

- In Chapter 1, the general introduction regarding the backgrounds and motivations of this study is described.
- In Chapter 2, the effect of the number of phenoxy linkages between the D and A units on the resulting memory property is studied.
- In chapter 3, for the purpose of expressing non-volatile memory characteristic, the induction of highly twisted conformational by a large steric hindrance is attempted. The stability of the resulting memory property is also discussed.
- In Chapter 4, the memory characteristics of three series of random copolyimides containing various diimide moieties as the A unit were studied to clarify the conjugation length and composition effects on the resulting memory properties.
- In Chapter 5, a series of copolyimides with widely conjugated pyrene moiety embedded as a D unit were prepared in order to tune the memory characteristics. In addition, the flexible memory device was prepared to demonstrate the future practical use of PI memory.

- Finally, this study of the development of PI memory materials is concluded in Chapter 6.

1-5. References

1. *International Technology Roadmap for Semiconductiors* *http://www.itrs.net/Links/2011ITRS/Home2011.htm* **2011**.
2. Ling, Q.-D.; Liaw, D.-J.; Zhu, C.; Chan, D. S.-H.; Kang, E.-T.; Neoh, K.-G., *Prog. Polym. Sci.* **2008**, *33*, 917-978.
3. Baek, S.; Lee, D.; Kim, J.; Hong, S.-H.; Kim, O.; Ree, M., *Adv. Funct. Mater.* **2007**, *17*, 2637-2644.
4. Ling, Q.-D.; Song, Y.; Lim, S.-L.; Teo, E. Y.-H.; Tan, Y.-P.; Zhu, C.; Chan, D. S. H.; Kwong, D.-L.; Kang, E.-T.; Neoh, K.-G., *Angew. Chem., Int. Ed.* **2006**, *45*, 2947-2951.
5. Pearson, C.; Ahn, J. H.; Mabrook, M. F.; Zeze, D. A.; Petty, M. C.; Kamtekar, K. T.; Wang, C. S.; Bryce, M. R.; Dimitrakis, P.; Tsoukalas, D., *Appl. Phys. Lett.* **2007**, *91*, 123506/1-123506/3.
6. Wu, H. C.; Yu, A. D.; Lee, W. Y.; Liu, C. L.; Chen, W. C., *Chem. Commun.* **2012**, *48*, 9135-9137.
7. Lai, Y.-C.; Ohshimizu, K.; Lee, W.-Y.; Hsu, J.-C.; Higashihara, T.; Ueda, M.; Chen, W.-C., *J. Mater. Chem.* **2011**, *21*, 14502-14508.
8. Liu, C.-L.; Hsu, J.-C.; Chen, W.-C.; Sugiyama, K.; Hirao, A., *ACS Appl. Mater. Interfaces* **2009**, *1*, 1974-1979.
9. Lim, S. L.; Ling, Q. D.; Teo, E. Y. H.; Zhu, C. X.; Chan, D. S. H.; Kang, E. T.; Neoh, K. G., *Chem. Mater.* **2007**, *19*, 5148-5157.
10. Fang, Y.-K.; Liu, C.-L.; Chen, W.-C., *J. Mater. Chem.* **2011**, *21*, 4778-4786.
11. Fang, Y. K.; Liu, C. L.; Yang, G. Y.; Chen, P. C.; Chen, W. C., *Macromolecules* **2011**, *44*, 2604-2612.
12. Teo, E. Y. H.; Ling, Q. D.; Song, Y.; Tan, Y. P.; Wang, W.; Kang, E. T.; Chan, D. S. H.; Zhu, C. X., *Org. Electron.* **2006**, *7*, 173-180.
13. Zhuang, X.-D.; Chen, Y.; Liu, G.; Li, P.-P.; Zhu, C.-X.; Kang, E.-T.; Noeh, K.-G.; Zhang, B.; Zhu, J.-H.; Li, Y.-X., *Adv. Mater.* **2010**, *22*, 1731-1735.
14. Liu, G.; Zhuang, X. D.; Chen, Y.; Zhang, B.; Zhu, J. H.; Zhu, C. X.; Neoh, K. G.; Kang, E. T., *Appl. Phys. Lett.* **2009**, *95*, 253301/1-253301/3.
15. Yu, A.-D.; Liu, C.-L.; Chen, W.-C., *Chem. Commun.* **2012**, *48*, 383-385.
16. Li, G. L.; Liu, G.; Li, M.; Wan, D.; Neoh, K. G.; Kang, E. T., *J. Phys. Chem. C* **2010**, *114*, 12742-12748.
17. Liu, J. Q.; Yin, Z. Y.; Cao, X. H.; Zhao, F.; Lin, A. P.; Xie, L. H.; Fan, Q. L.; Boey, F.; Zhang, H.; Huang, W., *ACS Nano* **2010**, *4*, 3987-3992.
18. Song, S.; Cho, B.; Kim, T. W.; Ji, Y.; Jo, M.; Wang, G.; Choe, M.; Kahng, Y.

H.; Hwang, H.; Lee, T., *Adv. Mater.* **2010,** *22*, 5048-5052.

19. Scott, J. C.; Bozano, L. D., *Adv. Mater.* **2007,** *19*, 1452-1463.
20. Ouyang, J. Y.; Chu, C. W.; Sieves, D.; Yang, Y., *Appl. Phys. Lett.* **2005,** *86*, 123507/1-123507/3.
21. Ouyang, J.; Chu, C.-W.; Szmanda, C. R.; Ma, L.; Yang, Y., *Nat. Mater.* **2004,** *3*, 918-922.
22. Feger, C.; Franke, H., *Plast. Eng.* **1996,** *36*, 759-814.
23. Lesieur, P.; Barraud, A.; Vandevyver, M., *Thin Solid Films* **1987,** *152*, 155-164.
24. Ling, Q.-D.; Chang, F.-C.; Song, Y.; Zhu, C.-X.; Liaw, D.-J.; Chan, D. S.-H.; Kang, E.-T.; Neoh, K.-G., *J. Am. Chem. Soc.* **2006,** *128*, 8732-8733.
25. Liu, Y.-L.; Ling, Q.-D.; Kang, E.-T.; Neoh, K.-G.; Liaw, D.-J.; Wang, K.-L.; Liou, W.-T.; Zhu, C.-X.; Chan, D. S.-H., *J. Appl. Phys.* **2009,** *105*, 044501/1-044501/9.
26. Liu, Y.-L.; Wang, K.-L.; Huang, G.-S.; Zhu, C.-X.; Tok, E.-S.; Neoh, K.-G.; Kang, E.-T., *Chem. Mater.* **2009,** *21*, 3391-3399.
27. Liu, C.-L.; Kurosawa, T.; Yu, A.-D.; Higashihara, T.; Ueda, M.; Chen, W.-C., *J. Phys. Chem. C* **2011,** *115*, 5930-5939.
28. Tian, G.; Wu, D.; Qi, S.; Wu, Z.; Wang, X., *Macromol. Rapid Commun.* **2011,** *32*, 384-389.
29. Liu, Y. W.; Zhang, Y.; Lan, Q.; Liu, S. W.; Qin, Z. X.; Chen, L. H.; Zhao, C. Y.; Chi, Z. G.; Xu, J. R.; Economy, J., *Chem. Mater.* **2012,** *24*, 1212-1222.
30. You, N.-H.; Chueh, C.-C.; Liu, C.-L.; Ueda, M.; Chen, W.-C., *Macromolecules* **2009,** *42*, 4456-4463.
31. Wang, K.-L.; Liu, Y.-L.; Shih, I. H.; Neoh, K.-G.; Kang, E.-T., *J. Polym. Sci., Part A: Polym. Chem.* **2010,** *48*, 5790-5800.
32. Wang, K.-L.; Liu, Y.-L.; Lee, J.-W.; Neoh, K.-G.; Kang, E.-T., *Macromolecules* **2010,** *43*, 7159-7164.
33. Cacelli, I.; Ferretti, A.; Girlanda, M.; Macucci, M., *Chem. Phys.* **2006,** *320*, 84-94.
34. Grabowski, Z. R.; Rotkiewicz, K.; Rettig, W., *Chem. Rev.* **2003,** *103*, 3899-4031.
35. Hu, J.; Li, Y.; Ji, Z.; Jiang, G.; Yang, L.; Hu, W.; Gao, H.; Jiang, L.; Wen, Y.; Song, Y.; Zhu, D., *J. Mater. Chem.* **2007,** *17*, 3530-3535.

Chapter 2. Effects of the Number of Phenoxy Linkages on the Memory Properties

ABSTRACT: Two TPA-based PIs, PI(AAPT-6FDA) and PI(APT-6FDA), were designed and synthesized for the purpose of verifying the effect of the number of mediated phenoxy linkage on the resulting memory properties. PI(AAPT-6FDA) and PI(APT-6FDA) exhibited distinct volatile memory characteristics of DRAM and SRAM, respectively. Moreover, each memory device showed a high ON/OFF current ratio of 10^9, a long retention time of 10^4 s, and device-to-device switching uniformity. The theoretical analysis suggested that the field induced charge transfer (CT) mechanism could be used to explain the memory characteristics of the PIs studied here. Also, it was clarified that the dual-mediated phenoxy linkages of PI(APT-6FDA) led to the more twisted conformation compared to PI(AAPT-6FDA), possessing mono-mediated phenoxy linkages. The twisted conformation of PI(APT-6FDA) produces a potential barrier for delaying the back CT process and explained the SRAM characteristic. However, the PI(AAPT-6FDA) device makes a more volatile ON state because of the possible lack of the back CT barriers due to the coplanar structure.

2-1. Introduction

During the past few years, enthusiastic studies have been carried out to clarify the relationship between the structures of functional polyimides (PIs) and the resulting memory properties.[1-11] In particular, revealing the non-volatile characteristics through the design of chemical structures is a subject of extreme difficulty. Over the years, approaches have been attempted to stabilize the charge transfer (CT) state and induce non-volatile memory characteristic in the polyimide (PI) system.[3-5] One of the effective ways to stabilize the CT state is inducing a twisted conformation of the active polymer. Since the CT state dissociates *via* back CT from the electron acceptor (A) to the electron donor (D), increasing the torsional angle between the D and A moiety generates an energy barrier for the suppression of the back CT and stabilizes the CT state. Therefore, it is obvious that the volatility of the resulting memory property can be modulated by controlling the conformation of the PI. Kang *et al.* found that the introduction of incorporated mediators in the polymer backbone, such as phenoxy linkage, leads to a twisted conformation, resulting in SRAM behavior, which is relatively a non-volatile characteristic comparing to the DRAM property.[6] The same group also reported that introducing the D moiety as a pendant group effectively increases the torsional displacement of the polymer back bone at the CT state, resulting in non-volatile WORM memory characteristic.[3-4] However, there also is a report on a PI containing D moiety at the pendent position which demonstrates the volatile DRAM property.[6] Therefore, comparing these previous reports, the design concept for inducing a large torsional angle for the revelation of non-volatile behavior still remains extremely unclear.

In this chapter, two types of functional PIs such as PI(AAPT-6FDA) derived from *N*-(4-(*p*-aminophenoxy)phenyl)-*N*-(*p*-aminophenyl)aniline (AAPT) and

4,4'-(hexafluoroisopropylidene)diphthalic anhydride (6FDA) and PI(APT-6FDA) from *N*,*N*-bis(4-(*p*-aminophenoxy)phenyl)aniline (APT) and 6FDA (shown in Scheme 2-2) were synthesized and their thermal, optical, electrochemical, and memory properties were evaluated. These two PIs were designed for the purpose of elucidating the effect of the number of phenoxy linkage between the D and A units on the resulting memory behavior. Moreover, in order to clarify the switching mechanism of the memory devices, theoretical calculations under the density functional theory (DFT) method was applied to analyze the geometry and electronic transitions of the studied PIs.

2-2. Results and discussion

2-2-1. Synthesis and characterization of monomers and polymers

The monomer synthesis of AAPT is described in the Experimental Section and also shown in Scheme 2-1a. First, the precursory 4-iodo-4'-nitrodiphenyl ether (INE) and *N*-(4-nitrophenyl)aniline were prepared from 4-fluoronitrobenzene and 4-iodophenol, and from 4-fluoronitrobenzene and aniline, respectively. Then, the Ullman reaction of *N*-(4-nitrophenyl)aniline and INE produced *N*-(4-(*p*-nitrophenoxy)phenyl)-*N*-(*p*-nitrophenyl)aniline (NNPT), which was further hydrogenated to AAPT. Similar to AAPT, APT was prepared in three steps as shown in Scheme 2-1b. The palladium catalyzed *N*-arylation reaction of aniline with two equivalents of INE produced *N*,*N*-bis(4-(*p*-nitrophenoxy)phenyl)aniline (NPT), which was converted to APT with the catalytic reduction.

Scheme 2-1. Synthesis of (a) AAPT and (b) APT.

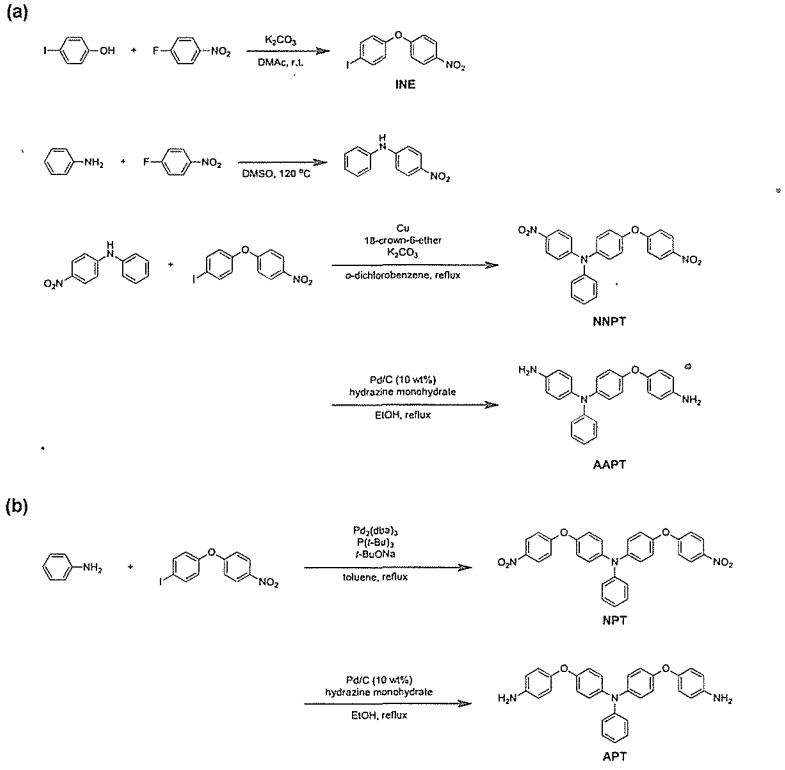

The characteristic nitro absorption peaks of both nitro compounds (NNPT and NPT) at around 1580 and 1340 cm^{-1} in the FT-IR spectra disappeared, and the new absorption peaks at around 3450 and 3370 cm^{-1} appeared after the reduction of NNPT and NPT, which were properly assigned to amino groups. The ^{1}H NMR spectra of these two diamine compounds are presented in Figure 2-1 with the assignments of all peaks. The signals at 4.92 and 4.82 ppm in Figure 2-1a are assigned to the asymmetric amino groups of AAPT, while the signal at 3.53 ppm in Figure 2-1b is assigned to the amino groups of APT. In addition, the ^{13}C NMR and elemental analysis clearly supported the formation of all monomers. The above results suggest the successful preparation of the AAPT and APT monomers.

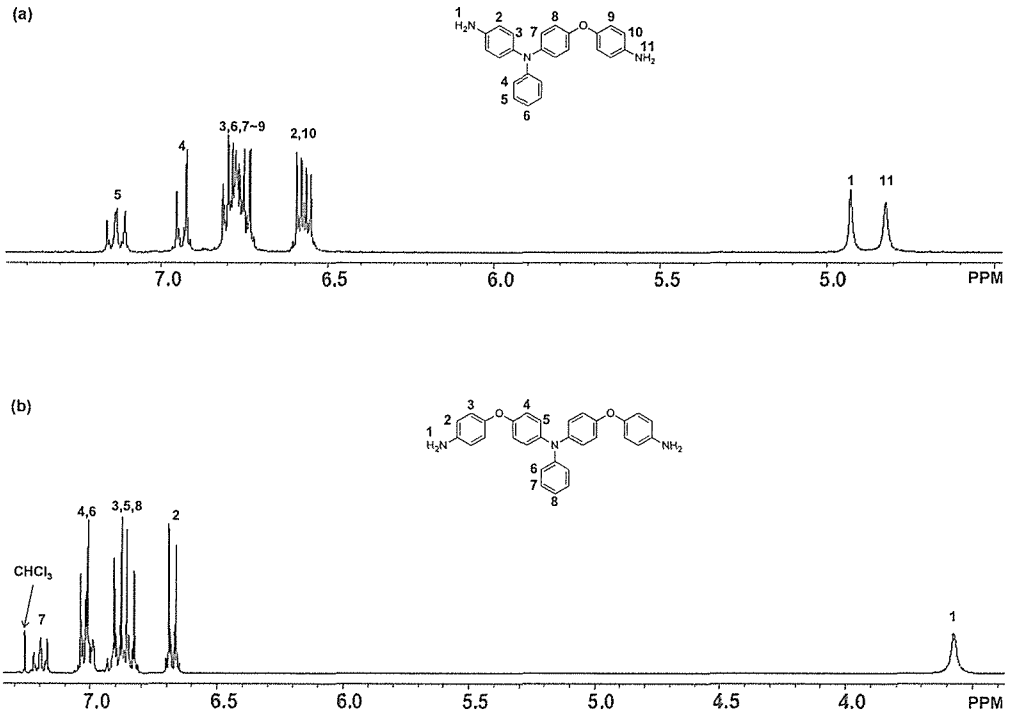

Figure 2-1. ^{1}H NMR spectra of (a) AAPT and (b) APT.

The polymers, PI(AAPT-6FDA) and PI(APT-6FDA), were prepared by the polycondensation reaction between diamines (AAPT and APT) and a diannhydride

(6FDA) in two steps, as shown in Scheme 2-2. First, the diamines and 6FDA were mixed in *N*,*N*-dimethylacetamine (DMAc) (solid content 15 wt%) under nitrogen to yield a viscous poly(amic acid) (PAA) solution. Then, chemical imidization was carried out by adding pyridine and acetic anhydride into the PAA solution to produce the PIs.

Scheme 2-2. Synthesis of PI(AAPT-6FDA) and PI(APT-6FDA).

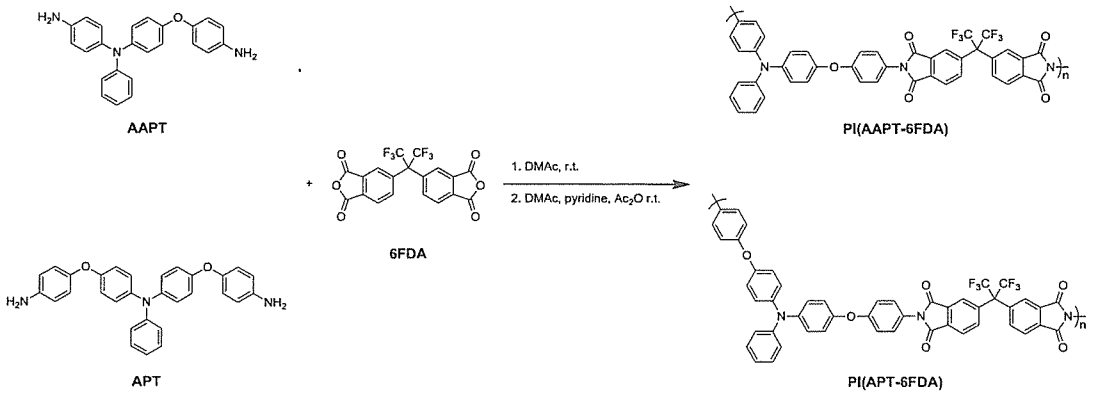

The desired structures of the PIs were confirmed by FT-IR spectra, which show the characteristic peaks of the imide group at 1780 cm^{-1} (symmetrical stretching of corbonyl) and 1720 cm^{-1} (asymmetrical stretching of carbonyl), and the C-N bond at around 1370 cm^{-1}, as presented in Figure 2-2. Moreover, the desired formations of all polymers were confirmed by ^{1}H NMR, shown in Figure 2-3, and elemental analysis. The number average molecular weight (M_n) values of PI(AAPT-6FDA) and PI(APT-6FDA) were 44,900 and 31,700, respectively, as determined by size exclusion chromatography (SEC). Both polymers were readily soluble in common organic solvents such as tetrahydrofuran (THF), *N*,*N*-dimethylformamide (DMF), DMAc, *N*-methylpyrrolidone (NMP), and chloroform. The high solubility may be attributed to the introduction of flexible ether linkages and hexafluoroisopropyl (6F) units in the polymer structure.

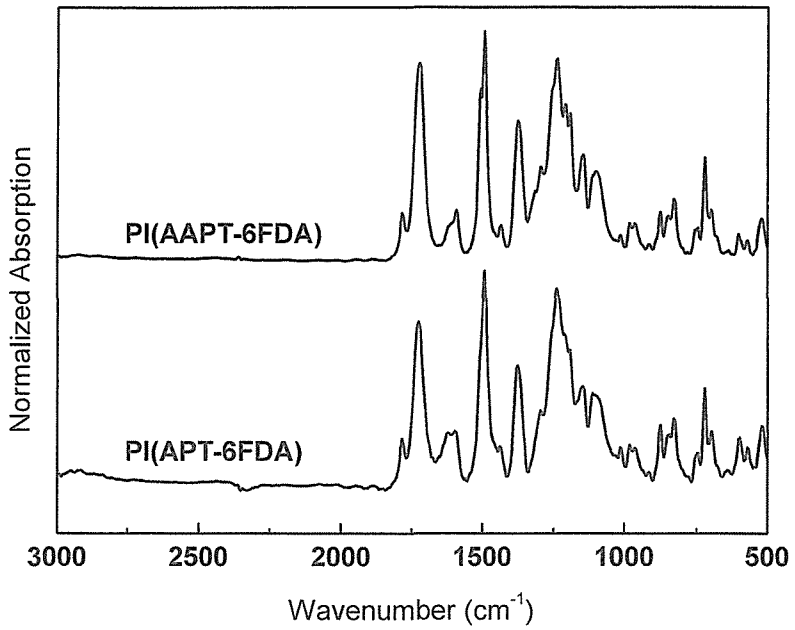

Figure 2-2. FT-IR absorption spectra of PI(AAPT-6FDA) and PI(APT-6FDA).

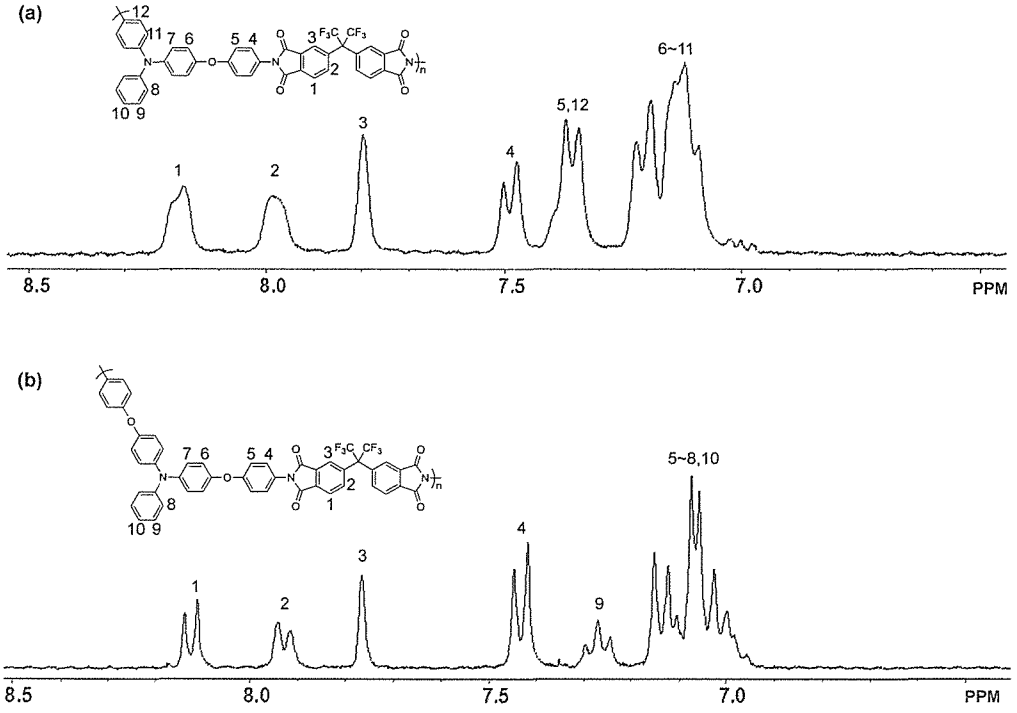

Figure 2-3. ^{1}H NMR spectra of (a) PI(AAPT-6FDA) and (b) PI(APT-6FDA).

The thermal stabilities of these two PIs were evaluated by thermo gravimetric analysis (TGA) under a nitrogen atmosphere (Figure 2-4). The 1% weight-loss temperatures (T_{d1}s) of PI(AAPT-6FDA) and PI(APT-6FDA) are determined to be 517 and 514 °C, respectively. These PIs not only showed excellent thermal stability but also possessed high glass transition temperatures (T_gs) of 276 and 252 °C for PI(AAPT-6FDA) and PI(APT-6FDA), respectively, which were estimated from differential scanning calorimetry (DSC) (see Figure 2-5). The excellent thermal stabilities of the PIs are expected to meet the requirement of heat resistance in the electronics industry.[12-13]

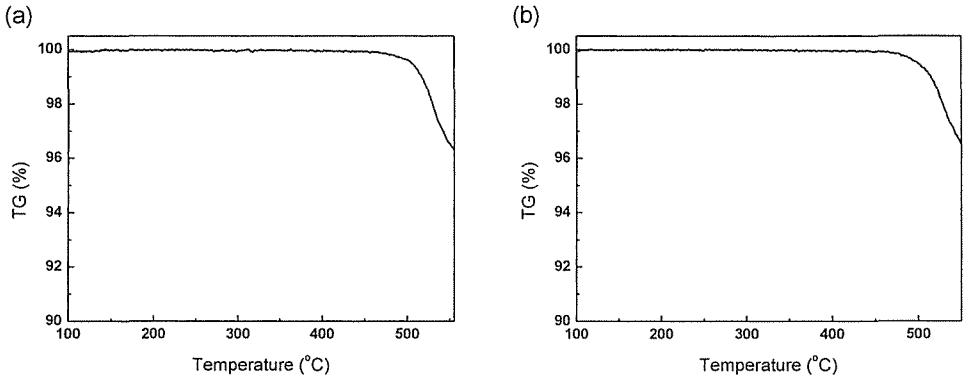

Figure 2-4. TGA curves of (a) PI(AAPT-6FDA) and (b) PI(APT-6FDA) under nitrogen atmosphere.

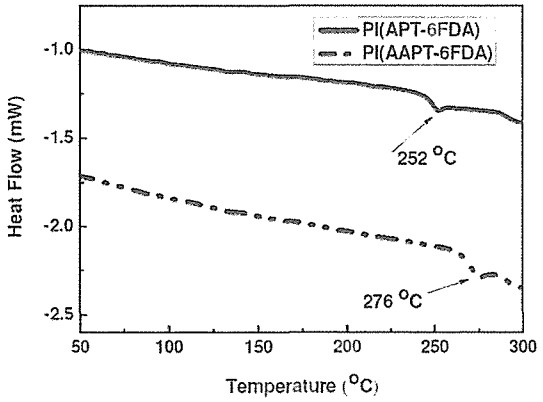

Figure 2-5. DSC curves of PI(AAPT-6FDA) and PI(APT-6FDA) under nitrogen atmosphere.

2-2-2. Optical and electrochemical properties

Figure 2-6 shows the solution and film state UV-vis absorption spectra of the studied PIs in. PI(AAPT-6FDA) exhibits absorption peak maxima (λ_{max}) 300 and 308 nm in the solution and thin film states, respectively, while those of PI(APT-6FDA) are 301 and 303 nm, respectively. The above absorption peaks are attributed to the π–π^* transition delocalized along the π-electronic system. Besides, as compared to PI(APT-6FDA) in the film state, PI(AAPT-6FDA) apparently exhibits more intense absorption intensity in the wavelength above 350 nm, probably resulting from the intermolecular π–π or CT interaction. As a result, the optical band gap (E_g^{opt}) of PI(AAPT-6FDA) and PI(APT-6FDA), estimated from the onset optical absorbance, are 3.15 and 3.55 eV, respectively. The larger E_g^{opt} of PI(APT-6FDA) than that of PI(AAPT-6FDA) indicates that the dual-mediated phenoxy linkage leads to a lower planarity than the mono-mediated one when both polymer structures are alike. To put it another way, the intermolecular interaction observed in the absorption spectra of PI(AAPT-6FDA) supports the higher planarity of PI(AAPT-6FDA) compared to PI(APT-6FDA)

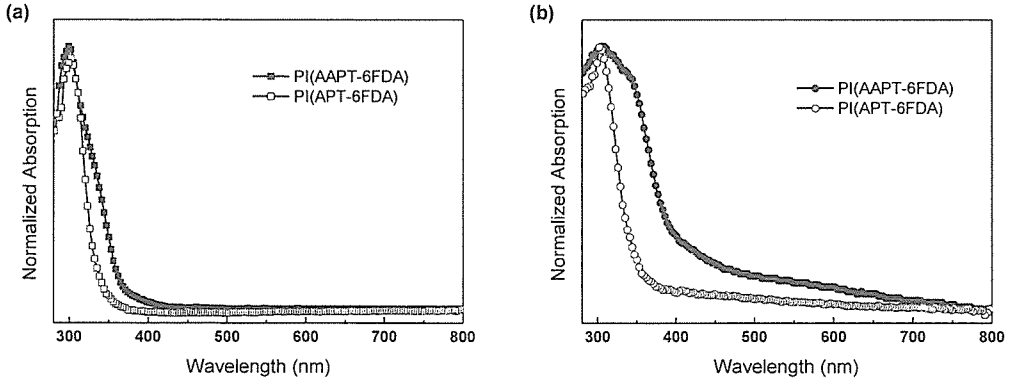

Figure 2-6. (a) Solution state and (b) film state UV-vis absorption spectra of PI(AAPT-6FDA) and PI(APT-6FDA).

Figure 2-7 shows the cyclic voltammetry (CV) results of PI(AAPT-6FDA) and PI(APT-6FDA) films on indium tin oxide (ITO) glass using a 0.1 M solution of tetrabutylammonium perchlorate (TBAP) in anhydrous acetonitrile. Both PIs exhibit reversible *p*-doping behavior during the anodic scan. The onset oxidation (E_{onset}^{OX}) values of PI(AAPT-6FDA) and PI(APT-6FDA) are 0.96 and 0.90 V *vs* Ag/Ag^{+}, respectively, and thus the estimated highest occupied molecular orbital (HOMO) energy levels are -5.32 and -5.26 eV, respectively.[14] Note that the potential of the external standard, the ferrocene/ferrocenium ion couple ($E_{ferrocene}$) was 0.44 V from the CV measurement without any polymer film coated on ITO glass. Besides, the lowest unoccupied molecular orbital (LUMO) energy levels of PI(AAPT-6FDA) and PI(APT-6FDA) estimated from the difference between the optical band gap and HOMO energy levels are -2.17 and -1.71 eV, respectively. The results provide us with the fact that additional phenoxy linkage does not conspicuously effect on the HOMO energy, while the LUMO energy is significantly affected. This indicates that the number of phenoxy likages effect on the geometry rather than the electronic state of the polymer.

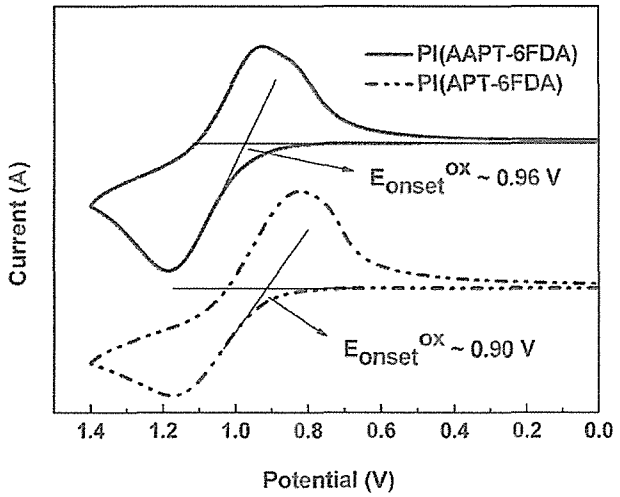

Figure 2-7. Cyclic voltammograms of PI(AAPT-6FDA) and PI(APT-6FDA).

2-2-3. Memory device characteristics of the polymers

The memory effects of PI(APT-6FDA) and PI(AAPT-6FDA) were demonstrated by the current-voltage (*I-V*) characteristics of an ITO/polymer/Al sandwich device. Figure 2-8 exhibits the typical *I-V* curves of the memory devices fabricated with PI(APT-6FDA) and PI(AAPT-6FDA). For the case of PI(AAPT-6FDA) (see Figure 2-8a), the device is initially in the OFF state ("0" signal in data storage) with a current in the range of 10^{-11}–10^{-14} A as the voltage is swept from 0 to -3.0 V. When the voltage increases further, an abrupt increase in the current is induced at a threshold value of about -3.5 V, and the device transits to the high conductivity ON state ("1" signal in data storage). The ON/OFF current ratio of the studied memory device is as high as 10^9, which leads to a low misreading rate for memory applications. This electronic transition from the OFF state to the ON state in the 1st sweep serves as the "writing" process. In addition, the device can be kept in the ON state during the subsequent 2nd sweep from 0 to -6 V. The 3rd sweep is conducted after turning off the power for 30 s. The device was reprogrammed, starting from the OFF state, to the ON state again with an accurate threshold voltage of -3.5 V and kept in the ON state (the 4th sweeps). This phenomenon suggests that the ON state of PI(AAPT-6FDA) can only be retained for an extremely short period of time after the removal of power and would immediately relax to the original OFF state. In addition, similar switching phenomena are observed during the positive voltage sweep (see the 5th and 6th sweeps). The short retention ability of the ON state determines the volatile DRAM type of PI(AAPT-6FDA). This field induced electronic transitions is similar to the previously reported device based on TP6F-PI[7] and PYTPA-PI,[8] shown in Chapter 1.

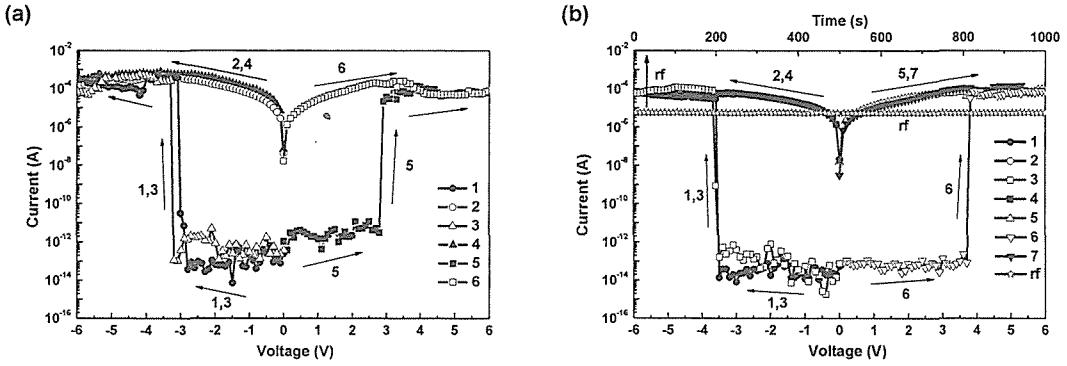

Figure 2-8. I-V characteristics of (a) PI(AAPT-6FDA) and (b) PI(APT-6FDA) memory device.

Meanwhile, the electrical behavior of the PI(APT-6FDA) device was also studied as shown in Figure 2-8b. The *I-V* curve observed during the 1st–7th sweeps still keeps the volatile characteristics. As compared to the PI(AAPT-6FDA) device, the main difference is the longer period of time for the retained ON state. Initially, the device is in the OFF state with quite a low current level of 10^{-12}–10^{-14} A. Further increasing the applied voltage higher than the threshold value, a transition from the OFF state to the ON state is observed with a bidirectional sharp current density increase (the 1st, 3rd, and 6th sweeps). The induced ON state did not relaxed to the initial OFF state after turning off the power supply for 30 s. However, after turning off the power for a longer time of 4 min, the device returns to low conductivity OFF state (3rd sweep), indicating that this memory device possesses a "remnant", yet volatile nature. The above switching behavior on remnant stored data and the volatile nature of memory device can explain the functionality of PI(APT-6FDA) as a SRAM.[6, 15] It should be noted that the *I-V* curves of the devices based on both PIs, exhibiting the volatile property, are measured in at least 10 devices with reproduced data.

The stability of the memory was also evaluated under the same conditions. Figure

2-9a shows the retention times and stress tests of both the ON and OFF states of PI(APT-6FDA). Initially, the memory device starts to turn ON or OFF to a high or low conductivity state. Under a constant stress of -1 V, no obvious degradation in current is observed for both ON and OFF states for at least 10^4 s during the readout test. The stimulus effect of read pulses on the ON and OFF states was also investigated for the long time test (Figure 2-9b). The pulse period and width are 3 and 2 μs, respectively, as shown in the inset of Figure 2-9b. The PI(APT-6FDA) memory device is stable for at least 10^8 continuous read pulses of -1 V.

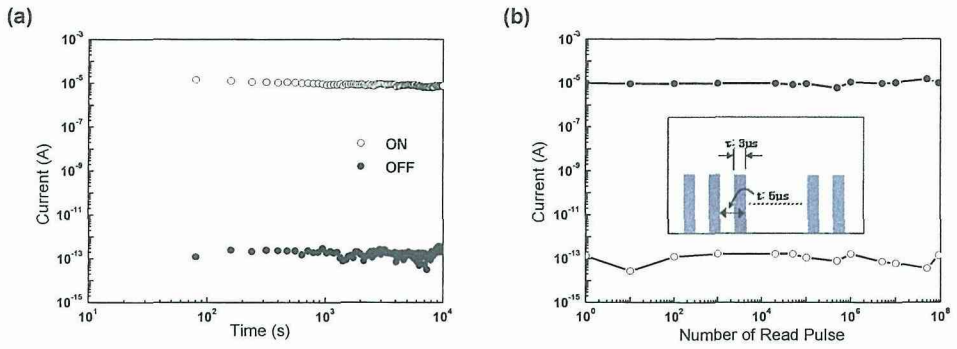

Figure 2-9. (a) Retention times on the ON and OFF states and (b) stimulus effect of read pulses on the ON and OFF states of the ITO/PI(APT-6FDA)/Al device. The insert of (b) shows the pulse shapes in the measurement.

In order to clarify the detailed converting mechanism, theoretical analysis was applied and discussed in the following section.

2-2-4. Proposed switching mechanism by theoretical analysis

Molecular simulation on the basic unit (BU) of PI(AAPT-6FDA) and PI(APT-6FDA) was carried out by DFT/B2LYP/6-31G(d) with the Gaussian 03 program.[16] The sketch map of the structures for the BU of PI(AAPT-6FDA) and PI(APT-6FDA) and optimized structures are plotted to the upper part of Figure 2-10. Note that the 6F group of the PIs

is not included in the BU since these fragments do not have significant differences in the electronic properties.[5-8] The PI(APT-6FDA) (represented as L-D-L-A) shows the more twisted conformation relative to the PI(AAPT-6FDA) (represented as D-L-A) due to the incorporation of the additional mediated noncoplanar geometry of phenoxy linkage. This is also supported by the blue-shifted absorbance of PI(APT-6FDA) than PI(AAPT-6FDA), as discussed in section 2-2-2.

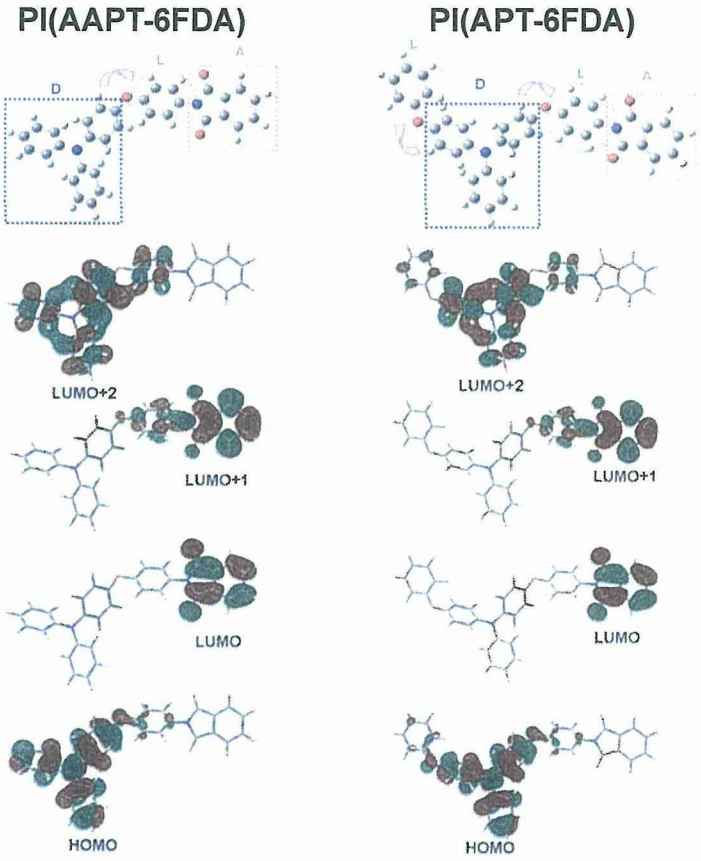

Figure 2-10. Electronic density contours of molecular orbitals and electrostatic potential surface (ESP) of the BUs of PI(AAPT-6FDA) and PI(APT-6FDA).

The bottom part of Figure 2-10 shows the charge density isosurfaces of the BUs of PI(AAPT-6FDA) and PI(APT-6FDA) with the most energetically favorable geometry. The relative ordering of the occupied and virtual molecular orbitals gives a reasonable

indication of the excited properties and charge transport ability. The HOMO and LUMO+2 isosurfaces tend to locate on the TPA (D), while the LUMO and LUMO+1 located on the phthalimide (A). As the applied bias reaches the threshold value, electrons at the HOMO with sufficient energy transit to LUMO+2 within TPA unit to give rise to the excited state. Basically, due to the fact that the HOMO and higher excited states (LUMO+1 and LUMO+2) are slightly distributed on the phenoxy linkages on PI(AAPT-6FDA) and PI(APT-6FDA), the charge transition comes next to the promotion of the electron from the ground state to the excited state. This means that the CT subsequent to the excitation of the AAPT or APT moiety leads to the high conductive CT state. Nevertheless, the CT can occur to form the conductive state through process such as directly from the HOMO to LUMO as well as indirectly from the HOMO to LUMO+2, LUMO+1, and then to the LUMO. Besides, the device switching to the ON state with a symmetrically comparable threshold voltage of either polarity also supports the switching mechanism of electric filed induced CT.[6, 8]

Generally, it is known that in the two distinct heterocyclic ring unit, the dihedral angle between the two rings tend to increase by applying an electric field.[17-19] Taking advantages of this view, it has been verified in the previous report on P(BPPO)-PI that the torsional angle between the D and A moieties increases during the CT process under the existence of phenoxy linkage.[6] The increased torsional angle generates a potential barrier for the back CT and possibly prevents the recombination of segregated charges, leading to a "remnant" behavior. For the case of PIs studied in this work, following the above theory, it can be said that PI(APT-6FDA) takes a more twisted conformation due to having larger amount of phenoxy linkages compared to PI(AAPT-6FDA). As a result, PI(APT-6FDA) shows a "remnant" behavior comparing to PI(AAPT-6FDA). Combined

with the remarkable difference in the film state UV absorption, it is suggested that PI(APT-6FDA) possessing dual-mediated phenoxy linkages would more possibly form temporary electric field induced CT state due to the larger inter- and intra-chain twisting effects, while the mono-mediated phenoxy linkage of PI(AAPT-6FDA) leads to a less twisted conformation and makes it behave as volatile DRAM. However, even in the case of PI(APT-6FDA), the twisted conformation relaxes to the initial state after removing the applied voltage and the potential barrier for the back CT disappears. Therefore, the back CT occurs from the phthalimide (A) to the TPA (D), which brings back the PIs from the CT state to the ground state, and confirms the volatile switching behavior. In addition, PI(AAPT-6FDA) and PI(APT-6FDA) showed close theoretical dipole moment values of 2.65 and 2.87 D, respectively. The smaller dipole moment value of PI(AAPT-6FDA) to PI(APT-6FDA) might contribute to the less volatile behavior. However, these values were much lower than that of the sulfur containing PIs showing a non-volatile property (around 6.00 D),[5] which might also explain the unstable CT state that leads to the volatile characteristics in both PIs.

2-3. Conclusion

Two TPA-based PIs, PI(AAPT-6FDA) and PI(APT-6FDA), were designed and synthesized in order to clarify the effect of the number of mediated phenoxy linkage between the D and A units on the resulting memory properties. The memory devices with the configuration of ITO/PI(APT-6FDA) or PI(AAPT-6FDA)/Al exhibited distinct volatile memory characteristics of SRAM or DRAM, respectively. Moreover, each memory device showed a high ON/OFF current ratio of 10^9, a long retention time of 10^4 s, and device-to-device switching uniformity. The theoretical analysis suggested that the

CT mechanism could be used to explain the memory characteristics of the PIs studied here. Also, it was clarified that the dual-mediated phenoxy linkages of PI(APT-6FDA) led to the more twisted conformation compared to PI(AAPT-6FDA) with mono-mediated phenoxy linkages. It thus produced a potential barrier for delaying the back CT process by the electric field and explained the SRAM characteristic. On the other hand, the PI(AAPT-6FDA) device showed a more volatile ON state because of the possible lack of the back CT barriers. These results reveal that the increase in the number of mediator gives rise to the increase in the torsional angle of the polymer structure, leading to a more stable CT state. The fundamental study on the structural effect on the resulting memory property provides us with the strategies for the design of functional PIs for advanced memory device applications.

2-4. Experimental section

Materials. *p*-Iodophenol, *p*-fluoronitrobenzene, aniline, tri-*t*-butylphosphine, copper powder, 18-crown-6-ether, palladium-activated carbon (Pd 10 wt%), DMAc, and toluene were purchased from Wako, Japan. Dehydrated dimethyl sulfoxide (DMSO), tris-(dibenzylideneacetone)dipalladium (0) ($Pd_2(dba)_3$) and 6FDA were purchased from TCI and were used as received.

Synthesis of INE. To a solution of *p*-diodophenol (5.05 g, 22.9 mmol) and potassium carbonate (3.73 g, 27.4 mmol) in a dehydrated DMAc (35 mL) was added *p*-fluoronitrobenzene (2.30 mL, 21.7 mmol) under a nitrogen atmosphere. The reaction mixture was stirred for 24 h at room temperature, and poured into a 1 M hydrochloric acid solution. The crude solid was purified by recrystallization from isopropanol and distilled water to give 7.17 g (96% in yield) of white crystal. IR (KBr), ν (cm^{-1}): 1508, 1342 (NO_2 stretching), 1246, 1053 (C–O–C stretching). ^1H NMR (300 MHz, $CDCl_3$, δ, ppm, 25 °C): 8.21 (d, J = 9.6 Hz, ArH, 2H), 7.73 (d, J = 8.7 Hz, ArH, 2H), 7.03 (d, J = 9.0 Hz, ArH, 2H), 6.86 (d, J = 9.0 Hz, ArH, 2H).

Synthesis of *N*-(4-nitrophenyl)aniline. A mixture of *p*-fluoronitrobenzene (2.10 mL, 19.8 mmol) and aniline (5.40 mL, 59.3 mmol) in dehydrated DMSO (50 mL) was stirred for 12 h at 120 °C under a nitrogen atmosphere. Then, the solution was poured into a 0.5 M hydrochloric acid solution. The precipitate was dissolved in ethyl acetate and the solution was then washed with 1 M hydrochloric acid solution, sodium hydrogen carbonate solution, and brine. The solution was died over magnesium sulfate, filtered, and concentrated. The crude product was purified by recrystallization from toluene and hexane to produce 3.22 g (76%) of yellow crystals. IR (KBr), ν (cm^{-1}): 3344 (N–H stretching), 1585 (NO_2 stretching). ^1H NMR (300 MHz, $CDCl_3$, δ, ppm, 25 °C):

8.12 (d, J = 9.3 Hz, ArH, 2H), 7.39 (d, J = 8.0 Hz, ArH, 2H), 7.23-7.14 (m, ArH, 3H), 6.94 (d, J = 8.7 Hz, ArH, 2H), 6.30 (s, N–H, 1H).

Synthesis of NNPT. A mixture of *N*-(4-nitrophenyl)aniline (4.17 g, 19.5 mmol), INE (9.50 g, 27.8 mmol), and excess amount of potassium carbonate (10.9 g, 78.6 mmol) in toluene (50 mL) was heated to reflux temperature using a Dean-Stark apparatus to remove water under a nitrogen atmosphere. After removing toluene, the mixture was cooled to room temperature and copper (4.96 g, 78.0 mmol), 18-crown-6-ether (1.60 g, 6.05 mmol), dichlorobenzene (30 mL) were added. The reaction mixture was refluxed for 12 h. After cooling to room temperature, the mixture was filtrated, washed with water, and poured into methanol. The crude solid was purified by recrystallization from 2-methoxyethanol to yield 6.13 g (74% in yield) of orange crystal. IR (KBr), v (cm^{-1}): 1585, 1342 (NO_2 stretching). ^{1}H NMR (300 MHz, DMSO-d_6, δ, ppm, 40 °C): 8.31 (d, J = 9.0 Hz, ArH, 2H), 8.12 (d, J = 9.6 Hz, ArH, 2H), 7.52 (t, J = 7.8 Hz, ArH, 2H), 7.41 (d, J = 9.0 Hz, ArH, 2H), 7.37-7.26 (m, ArH, 7H), 6.90 (d, J = 9.6 Hz, ArH, 2H). ^{13}C NMR (75 MHz, DMSO-d_6, δ, ppm, 40 °C): 163.23, 153.71, 152.59, 145.86, 143.34, 143.15, 140.80, 130.53, 128.57, 126.93, 126.44, 125.94, 122.15, 118.59, 117.78. *Anal.* Calcd. For $C_{24}H_{17}N_3$: C, 67.4; H, 4.01; N, 9.83. Found: C, 67.5; H, 4.23; N, 9.58.

Synthesis of NPT. Aniline (0.810 mL, 8.88 mmol) and tri-*t*-butylphosphine (0.200 mL, 0.808 mmol) were added to a mixture of INE (6.92 g, 20.3 mmol), (0.188 g, 0.203 mmol) in dehydrated toluene (90 mL) under a nitrogen atmosphere. The reaction mixture was refluxed for 16 h, and then filtered to remove sodium *tert*-butoxide and $Pd_2(dba)_3$. After concentrating the solution, the residual solid was dissolved in DMF and poured into water. The precipitate was collected by filtration and purified by column chromatography using dichloromethane as an eluent to give 4.19 g (91% in yield) of

yellow powder. IR (KBr), v (cm^{-1}): 1589, 1342 (NO_2 stretching). ^1H NMR (300 MHz, $CDCl_3$, δ, ppm, 25 °C): 8.22 (d, J = 9.0 Hz, ArH, 2H), 7.31 (t, J = 9.1 Hz, ArH, 2H), 7.17-6.99 (m, ArH, 15H). ^{13}C NMR (75 MHz, DMSO-d_6, δ, ppm, 40 °C): 163.94, 150.19, 147.83, 145.48, 142099, 129.97, 126.39, 125.89, 124.62, 123.85, 121.94, 117.27. *Anal.* Calcd. For $C_{30}H_{21}N_3$: C, 69.4; H, 4.07; N, 8.09. Found: C, 69.4; H, 4.62; N, 7.40.

Synthesis of AAPT. Hydrazine monohydrate (10 mL) was added dropwise to a solution of NNPT (2.14 g, 5.00 mmol) and palladium on activated carbon (22.4 mg) in ethanol (15 mL), and the mixture was refluxed for 24 h. The reaction solution was filtered through Celite to remove the palladium catalyst and washed with THF. The filtrate was concentrated and poured into water. The precipitate was collected by filtration and purified by recrystallization from chloroform and hexane to yield 1.26 g (69% in yield) of white crystals. IR (KBr), v (cm^{-1}): 3460, 3379 (N–H stretching). ^1H NMR (300 MHz, DMSO-d_6, δ, ppm, 40 °C): 7.13 (t, J = 8.0 Hz, ArH, 2H), 6.94 (d, J = 9.0 Hz, ArH, 2H), 6.80-6.73 (m, ArH, 9H), 6.59-6.55 (m, ArH, 4H), 4.92 (s, N–H, 2H), 4.82 (s, N–H, 2H). ^{13}C NMR (75 MHz, DMSO-d_6, δ, ppm, 40 °C): 154.83, 149.49, 147.13, 146.67, 145.86, 142.86, 136.42, 129.63, 128.43, 125.81, 121.16, 120.44, 120.06, 118.43, 115.79, 115.69. *Anal.* Calcd. For $C_{24}H_{21}N_3$: C, 78.5; H, 5.76; N, 11.4. Found: C, 78.4; H, 5.90; N, 11.2.

Synthesis of ATP. APT was prepared by a similar procedure according to the synthesis of AAPT, starting from NPT. APT was obtained as white crystals in 90% yield. IR (KBr), v (cm^{-1}): 3460, 3375 (N–H stretching). ^1H NMR (300 MHz, $CDCl_3$, δ, ppm, 25 °C): 7.19 (t, J = 7.8 Hz, ArH, 2H), 6.94 (d, J = 9.0 Hz, ArH, 2H), 7.03-6.98 (m, ArH, 6H), 6.89-6.81 (m, ArH, 9H), 6.73 (d, J = 8.1 Hz, ArH, 4H), 3.53 (s, N–H, 4H). ^{13}C

NMR (75 MHz, DMSO-d_6, δ, ppm, 40 °C): 154.87, 149.46, 148.80, 142.90, 142.83, 129.46, 126.37, 122.37, 121.74, 121.19, 118.64, 116.67. *Anal.* Calcd. For $C_{30}H_{25}N_3$: C, 78.4; H, 5.48; N, 9.14. Found: C, 78.3; H, 5.76; N, 8.96.

Synthesis of poly[*N*-(4-(*p*-aminophenoxy)phenyl-*N*-(*p*-aminophenyl)aniline-hexafluoroisopropylidenediphthalimide] (PI(AAPT-6FDA)). 6FDA (0.444 g, 1.00 mmol) was added into a solution of AAPT (0.367 g, 1.00 mmol) in dehydrated DMAc (solid contents 15 wt%) under nitrogen. The reaction mixture was stirred at room temperature for 24 h to give a poly(amic acid) (PAA) solution. A reaction mixture of acetic anhydride (0.148 g, 1.49 mmol) and pyridine (0.115 g, 1.49 mmol) was added to the above PAA solution. The reaction mixture was stirred at room temperature under a nitrogen atmosphere for 24 h. The resulting solution was poured into methanol, and the precipitate was collected by filtration and washed with methanol. The final product was dried at 200 °C under vacuum for 10 h, and the polymer yield was 92%. The M_n and M_w values estimated from SEC were 4.49×10^4 and 7.90×10^4, respectively, with the polydispersity index (PDI = M_w/M_n) of 1.76. IR (KBr), ν (cm-1): 1786, 1724 (C=O stretching), 1381 (C–N stretching). ^{1}H NMR (300 MHz, DMSO-d_6, δ, ppm, 40 °C): 8.20-8.00 (m, ArH, 4H), 7.80 (s, ArH, 2H), 7.49 (d, J = 8.7 Hz, ArH, 2H), 7.36 (d, J = 8.4 Hz, ArH, 4H), 7.22-7.09 (m, ArH, 11H). *Anal.* Calcd for $C_{43}H_{23}N_3$: C, 66.6; H, 2.99; N, 5.42; found, C, 66.2; H, 3.30; N, 5.17.

Synthesis of poly[*N*,*N*-bis(4-(*p*-aminophenoxy)phenyl)aniline-hexafluoroisopropylidenediphthalimide] (PI(APT-6FDA)). Using APT as a diamine, PI(APT-6FDA) was synthesized by a procedure similar to that use for PI(AAPT-6FDA). The yield of PI(APPA-6FDA) was

93%. M_n, M_w, and PDI values of PI-(AAPT-6FDA) were 3.17×10^4, 6.27×10^4, and 1.98, respectively. IR (KBr), v (cm^{-1}): 1786, 1728 (C=O stretching), 1377 (C–N stretching). ^1H NMR (300 MHz, DMSO-d_6, δ, ppm, 40 °C): 8.12 (d, J = 8.1 Hz, ArH, 2H), 7.93 (d, J = 8.7 Hz, ArH, 2H), 7.76 (s, N-H, 1H), 7.43 (d, J = 8.7 Hz, ArH, 4H), 7.27 (t, J = 7.8 Hz, ArH, 2H), 7.15-6.96 (m, ArH, 15H). *Anal.* Calcd for $C_{49}H_{27}N_3$: C, 68.2; H, 3.70; N, 4.68; found, C, 67.3; H, 3.35; N, 4.69.

Characterization. NMR spectra were recorded on a BRUKER DPX-300S spectrometer at resonant frequencies of 300 MHz for ^1H and 75 MHz for ^{13}C nuclei using $CDCl_3$ or DMSO-d_6 as the solvent and tetramethylsilane as the reference. FT-IR spectra were measured by a Horiba FT-120 Fourier transform spectrophotometer. M_n and M_w were evaluated by SEC on a JASCO PU-2080 Plus with two polystyrene gel columns (TSK GEKS GMH_{HR}-M). DMF containing 0.01 M LiBr was used as a solvent at a flow rate of 1.0 mL/min calibrated by polystyrene standard samples. The UV-visible optical absorption spectra were recorded on a Hitachi U-3210 spectrophotometer at room temperature. The absorbance of polymer solutions was evaluated in the wavelength range of 280-800 nm. Elemental analyses were performed on a Yanaco MT-6 CHN recorder elemental analysis instrument. Thermal properties were estimated from a Seiko TG/DTA 6300 thermal analysis system and TA instruments DSC-Q100 under a nitrogen atmosphere at a heating rate of 10 and 6 °C/min, respectively. CV was performed at room temperature using a working electrode (ITO, polymer film area of about 10×30 mm^2), a homemade reference electrode Ag/AgCl, and a counter electrode (Pt wire) at a sweep rate of 0.1 V/s (CHI611B electrochemical analyzer). A 0.1 M solution of TBAP in anhydrous acetonitrile was used as an electrolyte. The thickness of the polymer film was measured with a Microfigure Measuring Instrument (Surfcorder

ET3000, Kosaka Laboratory Ltd.).

Fabrication and measurement of the memory device. The memory device was fabricated on the ITO coated glass, with the configuration of ITO/polyimides/Al. Before the fabrication of the polymer layer, the ITO glass was precleaned by ultrasonication with water, acetone, and isopropanol each for 15 min. A 25 mg/mL of well-dissolved PI(AAPT-6FDA) or PI(APT-6FDA) polymer solution in DMAc was first filtered through 0.45 μm pore size of PTFE membrane syringe filter. Then, the filtered solution was spin-coated onto the ITO glass at a speed rate of 1000 rpm for 60 s and annealed at 150 °C for 30 min under nitrogen. The thickness of the thin film was determined to be around 40-50 nm. Finally, a 300-nm-thick Al top electrode was thermally evaporated through the shadow mask (recorded device units of 0.5×0.5 mm^2 in size) at a pressure of 10^{-7} torr with a uniform depositing rate of 3-5 Å/s. The electrical characterization of the memory device was performed by a Keithley 4200-SCS semiconductor parameter analyzer equipped with a Keithely 4205-PG2 arbitrary waveform pulse generator. ITO was used as the cathode (maintained as common), and Al was set as the anode during the voltage sweep. The probe tip used 10 μm diameter tungsten wire attached to a tinned copper shaft with a point radius < 0.1 μm (GGB Industries, Inc.). All of the electronic measurements were performed in a glovebox.

Computational methodology. Molecular calculations studied in this work were performed through the Gaussian 03 program package.[16] Equilibrium ground state geometry and electronic properties were optimized by means of the density functional theory (DFT) method at the B3LYP level of theory (Becke-style three-parameter density functional theory using the Lee–Yang–Parr correlation functional) with the 6-31 G(d) basic set.

2-5. References

1. Ling, Q.-D.; Liaw, D.-J.; Teo, E. Y.-H.; Zhu, C.; Chan, D. S.-H.; Kang, E.-T.; Neoh, K.-G., *Polymer* **2007,** *48*, 5182-5201.
2. Ling, Q.-D.; Liaw, D.-J.; Zhu, C.; Chan, D. S.-H.; Kang, E.-T.; Neoh, K.-G., *Prog. Polym. Sci.* **2008,** *33*, 917-978.
3. Wang, K.-L.; Liu, Y.-L.; Shih, I. H.; Neoh, K.-G.; Kang, E.-T., *J. Polym. Sci., Part A: Polym. Chem.* **2010,** *48*, 5790-5800.
4. Wang, K.-L.; Liu, Y.-L.; Lee, J.-W.; Neoh, K.-G.; Kang, E.-T., *Macromolecules* **2010,** *43*, 7159-7164.
5. You, N.-H.; Chueh, C.-C.; Liu, C.-L.; Ueda, M.; Chen, W.-C., *Macromolecules* **2009,** *42*, 4456-4463.
6. Liu, Y.-L.; Wang, K.-L.; Huang, G.-S.; Zhu, C.-X.; Tok, E.-S.; Neoh, K.-G.; Kang, E.-T., *Chem. Mater.* **2009,** *21*, 3391-3399.
7. Ling, Q.-D.; Chang, F.-C.; Song, Y.; Zhu, C.-X.; Liaw, D.-J.; Chan, D. S.-H.; Kang, E.-T.; Neoh, K.-G., *J. Am. Chem. Soc.* **2006,** *128*, 8732-8733.
8. Liu, Y.-L.; Ling, Q.-D.; Kang, E.-T.; Neoh, K.-G.; Liaw, D.-J.; Wang, K.-L.; Liou, W.-T.; Zhu, C.-X.; Chan, D. S.-H., *J. Appl. Phys.* **2009,** *105*, 044501/1-044501/9.
9. Liu, C.-L.; Kurosawa, T.; Yu, A.-D.; Higashihara, T.; Ueda, M.; Chen, W.-C., *J. Phys. Chem. C* **2011,** *115*, 5930-5939.
10. Tian, G.; Wu, D.; Qi, S.; Wu, Z.; Wang, X., *Macromol. Rapid Commun.* **2011,** *32*, 384-389.
11. Liu, Y. W.; Zhang, Y.; Lan, Q.; Liu, S. W.; Qin, Z. X.; Chen, L. H.; Zhao, C. Y.; Chi, Z. G.; Xu, J. R.; Economy, J., *Chem. Mater.* **2012,** *24*, 1212-1222.
12. *International Technology Roadmap for Semiconductiors http://www.itrs.net/Links/2011ITRS/Home2011.htm* **2011.**
13. Feger, C.; Franke, H., *Plast. Eng.* **1996,** *36*, 759-814.
14. Bredas, J. L.; Silbey, R.; Boudreaux, D. S.; Chance, R. R., *J. Am. Chem. Soc.* **1983,** *105*, 6555-6559.
15. Lee, W.-Y.; Kurosawa, T.; Lin, S.-T.; Higashihara, T.; Ueda, M.; Chen, W.-C., *Chem. Mater.* **2011,** *23*, 4487-4497.
16. Frisch, M. J. T., G. W.; Schlegel, H. B.; Scuseria, G. E.; Robb, M. A.; Cheeseman, J. R.; Montgomery, Jr., J. A.; Vreven, T.; Kudin, K. N.; Burant, J. C.; Millam, J. M.; Iyengar, S. S.; Tomasi, J.; Barone, V.; Mennucci, B.; Cossi, M.; Scalmani, G.; Rega, N.; Petersson, G. A.; Nakatsuji, H.; Hada, M.; Ehara, M.; Toyota, K.; Fukuda, R.; Hasegawa, J.; Ishida, M.; Nakajima, T.; Honda, Y.;

Kitao, O.; Nakai, H.; Klene, M.; Li, X.; Knox, J. E.; Hratchian, H. P.; Cross, J. B.; Bakken, V.; Adamo, C.; Jaramillo, J.; Gomperts, R.; Stratmann, R. E.; Yazyev, O.; Austin, A. J.; Cammi, R.; Pomelli, C.; Ochterski, J. W.; Ayala, P. Y.; Morokuma, K.; Voth, G. A.; Salvador, P.; Dannenberg, J. J.; Zakrzewski, V. G.; Dapprich, S.; Daniels, A. D.; Strain, M. C.; Farkas, O.; Malick, D. K.; Rabuck, A. D.; Raghavachari, K.; Foresman, J. B.; Ortiz, J. V.; Cui, Q.; Baboul, A. G.; Clifford, S.; Cioslowski, J.; Stefanov, B. B.; Liu, G.; Liashenko, A.; Piskorz, P.; Komaromi, I.; Martin, R. L.; Fox, D. J.; Keith, T.; Al-Laham, M. A.; Peng, C. Y.; Nanayakkara, A.; Challacombe, M.; Gill, P. M. W.; Johnson, B.; Chen, W.; Wong, M. W.; Gonzalez, C.; and Pople, J. A., *Gaussian, Inc., Wallingford CT* **2004**.

17. Cacelli, I.; Ferretti, A.; Girlanda, M.; Macucci, M., *Chem. Phys.* **2006**, *320*, 84-94.
18. Hu, J.; Li, Y.; Ji, Z.; Jiang, G.; Yang, L.; Hu, W.; Gao, H.; Jiang, L.; Wen, Y.; Song, Y.; Zhu, D., *J. Mater. Chem.* **2007**, *17*, 3530-3535.
19. Grabowski, Z. R.; Rotkiewicz, K.; Rettig, W., *Chem. Rev.* **2003**, *103*, 3899-4031.

Chapter 3. Inducing a Highly Twisted Conformation in the Polyimide Structure by Large Steric Hindrance for the Development of Non-volatile Memory

ABSTRACT: In order to clarify the structural effect on the resulting memory properties and also revealing non-volatile memory characteristic by extending the accomplishment acquired in chapter 2, two PIs, PI(DAT-6FDA) and PI(DAPT-6FDA), were designed and synthesized. The memory device based on PI(DAT-6FDA) showed unstable volatile behavior, while the device based on PI(DAPT-6FDA), with a more bulky D unit, exhibited a stable non-volatile FLASH type memory characteristic, showing a long retention time over 10^4 s. The theoretical simulation based on DFT suggested that the more distinct charge separation between the ground and CT states led to a highly stable memory behavior. Also, it was clarified that PI(DAPT-6FDA) exhibited a highly twisted conformation comparing to PI(DAT-6FDA) in the ground state and a more twisted dihedral angle between the D and A units was induced in the CT state, which led to a non-volatile memory characteristic.

3-1. Introduction

Since the first report on the polyimide (PI) memory,[1] almost all kinds of current memory characteristics, from volatile dynamic random access memory (DRAM)[1-5] and static random access memory (SRAM)[5-7] to non-volatile FLASH[8] and write once read many (WORM)[9-10] type characteristics, have been reproduced in the PI system. These attentive studies have elucidated that the field induced charge transfer (CT) between the electron donor (D) and electron acceptor (A) moieties is responsible for the revelation of memory switching behavior and, more importantly, the key factor to determine the volatility of the resulting memory behavior is the stability of the generated CT state, that is, unstable CT state leads to volatile memory property and *vice versa*.[1-12]

In Chapter 2, the fact that the number of mediating phenoxy linkages obviously contributed to the stabilization of the CT state by affecting the conformation of the PI has been revealed.[5-6] To be specific, PI(AAPT-6FDA) possessing mono-mediated phenoxy linkage showed DRAM property, while PI(APT-6FDA) with a dual-mediated phenoxy linkage showed SRAM property. However, since both of the resulting memory behaviors were volatile ones, twisting the conformation based on the concept of adding larger amount of phenoxy linkages is not sufficient enough for the revelation of non-volatile characteristic.

In this chapter, the synthesis and memory device characterization of two PIs, such as PI(DAT-6FDA) derived from *N*-(2,4-diaminophenyl)-*N*,*N*-diphenylamine (DAT) and 4,4'-(hexafluoroisopropylidene)diphthalic anhydride (6FDA) and PI(DAPT-6FDA) from *N*-(4-(2',4'-diaminophenoxy)phenyl-*N*,*N*-diphenylamine (DAPT) and 6FDA are reported (Scheme 3-2). Following the previous studies by Kang's group,[9-10] these two PIs possessing the D moiety (diphenylamine and triphenylamine for PI(DAT-6FDA) and

PI(DAPT-6FDA), respectively) at the pendent position have been designed intending to reveal a non-volatile memory behavior. The difference between Kang's group work and this work is that the D moieties were introduced at the ortho position of the benzene ring connected to the phthalimide, which is the A unit, to obtain absolute twisted conformation by utilizing the steric hindrance. In order to clarify the memory behavior, theoretical calculations of the geometry and electronic states under the density functional theory (DFT) method were also carried out.

3-2. Results and discussion

3-2-1. Synthesis and characterization of monomers and polymers

As shown in Scheme 3-1, the monomer synthesis of DAT was carried out according to the previously reported method.[13] The synthesis of DAPT was carried out in four steps as shown in Scheme 3-1. Using 1-chloro-2,4-dinitrobenzene and *N*-(4-hydroxyphenyl)-*N*,*N*-diphenylamine,[14] the precursory *N*-(4-(2',4'-dinitrophenoxy)phenyl-*N*,*N*-diphenylamine (DNPT) was synthesized by the aromatic nucleophilic substitution reaction which was further hydrogenated to DAPT. Due to its low oxidative stability, DAPT was immediately used for the polymerization reaction.

Scheme 3-1. Synthesis of (a) DAT and (b) DAPT.

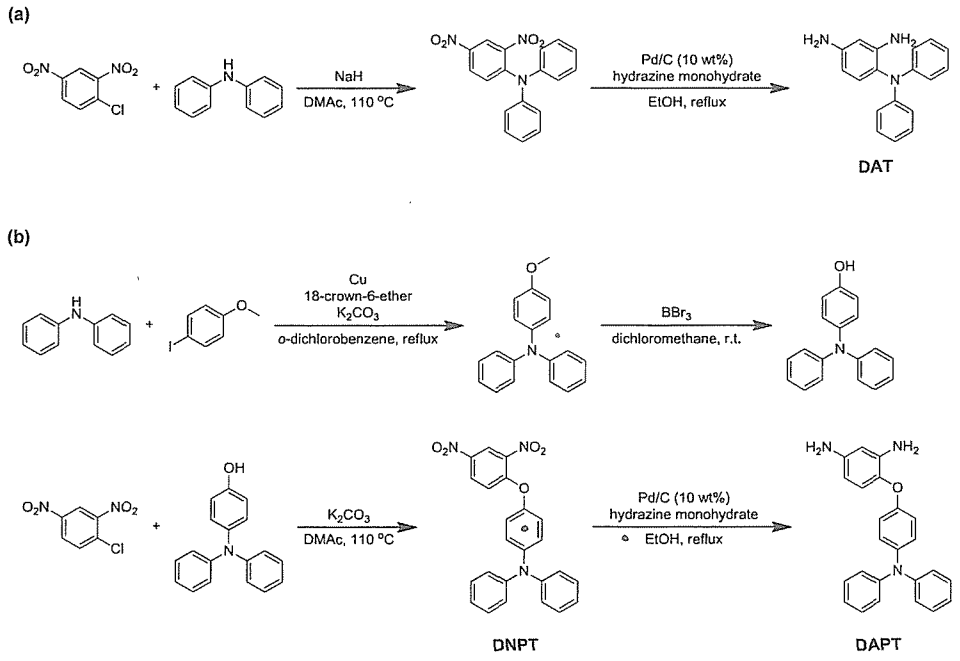

The characteristic nitro absorption peaks of DNPT at 1535 and 1346 cm^{-1} in the FT-IR spectra disappeared, and the new absorption peaks at 3460 and 3379 cm^{-1}

appeared after the reduction of DNPT, which were assigned to the amino groups. The ^{1}H NMR spectra of DAPT is presented in Figure 3-1. The signals at 4.89 and 4.60 ppm are assigned to the asymmetric amino groups of DAPT (#1 and 3). In addition, the ^{13}C NMR and elemental analysis clearly supported the formation of DAPT. It should be noted that, due to its low oxidative stability, quaternary ammonium chloride of DAPT was prepared before the elemental analysis.

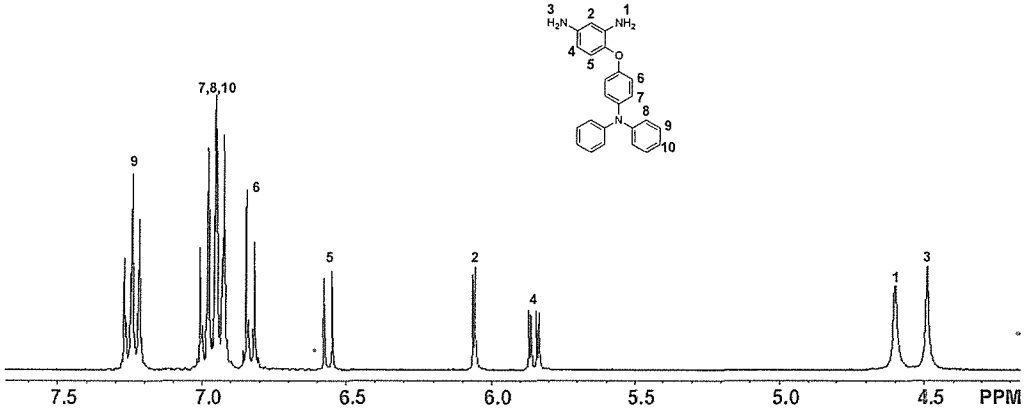

Figure 3-1. ^{1}H NMR spectra of DAPT.

The polymers, PI(DAT-6FDA) and PI(DAPT-6FDA), were prepared by the polycondensation reaction of diamines (DAT and DAPT) with a diannhydride (6FDA) in two steps, as shown in Scheme 3-2. First, the diamines and 6FDA were mixed in *N*,*N*-dimethylacetamine (DMAc) (solid content 15 wt%) under nitrogen to yield a viscous poly(amic acid) (PAA) solution. Then, chemical imidization was carried out by adding pyridine and acetic anhydride into the PAA solution to produce the PIs.

Scheme 3-2. Synthesis of PI(DAT-6FDA) and PI(DAPT-6FDA).

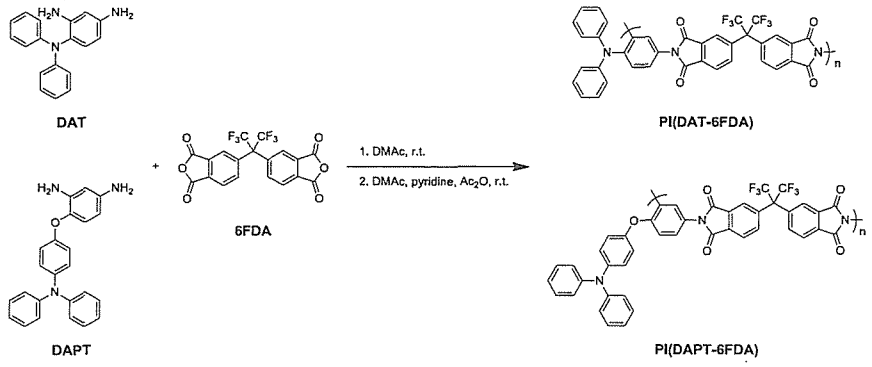

The desired structures of the PIs were confirmed by FT-IR spectra, which show the characteristic peaks of the imide group at around 1780 cm^{-1} (symmetrical stretching of corbonyl) and 1720 cm^{-1} (asymmetrical stretching of carbonyl), and the C-N bond at around 1370 cm^{-1}, as presented in Figure 3-2. Moreover, the desired formations of all polymers were confirmed by ^{1}H NMR with assignments of all peaks, shown in Figure 3-3, and elemental analysis. The number average molecular weight (M_n) values of PI(DAT-6FDA) and PI(DAPT-6FDA) were 16,000 and 21,000, respectively, as determined by size exclusion chromatography (SEC). Both polymers were readily soluble in common organic solvents such as *N*,*N*-dimethylformamide (DMF), DMAc, *N*-methylpyrrolidone (NMP), and toluene. The relatively low molecular weights are derived from steric hindrance of the bulky D units attached to the ortho position of amine moiety.[13] Also the high solubility attributes to the twisted conformation induced by the bulky D and hexafluoroisopropyl (6F) units in the polymer structure.

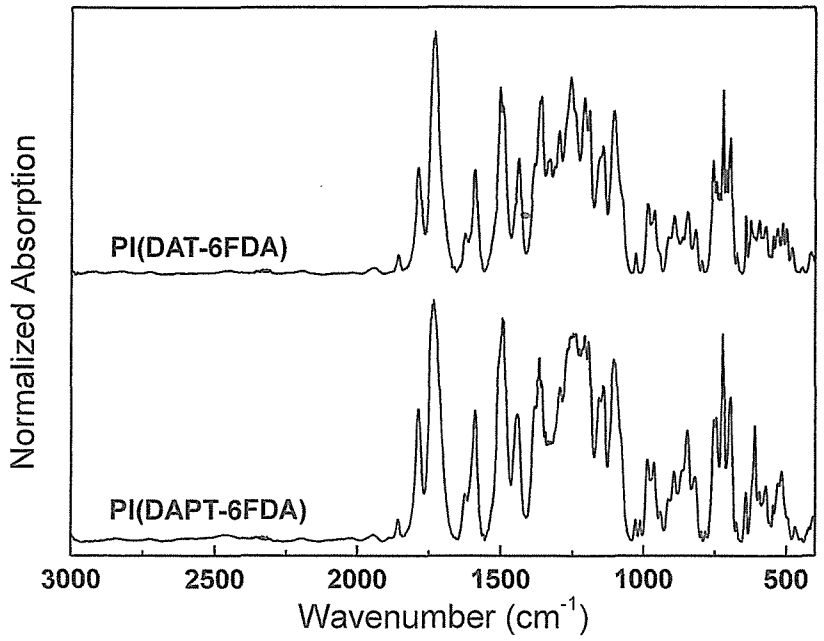

Figure 3-2. FT-IR absorption spectra of PI(DAT-6FDA) and PI(DAPT-6FDA).

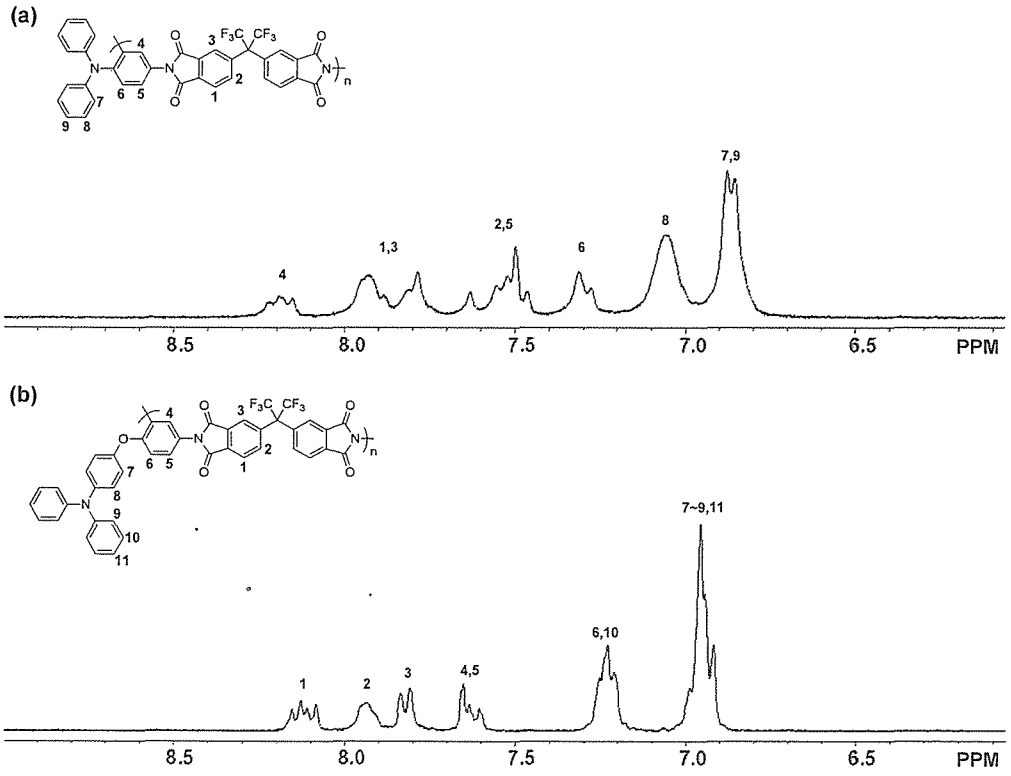

Figure 3-3. ^{1}H NMR spectra of PI(DAT-6FDA) and PI(DAPT-6FDA).

The thermal stabilities of these two PIs were evaluated by thermo gravimetric analysis (TGA) and differential scanning calorimetry (DSC) under a nitrogen atmosphere. The 5% weight-loss temperatures (T_{d5}s) of PI(DAT-6FDA) and PI(DAPT-6FDA) are determined to be 487 and 508 °C, respectively (Figure 3-4). Moreover, the glass transition temperatures (T_gs) of the PIs could not be observed during the DSC measurement in the range of 25–300 °C. These excellent thermal stabilities of the PIs are expected to meet the requirement of heat resistance in the electronics industry.

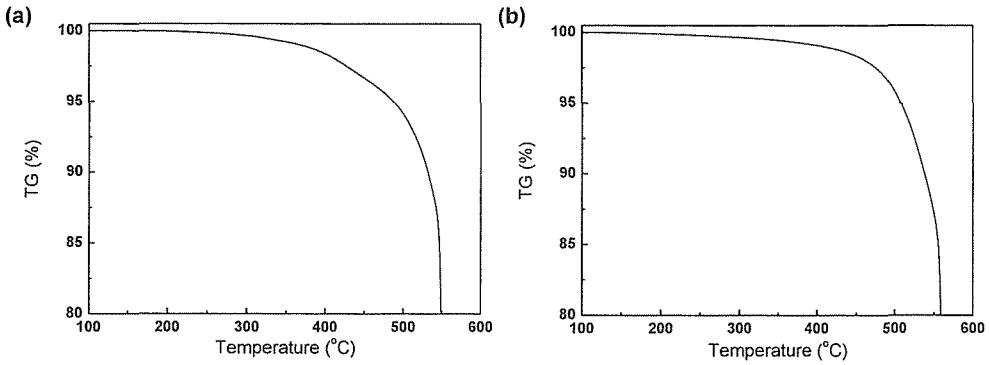

Figure 3-4. TGA curves of (a) PI(DAT-6FDA) and (b) PI(DAPT-6FDA).

3-2-2. Optical and electrochemical properties

Figure 3-5 shows the UV-vis absorption spectra of the studied PIs in DMAc solution and thin film states. Both PIs exhibit absorption peak maxima (λ_{max}) around 300 nm in solution and thin film states. This λ_{max} attributes to the π–π^* transition delocalized along the π-electronic system. Besides, one additional optical absorption around 320 and 340 nm are observed in the solution and film states of PI(DAT-6FDA), respectively. As the shoulder like absorption peak in the solution state changes to a clear absorption peak in the film state, this additional peak originates from the intermolecular π–π or CT interaction. As a result, the optical band gaps (E_g^{opt}s) of PI(DAT-6FDA) and

PI(DAPT-6FDA), estimated from the onset optical absorbance, are 3.32 and 3.47 eV, respectively. The result suggests that more dense intermolecular packing is promoted in the PI(DAT-6FDA) due to its coplanar structure compared to PI(DAPT-6FDA). In other words, the introduction of more bulky triphenylamine D unit of PI(DAPT-6FDA) results in a more twisted conformation.

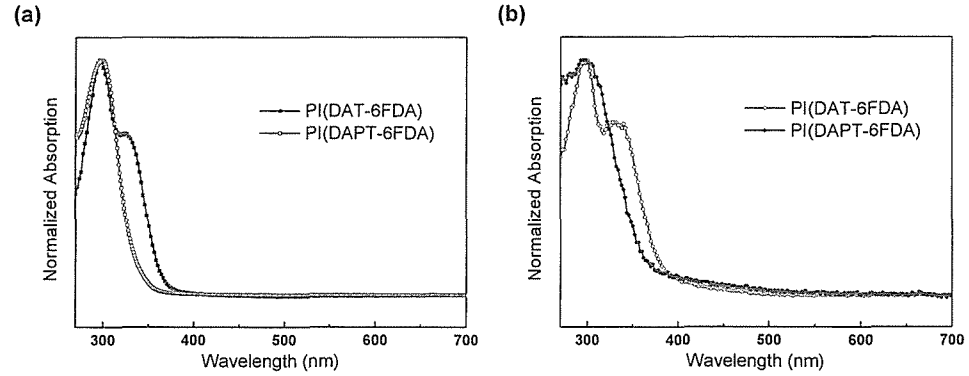

Figure 3-5. (a) Solution state and (b) film state UV-vis absorption spectra of PI(DAT-6FDA) and PI(DAPT-6FDA).

Figure 3-6 shows the cyclic voltammetry (CV) results of PI(DAT-6FDA) and PI(DAPT-6FDA) films on indium tin oxide (ITO) glass using a 0.1 M solution of tetrabutylammonium perchlorate (TBAP) in anhydrous acetonitrile. Both PIs exhibit reversible *p*-doping behavior during the anodic scan. The onset oxidation (E_{onset}^{ox}) values of PI(DAT-6FDA) and PI(DAPT-6FDA) are 1.05 and 0.75 V vs Ag/Ag^{+}, respectively, and thus the estimated highest occupied molecular orbital (HOMO) energy levels are -5.41 and -5.11 eV, respectively.[15] Note that the potential of the external standard, the ferrocene/ferrocenium ion couple ($E_{ferrocene}$) was 0.44 V from the CV measurement without any polymer film coated on ITO glass. Besides, the lowest unoccupied molecular orbital (LUMO) energy levels of PI(DAT-6FDA) and PI(DAPT-6FDA) estimated from the difference between the E_g^{opt}s and HOMO energy

levels are -2.09 and -1.64 eV, respectively. The result suggests that the frontier orbital of PI(DAT-6FDA) is more stabilized as compared to PI(DAPT-6FDA), and the more bulky D unit of PI(DAPT-6FDA) increased the LUMO energy level significantly, probably due to the non-linear or twisted conformation of the polymer backbone.

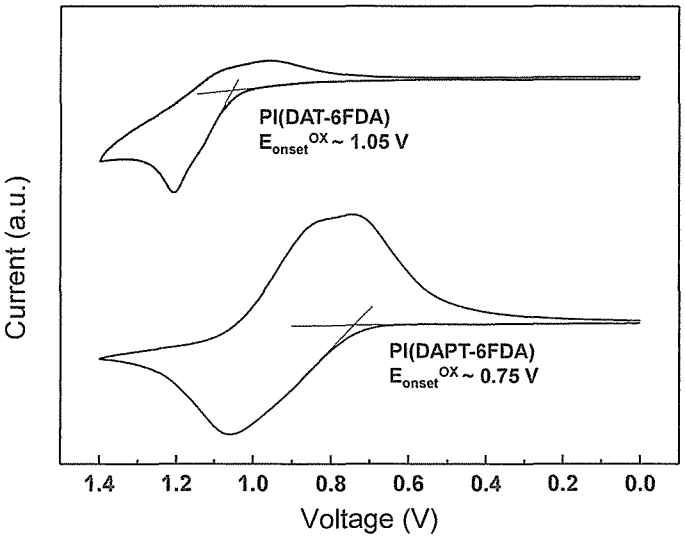

Figure 3-6. Cyclic voltammmograms of PI(DAT-6FDA) and PI(DAPT-6FDA).

3-2-3. Memory device characteristics of the polymers

The memory effects of PI(DAT-6FDA) and PI(DAPT-6FDA) are demonstrated by the current-voltage (*I-V*) characteristics of an Al/polymer/Al sandwich device. Figure 3-7 demonstrates the typical *I-V* curves of the memory devices based on PI(DAT-6FDA) and PI(DAPT-6FDA). For the case of PI(DAT-6FDA), as shown in Figure 3-7a, the device is initially in the low conductive OFF state with a current value in the range of 10^{-10}–10^{-6} A during the 1st voltage sweep from 0 to -2.5 V. When the voltage is further swept, an abrupt increase in the current value is observed at a threshold voltage of about -2.7 V, indicating an electronic switching from the OFF state to the high conductive ON state ("writing" process). The ON/OFF current ratio of the device based on

PI(DAT-6FDA) is around 10^4, which is quite sufficient to avoid misreading for memory applications. The ON state can be kept during subsequent 2nd voltage sweep from -4 to 0 V and also during the 3rd and 4th sweeps from 0 to 4 and 4 to 0 V, respectively, indicating the inerasable switching behavior. However, after turning off the electric power supply for 4 min, the device is reprogrammed, starting from the OFF state, to the ON state again with a threshold voltage of -3.2 V and keeps in the ON state (the 5th and 6th sweeps). This result suggests that the ON state can only be retained for a short period of time after removing the power and relaxes to the original OFF state. Thus, it can be concluded that the memory device based on PI(DAT-6FDA) possesses a volatile nature.

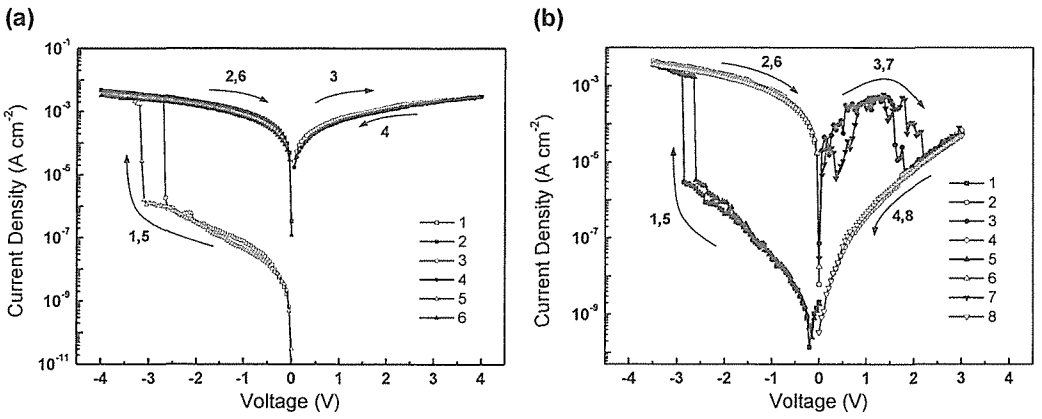

Figure 3-7. I-V curves of (a) PI(DAT-6FDA) and (b) PI(DAPT-6FDA).

On the other hand, the memory property of the device based on PI(DAPT-6FDA) is quite different to that of PI(DAT-6FDA) (Figure 3-7b). A sharp increase in the current value corresponding to the transition from the OFF state to the ON state is observed during the 1st sweep with the threshold voltage of -2.8 V. The switched ON state can be maintained during the subsequent 2nd voltage sweep and also after turning off the power supply for more than 30 min, indicating the non-volatile behavior. The induced ON state is initialized to the OFF state, corresponding to the "erasing" process, by applying a

voltage to the opposite direction from 0 to 3 V, as shown in the 3rd sweep. The recovered OFF state is kept during the subsequent 4th sweep from 3 to 0 V and can be reprogrammed to the ON state again by applying a voltage higher than the threshold value in the negative direction (see the 5th sweep). The rewritable and non-volatile switching behaviors discussed above indicate that the device based on PI(DAPT-6FDA) is a FLASH type memory. In addition, the above write read erase read (WRER) cycle can be continued for more than 10 times.

The stability of the memory was evaluated under the same condition. Figure 3-8 shows the retention times and stress tests of both the ON and OFF states of PI(DAT-6FDA) and PI(DATP-6FDA). For the case of PI(DAT-6FDA), the high current ON state starts to decrease after 10^3 s under the constant stress of -1 V and finally dies out after 10^4 s (Figure 3-8a). This means that the device based on PI(DAT-6FDA) cannot maintain the distinct two electronic states during the constant stress, resulting in an unstable memory characteristic. Meanwhile, no obvious degradation in the current is observed for both ON and OFF states of PI(DAPT-6FDA) for at least 10^4 s during the readout test, indicating a very stable memory behavior (Figure 3-8b).

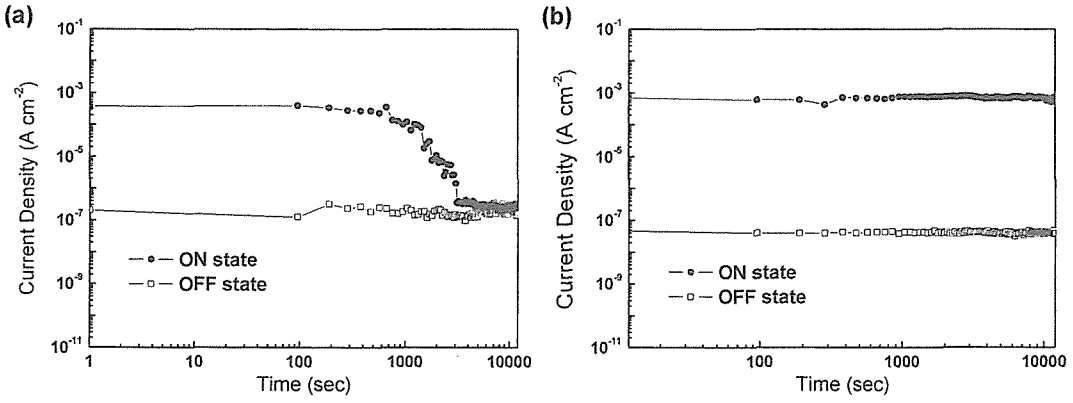

Figure 3-8. Retention times on the ON and OFF states of device based on (a) PI(DAT-6FDA) and (b) PI(DAPT-6FDA).

3-2-4. Theoretical analysis

As have been discussed in Chapter 2, the mechanism of electrical transition observed in both PIs system can be explained from electric field induced CT between the pendant D (diphenyl amine or triphenylamine) units and A (phthalimide) unit. To simplify the theoretical analysis, molecular simulations only on the basic units (BUs) of the ground and CT states of both PIs were carried out by DFT/B2LYP/6-31G(d) with the Gaussian 03 program.[16] Similar to Chapter 2, the 6F unit was not included in the BU.[1-2, 6, 8] Figure 3-9 shows the chemical structures for the BUs of PI(DAT-6FDA) and PI(DAPT-6FDA) and charge density isosurfaces with the most energetically favorable geometry. As can be seen, the electrons tend to locate on the D units of both PIs in the ground state and on the A units in the CT state. Comparing the two CT states, the electrons of PI(DAT-6FDA) are widely distributed among the whole BU, while those of PI(DAPT-6FDA) are relatively localized upon the A unit, indicating that charges of PI(DAPT-6FDA) at the CT state are more separated. This result provides us a good reason for the difference between the stabilities of the two memory behaviors. Since the electrons are widely distributed among the BU in the CT state of PI(DAT-6FDA), the separated charges can easily recombine and return to the ground state even under the constant voltage stress, resulting in an unstable memory behavior as shown in Figure 3-8a. On the other hand, the distinctly separated charges in the CT state of PI(DAPT-6FDA) suggest the difficulty of the recombination under the constant bias, leading to the stable memory characteristic described in Figure 3-8b.

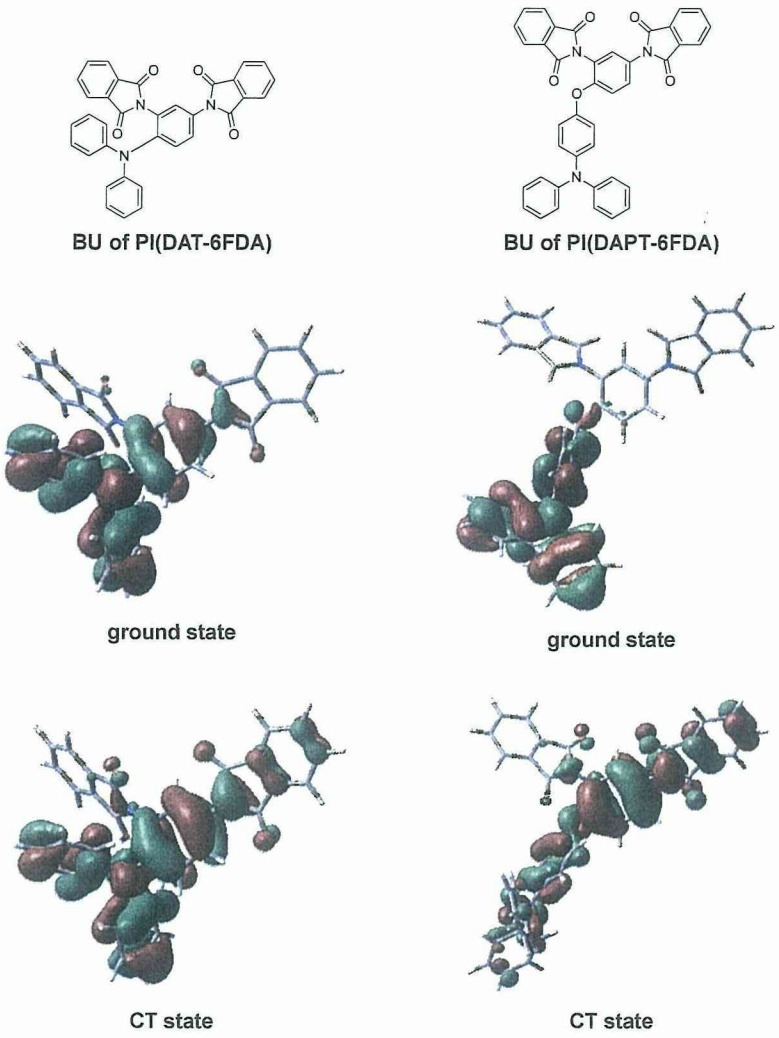

Figure 3-9. Chemical structures and electrostatic potential surface of the BUs of PI(DAT-6FDA) and PI(DAPT-6FDA) in the ground and CT states.

To gain further insight into the memory behavior, specifically the volatility, the structures of the BUs of both PIs were also discussed. Figure 3-10 shows the sketch maps of the optimized structures for the BUs of PI(DAT-6FDA) and PI(DAPT-6FDA) in both ground and CT states. For the case of PI(DAT-6FDA), a slight difference between the conformations of ground and CT states is observed. On the other hand, quite a big difference between the structures of PI(DAPT-6FDA) in the ground and CT states can

be observed. Paying attention to the two benzene rings, one connected to the phthalimide (represented as the blue square in the right side of Figure 3-10) and the other which is a part of triphenylamine D (red square), a large increase in the dihedral angle between these two rings is observed. Surprisingly, the increase in the dihedral angle between these two planes is around 20° which is a similar value to that of previously reported AZTA-PI showing non-volatile characteristic.[9] As have been discussed in chapter 2, a large dihedral angle between the D and A moieties generates an energy barrier to suppress the back CT. Since the back CT is the cause of the dissociation of the CT state, hampering the back CT leads to the revelation of non-volatile behavior. Therefore, following this theory, the results of theoretical calculations are quite reasonable to discuss the difference in volatility of PI(DAT-6FDA) and PI(DAPT-6FDA). As confirmed by the optical properties of both PIs, the conformation of PI(DAT-6FDA) is relatively planar comparing to that of PI(DAPT-6FDA). Since this coplanar structure does not change even in the CT state, the segregated charges in PI(DAT-6FDA) can easily recombine after removing the electrical power supply, resulting in a volatile behavior. Meanwhile, PI(DAPT-6FDA) takes a more twisted conformation comparing to PI(DAT-6FDA), which provides a potential barrier for delaying the back CT.[5-6] Moreover, from the theoretical calculation, a large mutation in the dihedral angle between the D and A units is confirmed after the formation of CT state. This increase in the dihedral angle generates an energy barrier which is large enough to suppress the back CT. As a result, PI(DAPT-6FDA) exhibits non-volatile characteristic.[9-10]

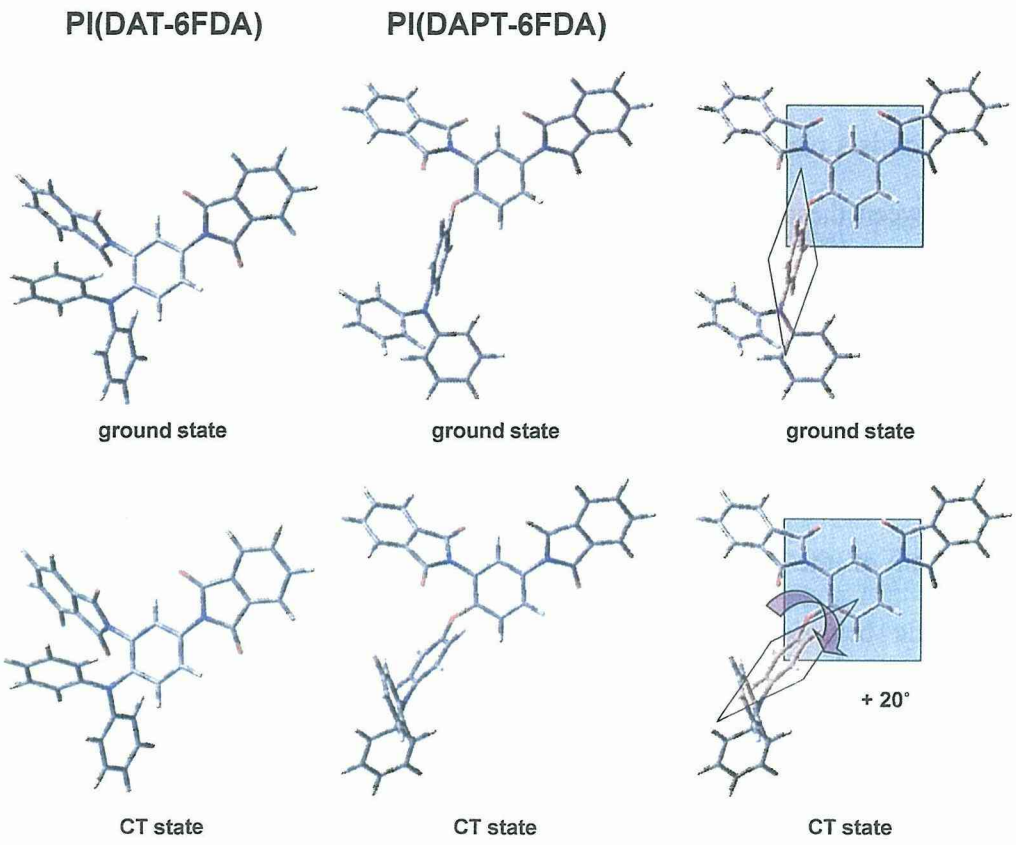

Figure 3-10. Optimized geometry of the BUs of PI(DAT-6FDA) and PI(DAPT-6FDA).

3-3. Conclusion

We have designed and synthesize two PIs, PI(DAT-6FDA) and PI(DAPT-6FDA), for the purpose of clarifying the structural effect on the resulting memory properties and also revealing non-volatile memory characteristic by extending the accomplishment acquired in Chapter 2. Two types of bulky D units were introduced to the ortho position of the benzene ring connected to the phthalimide to induce highly twisted conformation. The memory device based on PI(DAT-6FDA) showed unstable volatile behavior, while the device based on PI(DAPT-6FDA) exhibited a stable non-volatile FLASH type memory characteristic, showing a long retention time over 10^4 s. The theoretical simulation based on DFT suggested that the more distinct charge separation between the

ground and CT states leads to a highly stable memory behavior. Also, on the basis of optical measurement and theoretical analysis, PI(DAPT-6FDA) exhibits a highly twisted conformation comparing to PI(DAT-6FDA) in the ground state and a more twisted dihedral angle between the D and A units is induced in the CT state, leading to a non-volatile memory characteristic. The results provide us the possibility of aiming a specific memory property through structural design of the PI based on a certain concept.

3-4. Experimental section

Materials. The materials were used without further purification unless otherwise noted. Dehydrated DMAc, NMP, dehydrated pyridine, and acetic anhydride were purchased from Wako Pure Chemical Industries, Ltd., Japan. 1-Chloro-2,4-dinitrobenzene and 6FDA were purchased from TCI. 6FDA was purified by sublimation. DAT[13] and *N*-(4-hydroxyphenyl)-*N*,*N*-diphenylamine[14] were synthesized according to the previous reports.

Synthesis of DNPT. A mixture of *N*-(4-hydroxyphenyl)-*N*,*N*-diphenylamine (0.490 g, 1.88 mmol), 1-chloro-2,4-dinitrobenzene (0.381 g, 1.88 mmol), and K_2CO_3 (0.451 g, 3.00 mmol) in dehydrated DMAc (7 mL) was stirred at 90 °C for 24 h. After the reaction, the solution was poured into a large amount of 1M hydrochloric acid solution and the precipitate was collected by filtration. The crude product was purified by recrystallization from a mixture of ethanol and water to give 0.626 g (78% in yield) of a yellow crystal. IR (KBr), ν (cm^{-1}): 1535, 1346 (NO_2 stretching). ^{1}H NMR (300 MHz, DMSO-d_6, δ, ppm, 40 °C): 8.87 (d, J = 2.4 Hz, ArH, 1H), 8.46 (dd, J = 9.3 and 3.0 Hz, ArH, 1H), 7.36-7.27 (m, ArH, 5H), 7.19 (d, J = 9.3 Hz, ArH, 2H), 7.11-7.05 (m, ArH, 8H). ^{13}C NMR (75 MHz, DMSO-d_6, δ, ppm, 40 °C): 156.16, 149.53, 147.97, 146.29, 142.17, 140.17, 130.50, 130.41, 125.96, 124.84, 124.19, 122.63, 122.38, 119.87. *Anal.* Calcd. For $C_{24}H_{17}N_3O_5$: C, 67.4; H, 4.01; N, 9.83. Found: C, 67.4; H, 4.31; N, 9.54.

Synthesis of DAPT. To a solution of DNPT (0.855 g, 2.00 mmol) in DMF (5.0 mL) were added palladium on activated carbon (91.9 mg) and ethanol (5.0 mL). The suspension was stirred at room temperature for 24 h under H_2 atmosphere. Then, the palladium catalyst was removed by filtering through Celite. The filtrate was poured into water and the precipitate was dried under vacuo to obtain 0.674 g of white powder (92%

in yield). The obtained product was used without further purification. IR (KBr), ν (cm^{-1}): 3460, 3379 (N–H stretching). ^1H NMR (300 MHz, DMSO-d_6, δ, ppm, 40 °C): 7.23 (t, J = 8.7 Hz, ArH, 4H), 7.01-6.92 (m, ArH, 8H), 6.83 (d, J = 9.0 Hz, ArH, 2H), 6.56 (d, J = 8.4 Hz, ArH, 1H), 6.06 (d, J = 2.4 Hz, ArH, 1H), 5.85 (dd, J = 8.4 and 2.4 Hz, ArH, 1H), 4.60 (s, N–H, 2H), 4.49 (s, N–H, 2H). ^{13}C NMR (75 MHz, DMSO-d_6, δ, ppm, 40 °C): 156.38, 148.54, 146.93, 141.66, 141.53, 133.48, 130.15, 127.89, 123.30, 122.85, 122.50, 117.62, 104.18, 102.42. *Anal.* Calcd. For $C_{24}H_{23}N_3OCl_2$: C, 65.5; H, 5.26; N, 9.54. Found: C, 65.5; H, 5.58; N, 9.26.

Synthesis of poly[*N*-(2,4-diaminophenyl)-*N*,*N*-diphenylamine-hexafluoroisopropylidenediphthal i-mide] (PI(DAT-6FDA)) 6FDA (0.444 g, 1.00 mmol) was added into a solution of DAT (0.275 g, 1.00 mmol) in dehydrated DMAc (solid contents 15 wt%) under nitrogen. The reaction mixture was stirred at room temperature for 24 h to give a poly(amic acid) (PAA) solution. A reaction mixture of acetic anhydride (1.5 mL) and pyridine (1.5 mL) was added to the above PAA solution. The reaction mixture was stirred at room temperature under a nitrogen atmosphere for 24 h. The resulting solution was poured into methanol, and the precipitate was collected by filtration and washed with methanol. The final product was dried at 200 °C under vacuum for 10 h, and the polymer yield was 97%. The M_n and M_w values estimated from SEC were 1.60×10^4 and 3.60×10^4, respectively, with the polydispersity index (PDI = M_w / M_n) of 2.25. IR (KBr), ν (cm^{-1}): 1786, 1728 (C=O stretching), 1362 (C–N stretching). ^1H NMR (300 MHz, DMSO-d_6, δ, ppm, 40 °C): 8.30-8.13 (m, ArH, 1H), 8.03-7.70 (m, ArH, 4H), 7.70-7.42 (m, ArH, 3H), 7.29 (d, J = 12 Hz, ArH, 1H), 7.18-6.98 (m, ArH, 4H), 6.96-6.78 (m, ArH, 6H). *Anal.* Calcd. For $C_{37}H_{19}N_3O_4F_6$: C, 65.0; H, 2.80; N, 6.15. Found: C, 65.1; H, 3.01; N, 6.32.

Synthesis of poly[*N*-(4-(2',4'-diaminophenoxy)phenyl-*N*,*N*-diphenylamine-hexafluoroisopropylidenediphthali-mide] (PI(DAPT-6FDA)) Using DAPT as a diamine monomer, PI(DAPT-6FDA) was synthesized in a similar procedure to that used for PI(DAT-6FDA). The yield of PI(DAPT-6FDA) was 93%. M_n, M_w, and PDI values of PI-(AAPT-6FDA) were 2.10×10^4, 4.10×10^4, and 1.95, respectively. IR (KBr), ν (cm^{-1}): 1788, 1739 (C=O stretching), 1377 (C–N stretching). ^1H NMR (300 MHz, DMSO-d_6, δ, ppm, 40 °C): 8.23-8.02 (m, ArH, 2H), 8.01-7.72 (m, ArH, 4H), 7.70-7.53 (m, ArH, 2H), 7.32-7.10 (m, ArH, 5H), 7.07-6.82 (m, ArH, 10H). *Anal.* Calcd. For $C_{43}H_{23}N_3O_5F_6$: C, 66.6; H, 2.99; N, 5.42. Found: C, 65.1; H, 3.21; N, 5.26.

Characterization. NMR spectra were recorded on a BRUKER DPX-300S spectrometer at resonant frequencies of 300 MHz for ^1H and 75 MHz for ^{13}C nuclei using $CDCl_3$ or DMSO-d_6 as the solvent and tetramethylsilane as the reference. FT-IR spectra were measured by a Horiba FT-120 Fourier transform spectrophotometer. M_n and M_w values were evaluated by SEC on a JASCO PU-2080 Plus with two polystyrene gel columns (TSK GEKS GMH_{HR}-M). DMF containing 0.01 M LiBr was used as a solvent at a flow rate of 1.0 mL/min calibrated by polystyrene standard samples. The UV-visible optical absorption spectra were recorded on a Hitachi U-3210 spectrophotometer at room temperature. The absorbance of polymer solutions was evaluated in the wavelength range of 280-800 nm. Elemental analyses were performed on a Yanaco MT-6 CHN recorder elemental analysis instrument. Thermal properties were estimated from a Seiko TG/DTA 6300 thermal analysis system and TA instruments DSC-Q100 under a nitrogen atmosphere at a heating rate of 10 and 6 °C/min, respectively. CV was performed at room temperature using a working electrode (ITO,

polymer film area of about 10×30 mm^2), a homemade reference electrode Ag/AgCl, and a counter electrode (Pt wire) at a sweep rate of 0.1 V/s (CHI611B electrochemical analyzer). A 0.1 M solution of TBAP in anhydrous acetonitrile was used as an electrolyte. The thickness of the polymer film was measured with a Microfigure Measuring Instrument (Surfcorder ET3000, Kosaka Laboratory Ltd.).

Fabrication and measurement of the memory device. The memory device was fabricated on the glass substrate, with the configuration of Al/polyimides/Al. Before the fabrication, the glass substrate was precleaned by ultrasonication with water, acetone, and isopropanol each for 15 min. 30 nm thick Al bottom electrode patterns were deposited by a thermal evaporator at a pressure of 10^{-5} Torr with a depositing rate of 1 Å s^{-1}. A 25 mg/mL of well-dissolved PI(AAPT-6FDA) or PI(APT-6FDA) polymer solution in DMAc was first filtered through 0.45 μm pore size of poly(tetrafluoroethylene) (PTFE) membrane syringe filter. Then, the filtered solution was spin-coated onto the bottom Al electrode/glass substrate at a speed rate of 1000 rpm for 60 s and annealed at 150 °C for 30 min under nitrogen. The thickness of the thin film was determined to be around 40-50 nm. Finally, a 30 nm-thick Al top electrode was deposited and patterned by a metal mask with a cross-point device joint area of 0.2×0.2, 0.4×0.4 and 0.6×0.6 mm^2. The electrical characterization of the memory device was performed by a Keithley 4200-SCS semiconductor parameter analyzer (with low noise pre-amplifier) and a probe station at room temperature in a N_2-filled glovebox. The programming pulse signals were generated by a Keithley 4220-PGU pulse generator unit. The bottom electrode was grounded during all the electrical measurement with a swept step of 0.05 V.

Computational methodology. Molecular calculations studied in this work were performed through the Gaussian 03 program package.[16] Equilibrium ground state

geometry and electronic properties were optimized by means of the density functional theory (DFT) method at the B3LYP level of theory (Becke-style three-parameter density functional theory using the Lee–Yang–Parr correlation functional) with the 6-31 G(d) basic set.

3-5. References

1. Ling, Q.-D.; Chang, F.-C.; Song, Y.; Zhu, C.-X.; Liaw, D.-J.; Chan, D. S.-H.; Kang, E.-T.; Neoh, K.-G., *J. Am. Chem. Soc.* **2006,** *128*, 8732-8733.
2. Liu, Y.-L.; Ling, Q.-D.; Kang, E.-T.; Neoh, K.-G.; Liaw, D.-J.; Wang, K.-L.; Liou, W.-T.; Zhu, C.-X.; Chan, D. S.-H., *J. Appl. Phys.* **2009,** *105*, 044501/1-044501/9.
3. Liu, C.-L.; Kurosawa, T.; Yu, A.-D.; Higashihara, T.; Ueda, M.; Chen, W.-C., *J. Phys. Chem. C* **2011,** *115*, 5930-5939.
4. Tian, G.; Wu, D.; Qi, S.; Wu, Z.; Wang, X., *Macromol. Rapid Commun.* **2011,** *32*, 384-389.
5. Kuorosawa, T.; Chueh, C.-C.; Liu, C.-L.; Higashihara, T.; Ueda, M.; Chen, W.-C., *Macromolecules* **2010,** *43*, 1236-1244.
6. Liu, Y.-L.; Wang, K.-L.; Huang, G.-S.; Zhu, C.-X.; Tok, E.-S.; Neoh, K.-G.; Kang, E.-T., *Chem. Mater.* **2009,** *21*, 3391-3399.
7. Liu, Y. W.; Zhang, Y.; Lan, Q.; Liu, S. W.; Qin, Z. X.; Chen, L. H.; Zhao, C. Y.; Chi, Z. G.; Xu, J. R.; Economy, J., *Chem. Mater.* **2012,** *24*, 1212-1222.
8. You, N.-H.; Chueh, C.-C.; Liu, C.-L.; Ueda, M.; Chen, W.-C., *Macromolecules* **2009,** *42*, 4456-4463.
9. Wang, K.-L.; Liu, Y.-L.; Shih, I. H.; Neoh, K.-G.; Kang, E.-T., *J. Polym. Sci., Part A: Polym. Chem.* **2010,** *48*, 5790-5800.
10. Wang, K.-L.; Liu, Y.-L.; Lee, J.-W.; Neoh, K.-G.; Kang, E.-T., *Macromolecules* **2010,** *43*, 7159-7164.
11. Ling, Q.-D.; Liaw, D.-J.; Teo, E. Y.-H.; Zhu, C.; Chan, D. S.-H.; Kang, E.-T.; Neoh, K.-G., *Polymer* **2007,** *48*, 5182-5201.
12. Ling, Q.-D.; Liaw, D.-J.; Zhu, C.; Chan, D. S.-H.; Kang, E.-T.; Neoh, K.-G., *Prog. Polym. Sci.* **2008,** *33*, 917-978.
13. Hsiao, S.-H.; Chen, C.-W.; Liou, G.-S., *J. Polym. Sci., Part A: Polym. Chem.* **2004,** *42*, 3302-3313.
14. El-Khouly, M. E.; Shim, S. H.; Araki, Y.; Ito, O.; Kay, K.-Y., *J. Phys. Chem. B* **2008,** *112*, 3910-3917.
15. Bredas, J. L.; Silbey, R.; Boudreaux, D. S.; Chance, R. R., *J. Am. Chem. Soc.* **1983,** *105*, 6555-6559.
16. Frisch, M. J. T., G. W.; Schlegel, H. B.; Scuseria, G. E.; Robb, M. A.; Cheeseman, J. R.; Montgomery, Jr., J. A.; Vreven, T.; Kudin, K. N.; Burant, J. C.; Millam, J. M.; Iyengar, S. S.; Tomasi, J.; Barone, V.; Mennucci, B.; Cossi, M.; Scalmani, G.; Rega, N.; Petersson, G. A.; Nakatsuji, H.; Hada, M.; Ehara,

M.; Toyota, K.; Fukuda, R.; Hasegawa, J.; Ishida, M.; Nakajima, T.; Honda, Y.; Kitao, O.; Nakai, H.; Klene, M.; Li, X.; Knox, J. E.; Hratchian, H. P.; Cross, J. B.; Bakken, V.; Adamo, C.; Jaramillo, J.; Gomperts, R.; Stratmann, R. E.; Yazyev, O.; Austin, A. J.; Cammi, R.; Pomelli, C.; Ochterski, J. W.; Ayala, P. Y.; Morokuma, K.; Voth, G. A.; Salvador, P.; Dannenberg, J. J.; Zakrzewski, V. G.; Dapprich, S.; Daniels, A. D.; Strain, M. C.; Farkas, O.; Malick, D. K.; Rabuck, A. D.; Raghavachari, K.; Foresman, J. B.; Ortiz, J. V.; Cui, Q.; Baboul, A. G.; Clifford, S.; Cioslowski, J.; Stefanov, B. B.; Liu, G.; Liashenko, A.; Piskorz, P.; Komaromi, I.; Martin, R. L.; Fox, D. J.; Keith, T.; Al-Laham, M. A.; Peng, C. Y.; Nanayakkara, A.; Challacombe, M.; Gill, P. M. W.; Johnson, B.; Chen, W.; Wong, M. W.; Gonzalez, C.; and Pople, J. A., *Gaussian, Inc., Wallingford CT* **2004**.

Chapter 4. Influence of the Acceptor Conjugation Length and Composition in the Electrical Memory Characteristics of Random Copolyimides

ASBSTRACT: Three series of random copolyimides (coPIs), PI-PTCDIX, PI-NTCDIX, and PI-BTCDIX that contains perylene diimide (PTCDI), naphthalene diimide (NTCDI), and benzene diimide (BTCDI), respectively, were designed and synthesized with the view of modulating the volatility and clarifying the effects of the acceptor (A) ring conjugation length on the resulting memory properties. The memory devices based on these coPIs exhibited distinct switching characteristics which were found to be varied continuously with copolymer composition. The theoretical simulation suggested that the CT mechanism could be used to explain the memory behavior. Also, comparative studies of the energy levels of the components revealed that the stable CT complex was obtained through stabilization of the radical anion by means of long conjugation and high electron affinity of the A moieties, leading to non-volatile memory characteristics.

4-1. Introduction

Despite the fact that polyimides (PIs) showing specific memory properties are extensively reported,[1-12] the relationship between the PIs structure and its memory characteristics still remains unclear.[11-12] In particular, clarifying the effect of PIs structure on the volatility is a subject of utmost importance in the development of PI memory devices. In chapter 3, extending the concept of chapter 2, we have successfully developed a non-volatile memory characteristic by increasing the dihedral angle between the electron donor (D) and electron acceptor (A) units to suppress the back charge transfer (CT) and to stabilize the CT state. However, based on this concept, the design of PI structure for further development is quite difficult. One reason for this difficulty is that the large steric hindrance to induce large torsional angle simultaneously prohibits the reactivity of the monomer, which makes it difficult to obtain a high molecular weight polymer. Another reason is that the increase in dihedral angle depends strongly on the inherent structure and it cannot be predicted. Therefore, it would be significant to establish a more simple and versatile guideline for controlling the volatility through the design of PIs structure.

Meanwhile, a variety of perylene and naphthalene diimide derivatives are well known for their excellent n-type semiconducting properties originating from the large conjugation and high electron affinity of the core arene unit.[13] When these diimides are introduced as an A in the donor-acceptor (D-A) polymers, such distinctive natures of the diimides are effective to the stabilization of radical anion induced by the CT from D to A, resulting in a stable CT state. On the other hand, pyromellitic dimide does not possess a large conjugation and is rarely employed as carrier transporting materials. However, relatively high organic field effect transistor electron mobility (approaching

0.4 $cm^2V^{-1}s^{-1}$) of pyromellitic diimide was reported,[13-14] indicating its potential of stabilizing the radical species in the CT state. As have always been discussed for memory properties, the key factor to determine the volatility is the stability of the CT state. Therefore, introducing these diimides in the polymer structure could induce non-volatile memory by stabilizing the radical anions in the CT complex. Also, it might be possible to control the volatility by changing the content of the diimides.

In this chapter, the synthesis and memory properties on three series of random copolyimides (coPIs), PI-PTCDIX, PI-NTCDIX, and PI-BTCDIX, with different compositions of *N,N*-bis(4-aminophenyl)-*p*-toluidine (AMTPA), 4,4'-(hexafluoroisopropylidene)diphthalic anhydride (6FDA), and *N,N'*-bis(4-aminophenyl)-3,4,9,10-perylenetetracarboxydiimide (PTCDI), *N,N'*-bis-(4-aminophenyl)-1,4,5,8-naphthalenetetracarboxydiimide (NTCDI), or *N,N'*-bis-(4-aminophenyl)-1,2,4,5-benzenetetracarboxydiimide (BTCDI) shown in Scheme 4-1, where X is the molar content of the repeating unit containing PTCDI, NTCDI, or BTCDI, are reported. They were designed for the purpose of controlling the volatility and revealing non-volatile memory characteristics by introducing the varied ratio of diimide comonomers described above. Also, the ring size effect of the diimide moiety (PTCDI > NTCDI > BTCDI) on the electrical memory characteristics were explored.

4-2. Results and discussion

4-2-1. Synthesis and characterization of coPIs

The general synthetic strategy is shown in Scheme 4-1. The coPIs (PI-PTCDIX, PI-NTCDIX, and PI-BTCDIX) were synthesized by a two-step polycondensation of aromatic dianhydride (6FDA) with aromatic diamines (AMTPA and PTCD, NTCDI, or BTCDI), followed by chemical imidization using pyridine and acetic anhydride. The syntheses of PI-PTCDIX and PINTCDIX were carried out in *m*-cresol, which was well known as a good solvent for perylene and naphthalene diimide system. The feed molar ratios of PTCDI or NTCDI to AMTP were set to be 1, 2.5, 5, and 10%. Meanwhile, the synthesis of PI-BTCDIX was carried out in *N*-methylpyrrolidone (NMP). Different to the synthetic procedure of PI-PTCDIX or PI-NTCDIX, due to its extremely low solubility, BTCDI had to be dissolved in a large amount of NMP in the first place to obtain a sufficient molecular weight polymer.[15] The feed molar ratios of BTCDI to AMTPA were also set to be 1, 2.5, 5, and 10%.

Scheme 4-1. Synthesis of PI-PTCDIX, PI-NTCDIX, and PI-BTCDIX.

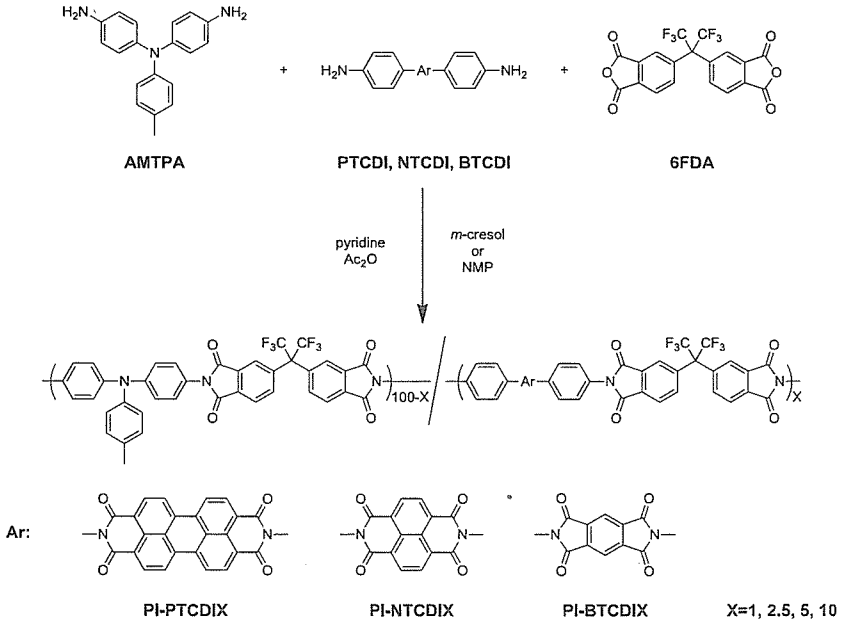

The chemical imidization were characterized by FT-IR spectra. All the coPIs exhibited similar FT-IR absorption peaks originated from the imide moieties located at 1780 cm^{-1} (ν_s, C=O), 1720 cm^{-1} (ν_{as}, C=O), and 1370 cm^{-1} (ν, C–N) as presented in Figure 4-1. The characteristic peaks at 1650 cm^{-1}, originating from the asymmetric vibration of the carbonyl groups in perylene and naphthalene diimide, are also observed in all FT-IR spectra, indicated by arrows in Figure 4-1a and Figure 4-1b. The intensity of these peaks gradually increase as the X values increase from 1 to 10, which are consistent with the molar composition of the PTCDI or NTCDI unit in each coPIs.

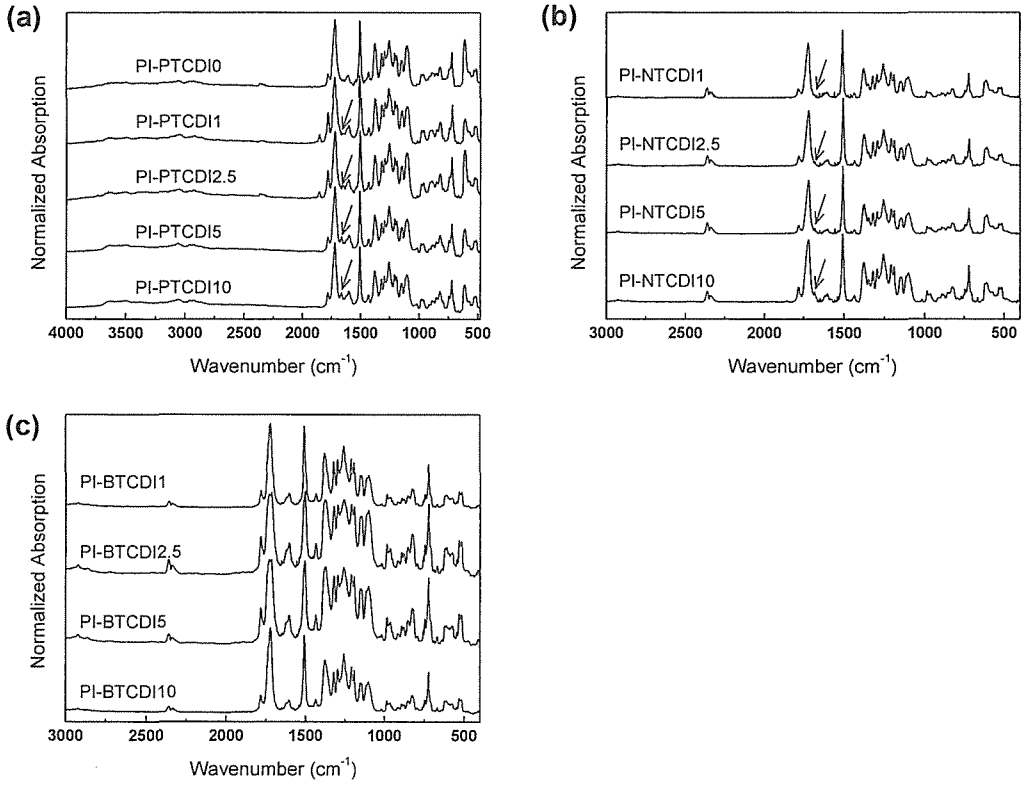

Figure 4-1. IR spectra of (a) PI-PTCDIX, (b) PI-NTCDIX, and (c) PI-BTCDIX

The structures of the coPIs were also characterized by ^1H NMR, as shown in Figure 4-2. The characteristic signals for perylene units of PI-PTCDIX are observed but very

broadly in the range of 7.0–8.4 ppm. Thus, the structure determination and molar composition of PTCDI in PI-PTCDIX are performed by comparing the integral values of the whole ArH spectra (#1–7 and #1'–7' in Figure 4-2a) with the $ArCH_3$ (#8) of AMTPA unit. When the integral value of $ArCH_3$ signal is set to be 3, the observed integral values of ArH signals of PI-PTCDI1, PI-PTCDI2.5, PI-PTCDI5, and PI-PTCDI10 are 18.2, 18.8, 19.3, and 20.5, respectively, which are in good agreement with those calculated values of 18.2, 18.6, 19.2, and 20.4, respectively. Similar to PI-PTCDIX, the characteristic signals for NTCDI and BTCDI containing units of PI-NTCDIX and PI-BTCDI, respectively, are observed very broadly in the range of 7.50–8.80 and 7.50–8.50 ppm, respectively, in the ^1H NMR spectra (Figure 4-2b and c). Thus the molar composition of NTCDI and BTCDI in PI-NTCDIX and PI-BTCDI, respectively, are also confirmed by comparing the integral values of the whole ArH spectra (#1–7 and #1'–6') with the $ArCH_3$ signal (#8) of the AMTPA unit. Also, all the expected structures of coPIs were confirmed by elemental analysis. The results suggest that the molar ratios of PTCDI, NTCDI, or BTCDI to AMTP in PI-PTCDIX, PI-NTCDIX, or PI-BTCDIX, respectively, are close to the original relative feeding ratios of monomer.

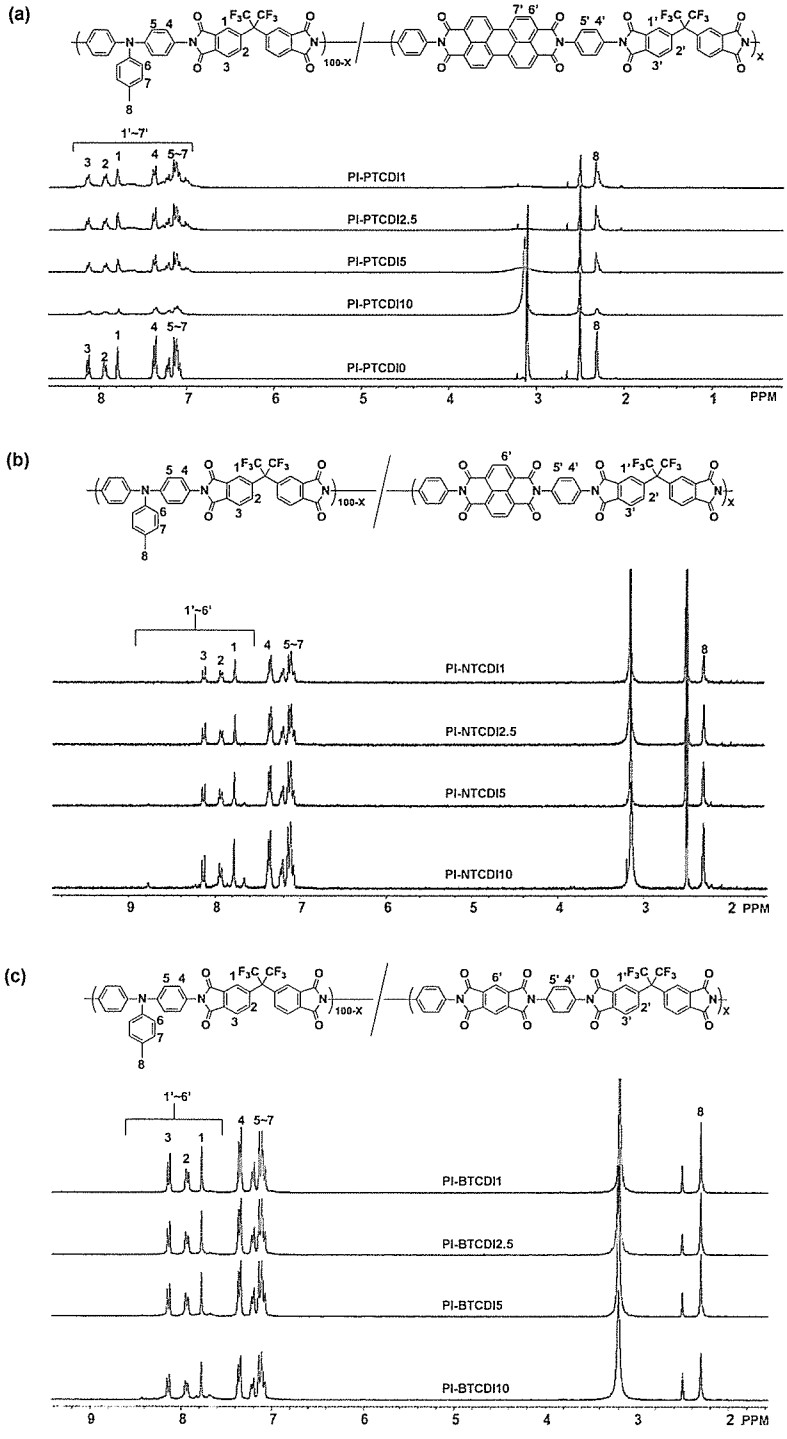

Figure 4-2. ^{1}H NMR spectra of (a) PI-PBIX, (b) PI-NTCDIX, and (c) PI-BTCDIX.

In addition, all the coPIs showed high number average molecular weights (M_ns) over 18 kDa (Table 4-1) and were readily soluble in common organic solvents such as *N*,*N*-dimethylacetamide (DMAc), dimethyl sulfoxide (DMSO), and NMP. The thermal properties of the coPIs were evaluated by thermo gravimetric analysis (TGA) and differential scanning calorimetry (DSC) as summarized in Table 4-1. All the coPIs possess high thermal stabilities with a high decomposition temperature (T_d) over 500 °C and glass transition temperature (T_g) not being observed below 300 °C. The excellent thermal properties of the coPIs are expected to meet the requirement of high heat resistance in electronic industry.

Table 4-1. Molecular weights and physical properties of the prepared coPIs.

coPIs	M_n (g/mol)[a]	M_w (g/mol)[a]	PDI[a]	T_d (°C)[b]	T_g (°C)[c]	E_g^{opt} (eV)[d]	HOMO (eV)[e]	LUMO (eV)[f]
PI-PTCDI0	43,000	112,000	2.60	515	—	3.14	-5.31	-2.17
PI-PTCDI1	19,000	42,000	2.21	507	—	3.14	-5.31	-2.17
PI-PTCDI2.5	19,000	42,000	2.21	508	—	3.14	-5.31	-2.17
PI-PTCDI5	18,000	36,000	2.00	510	—	3.14	-5.31	-2.17
PI-PTCDI10	32,000	67,000	2.09	496	—	2.05	-5.31	-3.26
PI-NTCDI1	38,000	70,000	1.84	515	—	3.14	-5.28	-2.14
PI-NTCDI2.5	33,000	64,000	1.94	514	—	3.14	-5.28	-2.14
PI-NTCDI5	28,000	63,000	2.25	517	—	3.14	-5.28	-2.14
PI-NTCDI10	24,000	53,000	2.21	516	—	3.14	-5.28	-2.14
PI-BTCDI1	53,000	118,000	2.23	521	—	3.14	-5.26	-2.12
PI-BTCDI2.5	50,000	106,000	2.12	525	—	3.14	-5.26	-2.12
PI-BTCDI5	49,000	108,000	2.2	525	—	3.14	-5.26	-2.12
PI-BTCDI10	40,000	87,000	2.18	524	—	3.14	-5.26	-2.12

[a]Determined by SEC. [b]Determined by TGA measurement. The values indicate the 5% weight loss temperature. [c]Determined by DSC measurement. The measurement was carried out in the range of -10-300 °C. [d]Estimated from the UV absorption spectra. [e]Estimated from CV. [f]LUMO = HOMO + band gap.

4-2-2. Optical and electrochemical properties

The UV-vis absorption spectra of the studied coPIs on thin films are shown in Figure 4-3. The maximum absorption wavelength (λ_{max}) of both coPIs are observed around 300 nm attribute to the π–π^* transition along the main chain. On the other hand, the shoulder like absorption peak around 350 nm in the solution state (data not shown) changes to a clear absorption peak, indicating that this peak originates from the intermolecular π–π or CT interaction. For the case of PI-PTCDI10, one additional broad low energy optical absorption (peak at 497 and 544 nm shown in Figure 4-3a) is observed. It is well known that PTCDI has a strong π–stacking ability due to its extended π conjugation and coplanar structure.[16] Therefore, the additional absorption in the low energy region only observed in PI-PTCDI10 corresponds to the existence of PTCDI fragments induced from this stacking behavior. The band gaps (E_g^{opt}s) of the coPIs estimated from the onset of the film state absorption spectra are also summarized in Table 4-1. As can be seen, except for PI-PTCDI10, all the E_g^{opt} values were the same regardless of the content of PTCDI, NTCDI, or BTCDI unit. This indicates that the introduction of a very small amount of diimides does not change the energy level values of the coPIs.

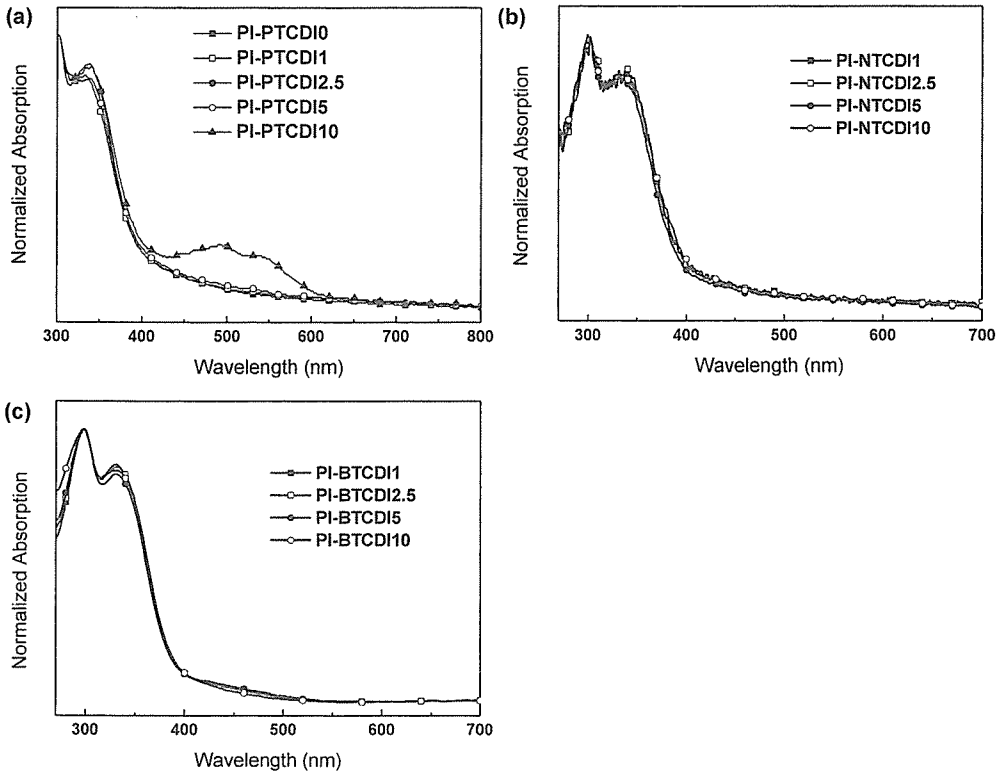

Figure 4-3. UV-vis absorption spectra of (a) PI-PTCDIX, (b) PI-NTCDIX, and (c) PI-BTCDIX.

The highest occupied molecular orbital (HOMO) energy levels of the coPIs were calculated from the results of cyclic voltammetry (CV) measurement with reference to ferrocence by the following equation: HOMO = $-(E_{onset}^{ox}+4.8-E_{ferrocene})$,[17] as summarized in Table 4-1. Note that the E_{onset}^{ox} is the onset oxidation value and $E_{ferrocene}$ is the potential of the external standard, the ferrocene/ferrocenium ion couple, which value was 0.44 V. In addition, the LUMO energy levels of the coPIs estimated from the difference between the E_g^{opt}s and HOMO energy levels are also summarized in Table 4-1. Similar to the tendency of E_g^{opt} values, all the energy levels were comparable apart from the existing amount of the diimide fragments.

4-2-3. Memory device characteristics of the coPIs

The effects of relative AMTPA/PTCDI, NTCDI, and BTCDI composition in random coPIs on memory device performance were systematically investigated. The memory behaviors of the coPIs were tested by the current-voltage (*I-V*) characteristics of indium tin oxide (ITO)/polymer/Al cross-point structured devices. ITO was used as the anode, and Al was set as cathode (maintained as common) in all electrical measurements. Representative *I-V* curve for memory device based on PI-PTCDI0 is shown in Figure 4-4a. Starting with low-conductivity OFF state of as-fabricated device, the current increases slowly in the range of 10^{-13}–10^{-11} A with the applied negative voltage. The current remaines low until the threshold voltage of about −2.8 V. When the voltage is increased further, the current increases abruptly from 10^{-11} to 10^{-5} A (sweep 1), thus indicating electronic transition to high-conductivity ON state that can serve as the "writing" process. A distinct hysteresis is observed in the bistable PI–PTCDI0 device with an ON/OFF current ratio up to 10^{6}. The ON state could be kept during a subsequent sweep from 0 to −8 V (sweep 2). After reading the ON state in the negative sweep and turning off the power for less than 1 min, the device can be conducted to reprogram from OFF state to ON state again with a negative biased sweep (sweep 3) and remains in the ON state (sweep 4). The PI–PTCDI0 memory device exhibits repeated operation from the sweep 5 and sweep 6, and the ON state cannot be maintained after the removal of power and would immediately relax back to the OFF state. The electrical switching behavior concludes that the PI–PTCDI0 memory device exhibits the volatile dynamic random access memory (DRAM) property because the stored data is instantly lost without the power supply.

The memory properties of PI-PTCDIX (X > 1) continuously shifted in accordance

with increasing the molar ratio of the PTCDI unit (Figure 4-4b-d). Similar to PT-PTCDI0, PI-PTCDI1 exhibits the volatile DRAM characteristic (Figure 4-4b). Meanwhile, the memory property of PI-PTCDI2.5 is somewhat different. As shown in Figure 4-4c, similar electric transition is observed during the initial sweep, and the switched ON state can be maintained during the subsequent 2nd sweep. The difference between PI-PTCDI1 and PI-PTCDI2.5 was the retainability of the ON state. As can be seen in the 3rd voltage sweep from 0 to -8 V, after turning off the power supply for about 4 min, the ON state of the device based on PI-PTCDI2.5 can still be sustained, indicating a relatively non-volatile behavior to PI-PTCDI1. However, after removing the power for a longer time, the device eventually returns to the initial OFF state, which can be determined as a volatile characteristic. As a result, the memory property of PI-PTCDI2.5 can be concluded to be a static random access memory (SRAM) type due to its "remnant", yet volatile behavior. Further increasing fraction in the PTCDI moieties, PI–PTCDI5 exhibits the typical write once read many (WORM) type memory effect. The device based on PI–PTCDI5 was scanned through five voltage sequences: 0 to −8.0 V (for sweep 1 to 4) and 0 to 8.0 V (sweep 5) in steps of 0.1 V, as shown in Figure 4-4d. Initially, this device is in the OFF state, the current increases rapidly 6 orders of magnitude at −2.9 V, and it changes to the ON state. The device does not return to the OFF state even after removing the power supply for a long period of time (*e.g.*, longer than 1 h; sweep 2). The ON state can be retained permanently in the subsequent voltage sweeps (sweeps 3 and 4) and also during the voltage sweep to the reverse direction (sweep 5). This means that the PI–PTCDI5 thin film sandwiched between ITO and Al electrodes exhibited single resistive switch. The PI–PTCDI10 device with more PTCDI units also showed the irreversible WORM memory

performance, as shown in Figure 4-4e. A remarkable current hysteresis was observed at one-direction resistive switching from OFF to ON state.

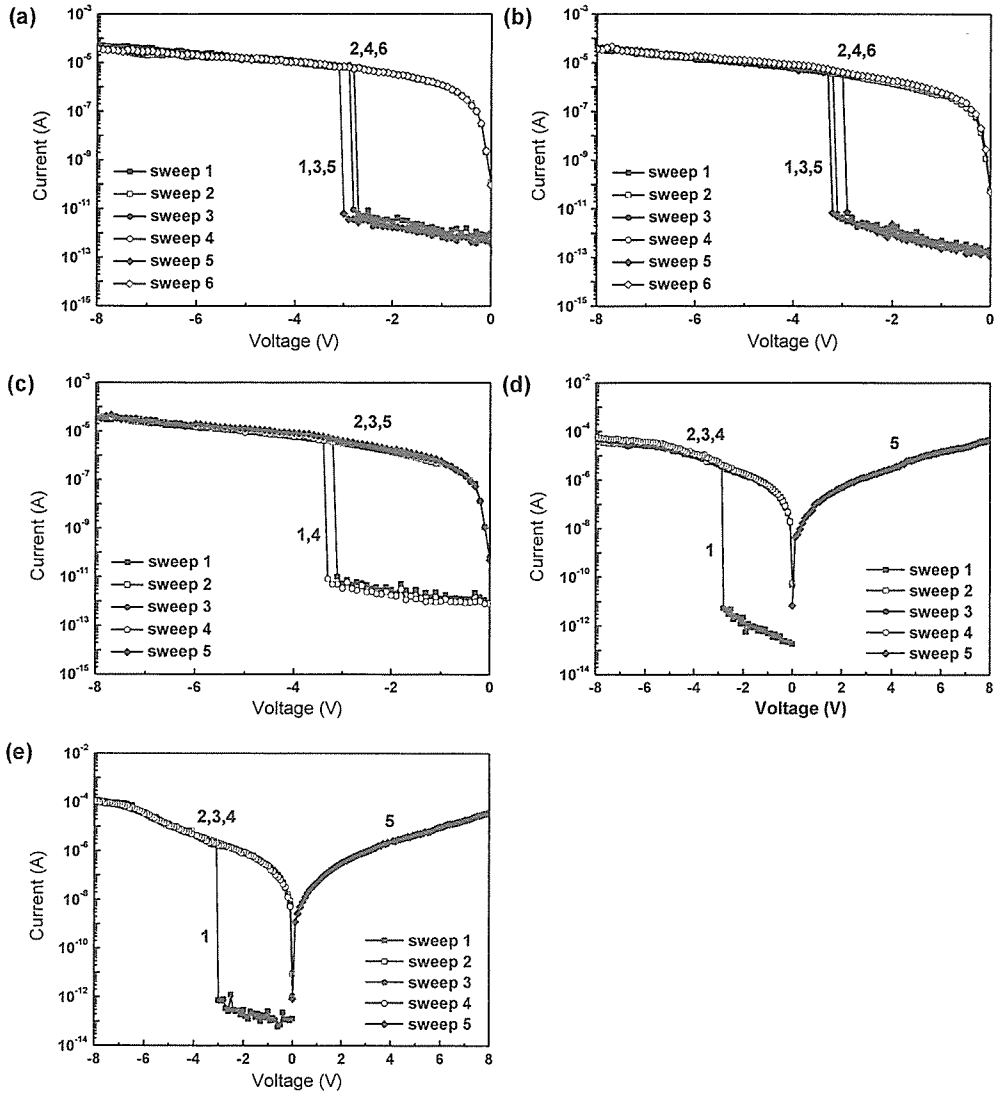

Figure 4-4. *I-V* characteristics of (a) PI-PTCDI0, (b) PI-PTCDI1, (c) PI-PTCDI2.5, (d) PI-PTCDI5, and (e) PI-PTCDI10.

Similar trend of the transition of memory properties to PI-PTCDIX is observed in the PI-NTCDIX system. Figure 4-5a shows the typical *I-V* characteristics of the memory devices fabricated with PI-NTCDI1. During the voltage sweep from 0 to -2.9 V, the

device is initially in the OFF state with a current value in the range of 10^{-9}–10^{-15} A. When the applied voltage is increased further, an abrupt jump in the current value occurs at a threshold voltage of about -3.0 V, indicating the transition from low-conductive OFF state to the high-conductive ON state. This electronic transition in the 1st sweep serves as the "writing" process of the current memory device. The electrical switching of PI-NTCDI1 device showes the distinctly bistable conductance state with the ON/OFF current ratio up to 10^6 at -1 V. In the 2nd sweep from 0 to -5.0 V, the memory device is kept in the ON state. The 3rd sweep was conducted after turning off the power for about 4 min. The device can be reprogrammed, starting from the OFF state, to the ON state again with an accurate threshold voltage of -2.8 V and remained in the ON state during the subsequent 4th sweep. This electrical switching concludes that the PI-NTCDI1 memory device exhibits the volatile nature of a DRAM (similar to PI-PTCDI1). Unlike PI-NTCDI1, PI-NTCDI5 with a higher NTCDI composition exhibits non-volatile memory characteristic as described below (Figure 4-5c). The device based on PI-NTCDI5 thin films are scanned through five voltage sequences: 0 to -5.0 V (sweep 1), 0 to -5.0 V (sweep 2), 0 to -5.0 V (sweep 3), 0 to -5.0 V (sweep 4), and 0 to 5.0 V (sweep 5) in steps of 0.1 V. During the 1st sweep (0 to -2.4 V), the current value initially remains at the low conductive OFF state. Further increasing the applied voltage, the current value abruptly increases several orders of magnitude at the threshold voltage of -2.5 V and changes to a high conductive state, indicating the transition from the OFF state to the ON state. The current value remains at the ON state during the subsequent negative sweep from 0 to -5.0 V (sweep 2-4) and positive sweep from 0 to 5.0 V (sweep 5). This means that the memory device based on PI-NTCDI5 does not return to the OFF state even after turning off the power for a long period of

time or applying a reverse bias, suggesting the WORM memory behavior with a high observed ON/OFF current ratio of 10^5 at -1 V (similar to PI-PTCDI5). Also, as shown in Figure 4-5d, the device based on PI-NTCDI10 (containing 10 mol% of NTCDI unit) also showes similar non-volatile WORM memory characteristics (similar to PI-PTCDI10). Meanwhile, the electrical behavior of the device based on PI-NTCDI2.5 is quite peculiar (Figure 4-5b). During the 1^{st} and 2^{nd} voltage sweeps, PI-NTCDI2.5 shows a similar switching behavior to PI-NTCDI1, PI-NTCDI5, and PI-NTCDI10. However, after turning off the power for about 8 min, the device transits to a medium conductive state which is different from PI-NTCDI1 or PI-NTCDI5 and PI-NTCDI10 (the 4^{th} sweep in Figure 4-5b). Further continuing the voltage sweep, the device transits to the ON state again and did not return to the initial state even after removing the applied voltage for a long period of time or by applying a reverse bias (the 5^{th} and 6^{th} sweeps in Figure 4-5b). This means that the device based on PI-NTCDI2.5 first shows a volatile memory property but eventually behaves as non-volatile memory, indicating a transition from SRAM type to WORM type memory.

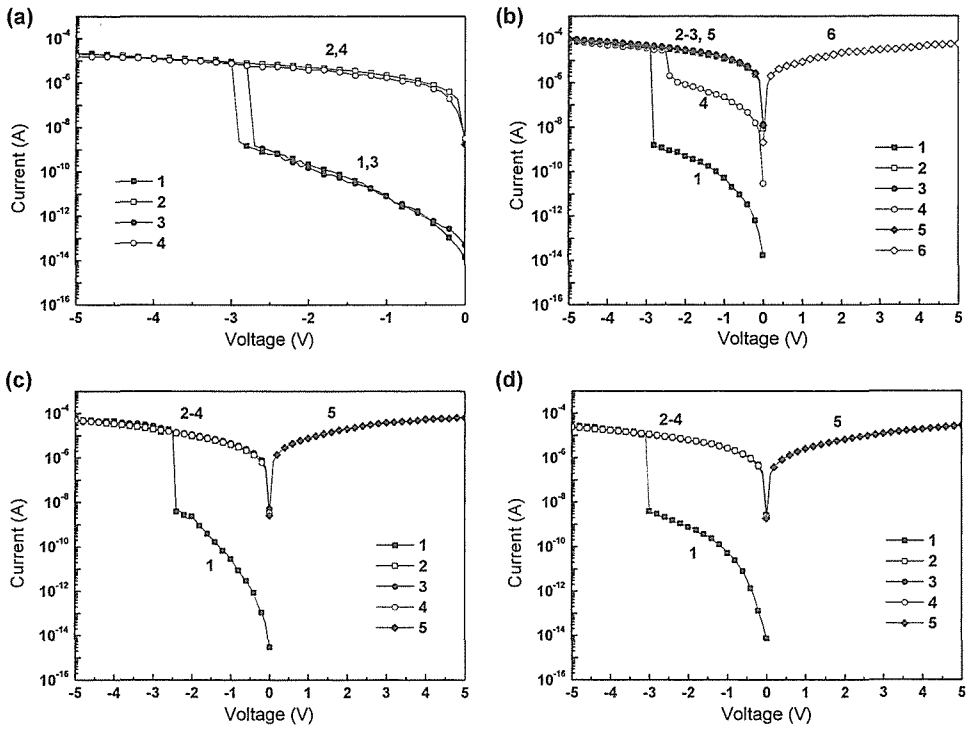

Figure 4-5. *I-V* characteristics of (a) PI-NTCDI1, (b) PI-NTCDI2.5, (c) PI-NTCDI5, and (d) PI-NTCDI10.

As have been discussed, the transition of the memory properties from volatile one to non-volatile one observed in the PI-NTCDIX system was similar to those of PI-PTCDIX system. However, the memory properties of PI-BTCDIX were rather unique to the other coPIs. The memory device based on PI-BTCDI1 and PI-BTCDI2.5 exhibits the DRAM memory behaviors similar to PI-PTCDI1 and PI-NTCDI1 devices (Figure 4-6a and b). Interestingly, further increasing the BTCDI content, PI-BTCDI5 always shows the low-conductive (OFF) state during the positive and negative scan and no switching behavior is observed (Figure 4-6c). Thus, PI-BTCDI5 had no memory characteristic but only shows an insulator behavior. This is also the case with PI-BTCDI10 (Figure 4-6d).

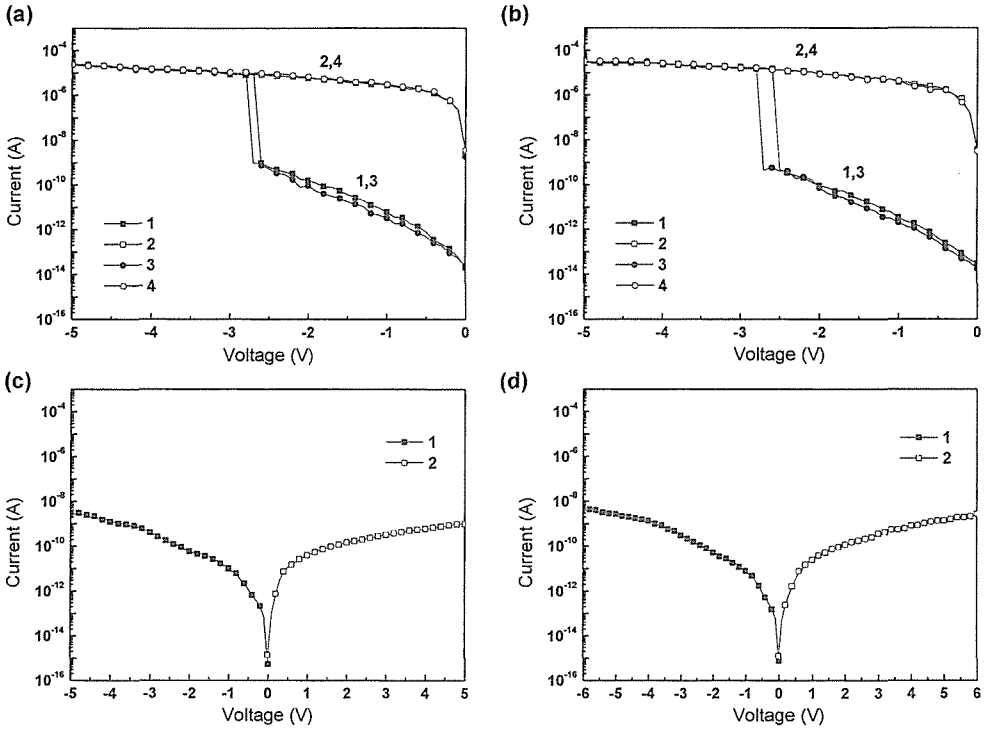

Figure 4-6. *I-V* characteristics of (a) PI-BTCDI1, (b) PI-BTCDI2.5, (c) PI-BTCDI5, and (d) PI-BTCDI10.

The long-term and stimulus stability of the memory effect of all the coPIs were also evaluated under the same condition. Figure 4-7a shows the representative retention times and stress tests of both the ON and OFF states using the device based on PI-PTCDI2.5. Initially, the memory device switches to a high conductivity state. The ON state can be maintained without obvious degradation for at least 10^4 s under a constant stress of -1 V. Then, the device is set back to the OFF state, it is persisted for the whole readout test period, and the ON/OFF current ratio is kept around 10^6. Figure 4-7b shows the cycles of a pulse voltage stress with a pulse width of 1 μs without significant change in ON and OFF states current for at least 10^8 continuous read pulses of -1 V. For the case of other coPIs showing electronic switching behavior, such as other

PI-PTCDIX series, PI-NTCDIX series, PI-BTCDI1, and PI-BTCDI2.5, all memory properties showed extremely high endurance during the long term operation tests as discussed above without exception.

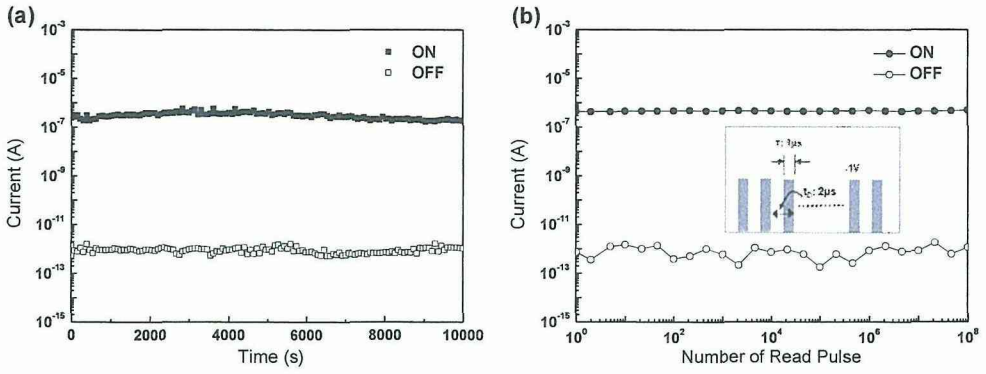

Figure 4-7. (a) Retention times on the ON and OFF states under a continuous readout voltage and (b) stimulus effect of read pulses on the ON and OFF states of the PI-PTCDI2.5 device. The inset of (b) shows the pulse shapes in the measurement.

4-2-4. Theoretical analysis and switching mechanism

To further investigate the switching mechanism, the electronic properties were studied by density functional theory and *I-V* characteristics of both ON and OFF states were analyzed. Calculations of the optimized geometry and molecular orbitals of the basic unit (BU) were carried out at the B3LYP/6-31G(d) level with the Gaussian 03 program package.[18] The mechanism of PI–PTCDI0 of electronic transition can be explained from electric field induced CT between the AMTPA (D) and 6FDA (A).[1-12] Similar molecular simulation of the BU of PI–PTCDI0 was demonstrated (Figure 4-8) relative to the TP6F–PI (without methyl group attached on the triphenylamine) proposed by Kang's group.[3] The relative ordering of the occupied and virtual molecular orbitals give a reasonable indication of the excited properties (from overlapping of the HOMO and third LUMO (LUMO+2)) and charge transport ability. The HOMO and

LUMO+2 orbitals are localized at the D while LUMO and LUMO+1 orbitals are located at A which implies that CT can occur to form a conductive channel through the process either indirectly from the LUMO+2 of D to the LUMO+1 and then to the LUMO of A (process 1-3 in Figure 4-8) or directly from the HOMO of D to the LUMO of A (process 1' in Figure 4-8).[3] The unstable CT state contributes to the charge recombination, and the device rapidly returns to the original OFF state due to the limited delocalization of AMTPA moieties.

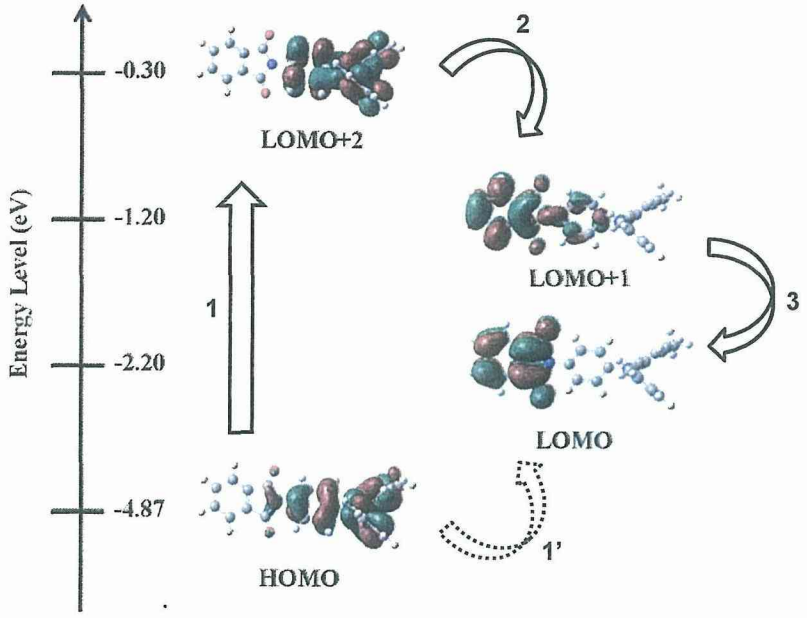

Figure 4-8. Optimized geometries and electronic density counters of molecular orbitals of PI-PTCDI0 basic units.

Figure 4-9 shows the I–V curves of PI–PTCDI5 device for OFF state, and the conduction states are well characterized by ohmic conduction relationship ($I \sim V$) and trap-limited space-charge-limited current (SCLC; $I \sim V^{m+1}$ ($m > 1$))[19-20] in the range of 0 to −1.7 V and −1.7 to −2.8 V, respectively, indicating that the carriers overcome the energy barrier and flow through the device by Ohmic conduction and trap-free SCLC

process sequentially at the higher bias. The power-law region indicates that the switching is triggered by carrier injection and hopping processes between the PIs chains. When the applied voltage exceeds the threshold value, the numerous generated charges and charge-transfer process rapidly yield a conducting path. As shown in inset of Figure 4-9, the obtained slope in a plot of $\log(I/V)$ vs $V^{1/2}$ of ON state is nearly equal to one. It indicates that the Poole–Frenkel (PF) emission is dominant in the ON state, reflecting the change in the conducting process at this stage.[21]

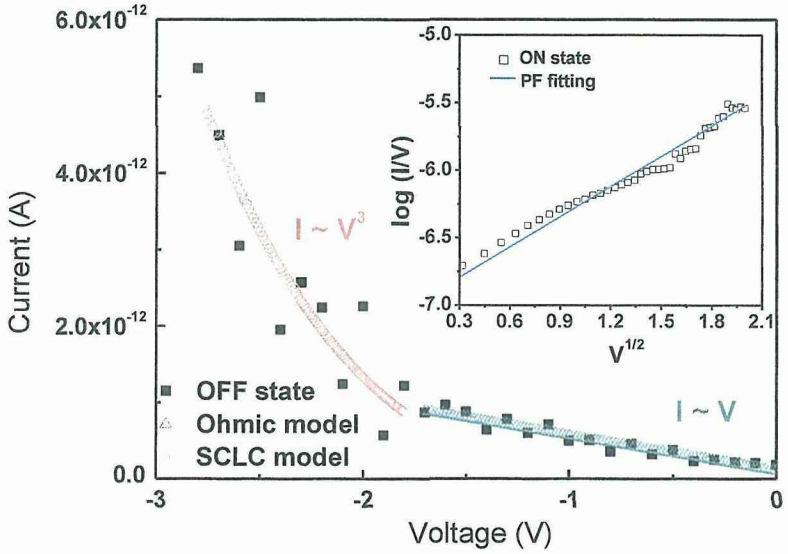

Figure 4-9. Experimental and fitted I-V characteristics of the PI-PTCDI5 memory device in the OFF and ON states.

Next, in order to understand the effect of the A moieties (PTCDI, NTCDI, and BTCDI) on the resulted memory behaviors, comparative studies of the energy levels of the components such as AMTPA, PTCDI, NTCDI, BTCDI, and 6FDA were carried out. The energy levels of AMTPA, PTCDI, NTCDI, BTCDI, and 6FDA were estimated by measuring the CV curves and UV-vis absorption spectra of model compounds shown in Figure 4-10.

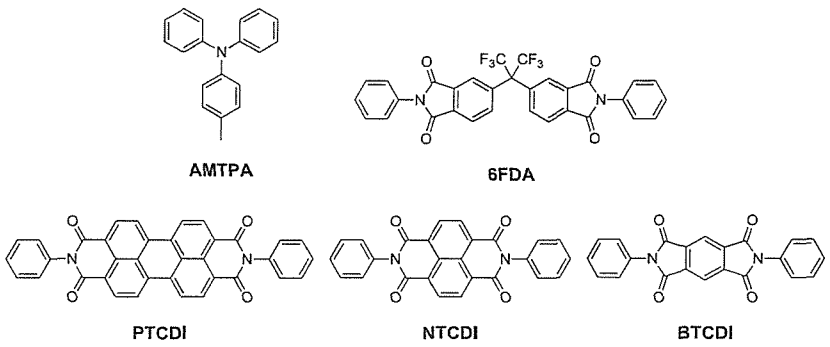

Figure 4-10. Chemical structures of the prepared model compounds.

All the results are summarized in Figure 4-11 and the switching mechanism can be described as the following. By applying an electric field, electron transfer from the HOMO of AMTPA to the LUMO of 6FDA is facilitated and forms a conductive CT state. Consequently, radical cation and anion are generated at AMTPA and 6FDA, respectively. The segregated radical species can localize at AMTPA and 6FDA units under an electric field. However, in the absence of NTCDI or PBI, the CT state dissociates after removing the applied electric field due to the recombination of the radical species. It is probably attributed to the short conjugation of AMTPA or 6FDA and low electron affinity of the 6FDA moiety (i.e. the LUMO energy level of 6FDA is high). By incorporating 5% or 10% of PTCDI or NTCDI moiety, the radical anion locating at the 6FDA unit transits to the PTCDI or NTCDI unit. After this transition, due to the large conjugation and high electron affinity (i.e. low LUMO energy level) of PTCDI or NTCDI, the radical anion is stabilized even after turning off the applied electric field or by applying an opposite voltage. As a result, the dissociation of CT state is suppressed and non-volatile memory property is revealed. On the other hand, when the content of PTCDI or NTCDI unit is too small, the amount of stabilized radical anion is not enough to suppress this dissociation, resulting in a volatile memory characteristic.

For the case of PI-NTCDI2.5, the amount of NTCDI meets the critical point for the stabilization of CT complex which leads to the DRAM-WORM transition. Meanwhile, for the case of PI-BTCDIX, the generated radical anion cannot be stabilized due to the short conjugation length and low electron affinity (high LUMO energy level) of BTCDI, resulting in no transition in the volatility by increasing the loading ratio of BTCDI from 1 to 2.5 mol%. Moreover, the low HOMO level of BTCDI moiety leads to a large energy barrier toward the work function of ITO electrode, which limits the carrier injection from the electrode to the HOMO of PI-BTCDI. Thus, no memory characteristics are observed under a large existence of BTCDI unit. The above experimental results demonstrate the significance of the A ring structure on the memory characteristics.

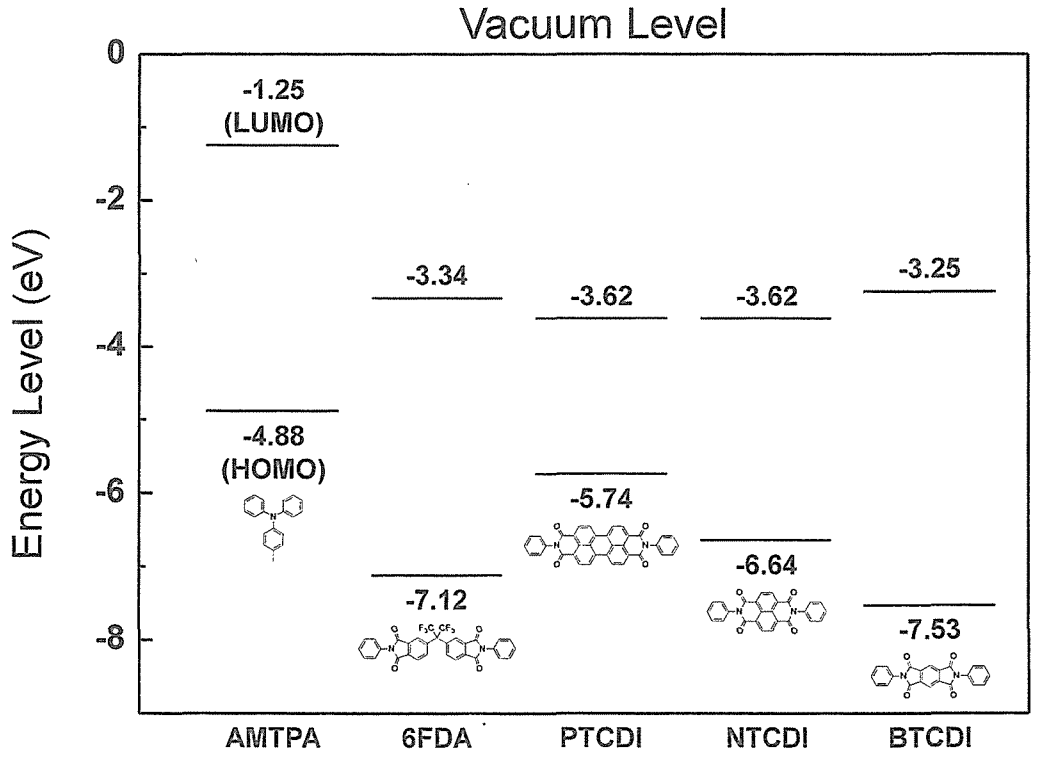

Figure 4-11. Estimated HOMO and LUMO energy levels of the D and A components.

4-3. Conclusion

Three series of random coPIs, PI-PTCDIX, PI-NTCDIX, and PI-BTCDIX were designed and synthesized, with the view of modulating the volatility and clarifying the effects of the A conjugation length on the resulting memory properties. The memory devices based on these coPIs exhibited distinct switching characteristics which were found to be varied continuously with copolymer composition. The (PI-PTCDI0, PI-PTCDI1), (PI-PTCDI2.5) and (PI-PTCDI5, PI-PTCDI10) devices provided volatile DRAM, SRAM, and non-volatile WORM behavior, respectively. For the case of PI-NTCDIX, the memory characteristics transited from volatile DRAM (PI-NTCDI1) to non-volatile WORM (PI-NTCDI5 and PI-NTCDI10), where PI-NTCDI2.5 showed a transition between DRAM and WORM type memory properties. Meanwhile, PI-BTCDIX based memory device exhibited the volatile memory characteristic at a low BTCDI composition (PI-BTCDI1 and PI-BTCDI2.5) and no switching behavior was observed at a high BTCDI composition (PI-BTCDI5 and PI-BTCDI10). The theoretical simulation suggested that the CT mechanism could be used to explain the memory behavior. Also, comparative studies of the energy levels of the components revealed that the stable CT state was obtained through stabilization of the radical anion by means of long conjugation and high electron affinity of the PTCDI and NTCDI moieties, leading to non-volatile memory characteristics. On the other hand, due to the low HOMO energy level of the BTCDI unit, a large energy barrier which prevents the hole injection from the ITO electrode to the polymer was generated, resulting in no switching behavior at a high BTCDI composition. Specifically, the importance of these results provided that coPIs with suitable A structure and ratio represent the design concept for a new class of PIs with readily tunable electronic memory performance.

4-4. Experimental section

Materials. The materials were used without further purification unless otherwise noted. Dehydrated DMAc, NMP, dehydrated pyridine, and acetic anhydride were purchased from Wako Pure Chemical Industries, Ltd., Japan. *m*-Cresol was purchased from Kanto Chemical Co., Inc (Japan). 6FDA was purchased from TCI and purified by sublimation. AMTPA was kindly donated by JSR Corp. PTCDI,[22] NTCDI,[22] BTCDI[15] and model compounds for AMTPA,[23] PBI,[22] NTCDI,[22] BTCDI,[24] 6FDA[24] (shown in Figure 4-10) were synthesized according to the previous reports.

Synthesis of Poly[4,4'-diamino-4"-methyltriphenylamine–hexafluoroisopropylidenediphthalimide] (PI–PTCDI0). To a solution of AMTPA (0.289 g, 1.00 mmol) in DMAc (5.00 mL) was added 6FDA (0.444 g, 1.00 mmol) under nitrogen. The mixture was stirred for 2 h at room temperature to give a viscous poly(amic acid) (PAA) solution. Excess amounts of acetic anhydride (1.50 mL) and pyridine (1.50 mL) were then added to the above PAA solution and stirred for 24 h. The resulting solution was poured into methanol, and the precipitate was collected by filtration. The final product was washed with methanol and dried at 200 °C for 5 h under vacuum to yield 0.666 g (95%). The M_n and weight-average molecular weight (M_w) estimated from size exclusion chromatography (SEC) were 4.25×10^4 and 11.2×10^4, respectively, with the polydispersity index (PDI = M_w/M_n) of 2.64. IR (KBr), ν (cm^{-1}): 1782, 1720 (C=O stretching), 1377 (C–N stretching). ^{1}H NMR (DMSO-d_6, δ, ppm, 40 °C): 8.13 (d, J = 7.8 Hz, ArH, 2H), 7.94 (d, J = 7.8 Hz, ArH, 2H), 7.79 (s, ArH, 2H), 7.36 (d, J = 9.0 Hz, ArH, 4H), 7.21 (d, J = 8.7 Hz, ArH, 2H), 7.15–7.08 (m, ArH, 6H), 2.30 (s, $ArCH_3$, 3H). *Anal.* Calcd for $C_{38}H_{21}N_3$: C, 65.4; H, 3.03; N, 6.02. Found: C, 64.9; H, 3.21; N, 6.17.

Synthesis of Poly[4,4'-diamino-4''-methyltriphenylamine–hexafluoroisopropylidenediphthalimide-co-*N*,*N*'-bis(4-aminophenyl)-3,4,9,10-perylenebis(dicarboximide)–hexafluoroisopropylidenediphthalimide] (PI-PTCDIX). 6FDA (0.444 g, 1.00 mmol) was added to a solution of AMTPA and PBI in *m*-cresol (5.00 mL), and the mixture was stirred for 2 h at room temperature to afford a viscous PAA solution. The total amount of AMTPA and PBI was set to 1.00 mmol. The molar ratios of PBI to AMTPA were set to be 1, 2.5, 5, and 10 mol % for PI-PTCDI1, PI-PTCDI2.5, PI-PTCDI5, and PI-PTCDI10, respectively. A reaction mixture of acetic anhydride (1.50 mL) and pyridine (1.50 mL) was added to the above PAA solution. The reaction mixture was stirred at room temperature under a nitrogen atmosphere for 24 h. The resulting solution was poured into methanol, and the precipitate was collected by filtration and washed with methanol. The product was finally dried at 200 °C for 5 h under vacuum. PI-PTCDI1, PI-PTCDI2.5, PI-PTCDI5, and PI-PTCDI10 were obtained in the yields of 85, 84, 81, and 92%, respectively. IR (KBr) of PI–PTCDI1, ν (cm^{-1}): 1786, 1724 (C=O stretching of phthalimide), 1662 (C=O stretching of PTCDI unit), 1381 (C–N stretching). IR (KBr) of PI–PTCDI2.5, ν (cm^{-1}): 1786, 1724 (C=O stretching of phthalimide), 1662 (C=O stretching of PTCDI unit), 1381 (C–N stretching). IR (KBr) of PI–PTCDI5, ν (cm^{-1}): 1786, 1724 (C=O stretching of phthalimide), 1658 (C=O stretching of PBI unit), 1377 (C–N stretching). IR (KBr) of PI–PTCDI10, ν (cm^{-1}): 1786, 1724 (C=O stretching of phthalimide), 1658 (C=O stretching of PTCDI unit), 1377 (C–N stretching). ^{1}H NMR (DMSO-d_6, δ, ppm, 40 °C) of PI–PTCDI1: 8.13 (d, J = 7.8 Hz, ArH, 2H), 7.94 (d, J = 7.8 Hz, ArH, 2H), 7.79 (s, ArH, 2H), 7.36 (d, J = 9.0 Hz, ArH, 4H), 7.21 (d, J = 8.7 Hz, ArH, 2H), 7.15–7.08 (m, ArH, 6H), 2.30 (s, $ArCH_3$, 3H), 6.8–8.4 (bm, ArH of PTCDI containing

unit, 0.23H (0.22H, calcd)). ^{1}H NMR (DMSO-d_6, δ, ppm, 40 °C) of PI–PTCDI2.5: 8.13 (d, J = 7.8 Hz, ArH, 2H), 7.94 (d, J = 7.8 Hz, ArH, 2H), 7.79 (s, ArH, 2H), 7.36 (d, J = 9.0 Hz, ArH, 4H), 7.21 (d, J = 8.7 Hz, ArH, 2H), 7.15–7.08 (m, ArH, 6H), 2.30 (s, $ArCH_3$, 3H), 6.8–8.4 (bm, ArH of PTCDI containing unit, 0.79H (0.56H, calcd)). ^{1}H NMR (DMSO-d_6, δ, ppm, 40 °C) of PI–PTCDI5: 8.13 (d, J = 7.8 Hz, ArH, 2H), 7.94 (d, J = 7.8 Hz, ArH, 2H), 7.79 (s, ArH, 2H), 7.36 (d, J = 9.0 Hz, ArH, 4H), 7.21 (d, J = 8.7 Hz, ArH, 2H), 7.15–7.08 (m, ArH, 6H), 2.30 (s, $ArCH_3$, 3H), 6.8–8.4 (bm, ArH of PTCDI containing unit, 1.3H (1.2H, calcd.)). ^{1}H NMR (DMSO-d_6, δ, ppm, 40 °C) of PI–PTCDI10: 8.13 (d, J = 7.8 Hz, ArH, 2H), 7.94 (d, J = 7.8 Hz, ArH, 2H), 7.79 (s, ArH, 2H), 7.36 (d, J = 9.0 Hz, ArH, 4H), 7.21 (d, J = 8.7 Hz, ArH, 2H), 7.15–7.08 (m, ArH, 6H), 2.30 (s, $ArCH_3$, 3H), 6.8–8.4 (bm, ArH of PTCDI containing unit, 2.5H (2.4H, calcd)). *Anal.* Calcd of PI–PTCDI1: C, 65.4; H, 3.02; N, 6.02. Found: C, 64.3; H, 3.37; N, 6.13. *Anal.* Calcd of PI–PTCDI2.5: C, 65.5; H, 3.01; N, 6.01. Found: C, 64.3; H, 3.36; N, 6.07. *Anal.* Calcd of PI–PTCDI5: C, 65.5; H, 2.99; N, 6.00. Found: C, 64.1; H, 3.58; N, 6.28. *Anal.* Calcd of PI–PTCDI10: C, 65.6; H, 2.95; N, 5.99. Found: C, 62.9; H, 3.34; N, 5.62.

Synthesis of Poly[4,4'-diamino-4''-methyltriphenylamine–hexafluoroisopropylidenediphthalimide-co-*N,N'*-bis(4-aminophenyl)-1,8:4,5-naphthalenetetracarboxdiimide-hexafluoroisopropylidenediphthalimide] (PI-NTCDIX). The synthesis of PI-NTCDIX was carried out according to the similar procedure to PI-PTCDX shown above. PI-NTCDI1, PI-NTCDI2.5, PI-NTCDI5, and PI-NTCDI10 were obtained in the yields of 93, 93, 94, and 97%, respectively. The M_ns of 3.80×10^4, 3.30×10^4, 2.80×10^4, and 2.40×10^4 g/mol with the PDI of 1.84, 1.94, 2.25, and 2.21 for PI-NTCDI1, PI-NTCDI2.5, PI-NTCDI5, and PI-NTCDI10 were determined,

respectively. IR (Si wafer) of PI-NTCDI1, ν (cm^{-1}): 1783, 1724 (C=O stretching of phthalimide), 1684 (C=O stretching of NTCDI unit), 1377 (C-N stretching). IR (Si wafer) of PI-NTCDI2.5, ν (cm^{-1}): 1784, 1724 (C=O stretching of phthalimide), 1684 (C=O stretching of NTCDI unit), 1377 (C-N stretching). IR (Si wafer) of PI-NTCDI5, ν (cm^{-1}): 1784, 1724 (C=O stretching of phthalimide), 1684 (C=O stretching of NTCDI unit), 1377 (C-N stretching). IR (Si wafer) of PI-NTCDI10, ν (cm^{-1}): 1786, 1724 (C=O stretching of phthalimide), 1686 (C=O stretching of NTCDI unit), 1377 (C-N stretching). ^{1}H NMR (DMSO-d_6, δ, ppm, 40 °C) of PI-NTCDI1: 8.13 (d, J = 7.8 Hz, ArH, 2H), 7.94 (d, J = 7.8 Hz, ArH, 2H), 7.79 (s, ArH, 2H), 7.36 (d, J = 9.0 Hz, ArH, 4H), 7.21 (d, J = 8.7 Hz, ArH, 2H), 7.15-7.08 (m, ArH, 6H), 2.31 (s, $ArCH_3$, 3H), 7.50-8.80 (bm, ArH of NTCDI containing unit, 0.17H (0.18H, calcd.)). ^{1}H NMR (DMSO-d_6, δ, ppm, 40 °C) of PI-NTCDI2.5: 8.13 (*d*, J = 7.8 Hz, ArH, 2H), 7.94 (d, J = 7.8 Hz, ArH, 2H), 7.79 (s, ArH, 2H), 7.36 (d, J = 9.0 Hz, ArH, 4H), 7.21 (d, J = 8.7 Hz, ArH, 2H), 7.15-7.08 (m, ArH, 6H), 2.31 (s, $ArCH_3$, 3H), 7.50-8.80 (bm, ArH of NTCDI containing unit, 0.74H (0.46H, calcd.)). ^{1}H NMR (DMSO-d_6, δ, ppm, 40 °C) of PI-NTCDI5: 8.13 (d, J = 7.8 Hz, ArH, 2H), 7.94 (d, J = 7.8 Hz, ArH, 2H), 7.79 (s, ArH, 2H), 7.36 (d, J = 9.0 Hz, ArH, 4H), 7.21 (d, J = 8.7 Hz, ArH, 2H), 7.15-7.08 (m, ArH, 6H), 2.31 (s, $ArCH_3$, 3H), 7.50-8.80 (bm, ArH of NTCDI containing unit, 1.0H (0.95H, calcd.)). ^{1}H NMR (DMSO-d_6, δ, ppm, 40 °C) of PI-NTCDI10: 8.13 (d, J = 7.8 Hz, ArH, 2H), 7.94 (d, J = 7.8 Hz, ArH, 2H), 7.79 (s, ArH, 2H), 7.36 (d, J = 9.0 Hz, ArH, 4H), 7.21 (d, J = 8.7 Hz, ArH, 2H), 7.15-7.08 (m, ArH, 6H), 2.31 (s, $ArCH_3$, 3H), 7.50-8.80 (bm, ArH of NTCDI containing unit, 1.8H (2.0H, calcd.)). *Anal.* Calcd of PI-NTCDI1: C, 65.4; H, 3.02; N, 6.03; found: C, 65.1; H, 3.26; N, 5.98. *Anal.* Calcd of PI-NTCDI2.5: C, 65.4; H, 3.00; N, 6.03; found: C, 65.0; H, 3.15; N, 5.98. *Anal.* Calcd

of PI-NTCDI5: C, 65.3; H, 2.98; N, 6.05; found: C, 64.7; H, 2.98; N, 6.96. *Anal.* Calcd of PI-NTCDI10: C, 65.2; H, 2.94; N, 6.07; found: C, 64.9; H, 3.13; N, 5.96.

Synthesis of Poly[4,4'-diamino-4''-methyltriphenylamine–hexafluoroisopropylidenediphthalimide-co-*N*,*N*'-bis(4-aminophenyl)-1,2:4,5-benzenetetracarboxdiimide-hexafluoroisopropylidenediphthalimide] (PI-BTCDIX). To a solution of BTCDI in NMP (7 mL) was added 6FDA (0.444 g, 1.00 mmol). The mixture was stirred at room temperature until the system became homogenious and then AMTPA was added. The total amount of BTCDI and AMTPA were set to 1.00 mmol, where the molar ratios of BTCDI to AMTPA were set to 1, 2.5, 5, and 10% for PI-BTCDI1, PI-BTCDI2.5, PI-BTCDI5, and PI-BTCDI10, respectively. The chemical imidization of the above PAA solution was carried out according to the similar procedure to PI-NTCDIX. PI-BTCDI1, PI-BTCDI2.5, PI-BTCDI5, and PI-BTCDI10 were obtained in the yields of 95, 95, 93, and 94%, respectively. The estimated M_n were 5.30×10^4, 5.00×10^4, 4.90×10^4, and 4.00×10^4 g/mol with the PDI of 2.23, 2.12, 2.20, and 2.18 for PI-BTCDI1, PI-BTCDI2.5, PI-BTCDI5, and PI-BTCDI10, respectively. IR (Si wafer) of PI-BTCDI1, ν (cm^{-1}): 1784, 1724 (C=O stretching), 1379 (C-N stretching). IR (Si wafer) of PI-NTCDI2.5, ν (cm^{-1}): 1784, 1716 (C=O stretching), 1375 (C-N stretching). IR (Si wafer) of PI-NTCDI5, ν (cm^{-1}): 1784, 1716 (C=O stretching), 1375 (C-N stretching). IR (Si wafer) of PI-NTCDI10, ν (cm^{-1}): 1784, 1720 (C=O stretching), 1376 (C-N stretching). ^{1}H NMR (DMSO-d_6, δ, ppm, 40 °C) of PI-BTCDI1: 8.13 (d, J = 7.8 Hz, ArH, 2H), 7.93 (d, J = 7.8 Hz, ArH, 2H), 7.78 (s, ArH, 2H), 7.36 (d, J = 9.0 Hz, ArH, 4H), 7.21 (d, J = 8.7 Hz, ArH, 2H), 7.14-7.07 (m, ArH, 6H), 2.30 (s, $ArCH_3$, 3H), 7.50-8.50 (bm, ArH of BTCDI containing unit, 0.19H (0.16H, calcd.)). ^{1}H NMR (DMSO-d_6, δ, ppm, 40 °C) of PI-BTCDI2.5: 8.13 (d, J = 7.8 Hz, ArH, 2H), 7.93 (d, J =

7.8 Hz, ArH, 2H), 7.78 (s, ArH, 2H), 7.36 (d, J = 9.0 Hz, ArH, 4H), 7.21 (d, J = 8.7 Hz, ArH, 2H), 7.14-7.07 (m, ArH, 6H), 2.30 (s, $ArCH_3$, 3H), 7.50-8.50 (bm, ArH of BTCDI containing unit, 0.51H (0.41H, calcd.)). ^{1}H NMR (DMSO-d_6, δ, ppm, 40 °C) of PI-BTCDI5: 8.13 (d, J = 7.8 Hz, ArH, 2H), 7.93 (d, J = 7.8 Hz, ArH, 2H), 7.78 (s, ArH, 2H), 7.36 (d, J = 9.0 Hz, ArH, 4H), 7.21 (d, J = 8.7 Hz, ArH, 2H), 7.14-7.07 (m, ArH, 6H), 2.30 (s, $ArCH_3$, 3H), 7.50-8.50 (bm, ArH of BTCDI containing unit, 0.91H (0.84H, calcd.)). ^{1}H NMR (DMSO-d_6, δ, ppm, 40 °C) of PI-BTCDI10: 8.13 (d, J = 7.8 Hz, ArH, 2H), 7.93 (d, J = 7.8 Hz, ArH, 2H), 7.78 (s, ArH, 2H), 7.36 (d, J = 9.0 Hz, ArH, 4H), 7.21 (d, J = 8.7 Hz, ArH, 2H), 7.14-7.07 (m, ArH, 6H), 2.30 (s, $ArCH_3$, 3H), 7.50-8.50 (bm, ArH of BTCDI containing unit, 1.8H (1.8H, calcd.)). *Anal.* Calcd of PI-BTCDI1: C, 65.4; H, 3.02; N, 6.03; found: C, 64.8; H, 3.46; N, 6.09. *Anal.* Calcd of PI-BTCDI2.5: C, 65.3; H, 3.00; N, 6.04; found: C, 64.7; H, 3.39; N, 6.10. *Anal.* Calcd of PI-BTCDI5: C, 65.2; H, 2.98; N, 6.05; found: C, 64.6; H, 2.93; N, 6.23. *Anal.* Calcd of PI-BTCDI10: C, 65.0; H, 2.93; N, 6.11; found: C, 64.6; H, 3.47; N, 6.16.

Characterization. FT-IR spectra were measured by a Horiba FT-120 Fourier transform spectrophotometer. M_n and PDI values were evaluated by HITACHI SEC with two polystyrene gel columns (Shodex GPC KD-804, KD-805). *N*,*N*-Dimethylformamide (DMF) containing 0.01 M LiBr was used as an eluent at a flow rate of 1.0 mL·min^{-1} calibrated by polystyrene standard samples. Elemental analyses were performed on a Yanaco MT-6 CHN recorder elemental analysis instrument. Thermal properties were estimated from a Seiko TG/DTA 6300 TGA system and a thermal analysis instrument of DSC-Q100 under a nitrogen atmosphere at a heating rate of 10 and 6 °C/min, respectively. Electrochemistry was performed with a CHI 611B electrochemical analyzer. Cyclic voltammetry was performed by a

three-electrode cell in which ITO (polymer films area about 0.7 × 0.5 cm^2) was used as a working electrode. A platinum wire was used as an auxiliary electrode. All cell potentials were taken with the use of a homemade Ag/AgCl, KCl (sat.) reference electrode. Absorption spectra were measured with a Hitachi U4100 UV-Vis-NIR spectrophotometer. The thickness of the polymer films were measured with a Microfigure Measuring Instrument (Surfcorder ET3000, Kosaka Laboratory Ltd).

Fabrication and Measurement of the Memory Device. The ITO glass substrates were cleaned stepwise by water, acetone, and isopropyl alcohol in an ultrasonic bath. The memory device was fabricated following the basic structures of ITO/PIs/Al. A well-dissolved polymer solution in DMAc was first filtered through 0.45 μm pore size of poly(tetrafluoroethylene) (PTFE) membrane syringe filter, spin-coated on top of an ITO glass substrate at a speed rate of 1000 rpm for 60 s, and then baked at 150 °C for 20 min in a nitrogen-filled glovebox. The thickness of the thin film was determined to be around 37–41 nm. The top electrode with a 300 nm of Al was deposited under vacuum through the shadow mask in a thermal evaporator. Each substrate contained the memory cells with a recorded area of 0.5×0.5 mm^2. The electrical characterization of the memory device was performed by a Keithley 4200-SCS semiconductor parameter analyzer equipped with a Keithley 4205-PG2 arbitrary waveform pulse generator. ITO was used as the cathode (maintained as common), and Al was set as the anode during the voltage sweep. All of the electronic measurements were performed in a glovebox.

Computational Methodology. All calculations were performed using the Gaussian 03 program package. [18] Optimized gas-phase ground states were calculated at the DFT method, using the hybrid B3LYP exchange correlation functional and the split valence 6-31G(d) basic set (DFT//B3LYP/6-31G(d)).

4-5. References

1. Liu, Y.-L.; Wang, K.-L.; Huang, G.-S.; Zhu, C.-X.; Tok, E.-S.; Neoh, K.-G.; Kang, E.-T., *Chem. Mater.* **2009,** *21*, 3391-3399.
2. Liu, Y. W.; Zhang, Y.; Lan, Q.; Liu, S. W.; Qin, Z. X.; Chen, L. H.; Zhao, C. Y.; Chi, Z. G.; Xu, J. R.; Economy, J., *Chem. Mater.* **2012,** *24*, 1212-1222.
3. Ling, Q.-D.; Chang, F.-C.; Song, Y.; Zhu, C.-X.; Liaw, D.-J.; Chan, D. S.-H.; Kang, E.-T.; Neoh, K.-G., *J. Am. Chem. Soc.* **2006,** *128*, 8732-8733.
4. Liu, Y.-L.; Ling, Q.-D.; Kang, E.-T.; Neoh, K.-G.; Liaw, D.-J.; Wang, K.-L.; Liou, W.-T.; Zhu, C.-X.; Chan, D. S.-H., *J. Appl. Phys.* **2009,** *105*, 044501/1-044501/9.
5. Liu, C.-L.; Kurosawa, T.; Yu, A.-D.; Higashihara, T.; Ueda, M.; Chen, W.-C., *J. Phys. Chem. C* **2011,** *115*, 5930-5939.
6. Kung, Y.-C.; Lee, W.-F.; Hsiao, S.-H.; Liou, G.-S., *J. Polym. Sci., Part A: Polym. Chem.* **2011,** *49*, 2210-2221.
7. Tian, G.; Wu, D.; Qi, S.; Wu, Z.; Wang, X., *Macromol. Rapid Commun.* **2011,** *32*, 384-389.
8. Kuorosawa, T.; Chueh, C.-C.; Liu, C.-L.; Higashihara, T.; Ueda, M.; Chen, W.-C., *Macromolecules* **2010,** *43*, 1236-1244.
9. Wang, K.-L.; Liu, Y.-L.; Lee, J.-W.; Neoh, K.-G.; Kang, E.-T., *Macromolecules* **2010,** *43*, 7159-7164.
10. You, N.-H.; Chueh, C.-C.; Liu, C.-L.; Ueda, M.; Chen, W.-C., *Macromolecules* **2009,** *42*, 4456-4463.
11. Ling, Q.-D.; Liaw, D.-J.; Teo, E. Y.-H.; Zhu, C.; Chan, D. S.-H.; Kang, E.-T.; Neoh, K.-G., *Polymer* **2007,** *48*, 5182-5201.
12. Ling, Q.-D.; Liaw, D.-J.; Zhu, C.; Chan, D. S.-H.; Kang, E.-T.; Neoh, K.-G., *Prog. Polym. Sci.* **2008,** *33*, 917-978.
13. Zhan, X.; Facchetti, A.; Barlow, S.; Marks, T. J.; Ratner, M. A.; Wasielewski, M. R.; Marder, S. R., *Adv. Mater.* **2011,** *23*, 268-284.
14. Zheng, Q. D.; Huang, J.; Sarjeant, A.; Katz, H. E., *J. Am. Chem. Soc.* **2008,** *130*, 14410-14411.
15. McKerrow, A. J.; Fox, M. A.; Leu, J. P.; Ho, P. S., *J. Polym. Sci., Part A Polym. Chem.* **1997,** *35*, 319-327.
16. Wurthner, F., *Chem. Commun.* **2004**, 1564-1579.
17. Bredas, J. L.; Silbey, R.; Boudreaux, D. S.; Chance, R. R., *J. Am. Chem. Soc.* **1983,** *105*, 6555-6559.
18. Frisch, M. J. T., G. W.; Schlegel, H. B.; Scuseria, G. E.; Robb, M. A.;

Cheeseman, J. R.; Montgomery, Jr., J. A.; Vreven, T.; Kudin, K. N.; Burant, J. C.; Millam, J. M.; Iyengar, S. S.; Tomasi, J.; Barone, V.; Mennucci, B.; Cossi, M.; Scalmani, G.; Rega, N.; Petersson, G. A.; Nakatsuji, H.; Hada, M.; Ehara, M.; Toyota, K.; Fukuda, R.; Hasegawa, J.; Ishida, M.; Nakajima, T.; Honda, Y.; Kitao, O.; Nakai, H.; Klene, M.; Li, X.; Knox, J. E.; Hratchian, H. P.; Cross, J. B.; Bakken, V.; Adamo, C.; Jaramillo, J.; Gomperts, R.; Stratmann, R. E.; Yazyev, O.; Austin, A. J.; Cammi, R.; Pomelli, C.; Ochterski, J. W.; Ayala, P. Y.; Morokuma, K.; Voth, G. A.; Salvador, P.; Dannenberg, J. J.; Zakrzewski, V. G.; Dapprich, S.; Daniels, A. D.; Strain, M. C.; Farkas, O.; Malick, D. K.; Rabuck, A. D.; Raghavachari, K.; Foresman, J. B.; Ortiz, J. V.; Cui, Q.; Baboul, A. G.; Clifford, S.; Cioslowski, J.; Stefanov, B. B.; Liu, G.; Liashenko, A.; Piskorz, P.; Komaromi, I.; Martin, R. L.; Fox, D. J.; Keith, T.; Al-Laham, M. A.; Peng, C. Y.; Nanayakkara, A.; Challacombe, M.; Gill, P. M. W.; Johnson, B.; Chen, W.; Wong, M. W.; Gonzalez, C.; and Pople, J. A., *Gaussian, Inc., Wallingford CT* **2004**.

19. Kim, K.; Park, S.; Hahm, S. G.; Lee, T. J.; Kim, D. M.; Kim, J. C.; Kwon, W.; Ko, Y.-G.; Ree, M., *J. Phys. Chem. B* **2009**, *113*, 9143-9150.
20. Shang, D. S.; Wang, Q.; Chen, L. D.; Dong, R.; Li, X. M.; Zhang, W. Q., *Phys. Rev. B Condens. Matter Mater. Phys.* **2006**, *73*, 245427/1-245427/7.
21. Sze, S. M.; Editor, *Modern Semiconductor Device Physics*. 1998; p 556 pp.
22. Kolhe, N. B.; Asha, S. K.; Senanayak, S. P.; Narayan, K. S., *J. Phys. Chem. B* **2010**, *114*, 16694-16704.
23. Hill, L. L.; Moore, L. R.; Huang, R.; Craciun, R.; Vincent, A. J.; Dixon, D. A.; Chou, J.; Woltermann, C. J.; Shaughnessy, K. H., *J. Org. Chem.* **2006**, *71*, 5117-5125.
24. Yu, J.-W.; Sung, C. S. P., *Macromolecules* **1995**, *28*, 2506-2511.

Chater 5. Tuning the Memory Characteristics from Volatile to Non-Volatile by Pyrene Composition in Radom Copolyimides and the Fabrication of Flexible Polymer Memory Devices

ABSTRACT: A series of Random copolyimides (coPIs) with pyrene containing donors were prepared and employed as the active layer for flexible resistance memory devices in a cross-point poly(ethylene naphthalene) PEN/Al/coPIs/Al platform. The pyrene moiety was introduced for the purpose of delocalizing the radical cation generated in the CT state and inducing non-volatile behavior. The memory behaviors varied from volatile to non-volatile one in accordance with increasing the pyrene content. Electrical bistability was ascribed to the field induced charge transfer (CT) as suggested by theoretical simulation and the largely conjugated pyrene moiety benefits the stable CT state with excellent non-volatile electrical properties. Also, the flexible device based on the coPIs exhibited superior retention stress and mechanical durability when operated under various bending conditions. The resistance switching characteristics have been successfully analyzed using a proper theoretical model.

5-1. Introduction

In Chapter 4, an effective and simple design concept to modulate the memory behavior has been established, which has introduced a largely conjugated and highly electron affinitive moieties such as perylene and naphthalene diimides as the electron accepting units and controlling their molar composition in random copolyimide (coPI) system. The basic notion of this concept is to stabilize the radical anions generated in the CT state through delocalization and trapping effect. Although remarkable effects to induce non-volatile behavior have been demonstrated, these functional moieties, at the same time, possess some disadvantages to be addressed, such as low solubility and complicated and relatively low yield synthetic strategies, which cannot be ignored from the view point of further developing PI memory materials.

Meantime, polycyclic arenes (PCAs), such as naphthalene, anthracene, pyrene, etc., have been widely studied for their remarkable ion stability, oxidation stability, and n- or p-type semiconducting properties derived from the large conjugation, high electron affinity, and high crystallinity.[1-2] Among the several PCAs, pyrene is well known not only for its excellent electronic properties but also for the wide variety of possible chemical modifications.[2-3] Thus, introducing pyrene into the electron-donating triaryl amine structure of donor–acceptor PIs would simultaneously increase the solubility and stabilize the radical cation in the CT state which might contribute to the expression of non-volatile memory characteristics. However, a detailed investigation on the stabilization of radical cations in the CT state for non-volatile memory characteristics of donor–acceptor PIs has never been reported.

In this chapter, modifying the concept established in Chapter 4, a series of random coPIs prepared from *N*,*N*-bis(4-aminophenyl)-*p*-toluidine (AMTPA),

N,*N*-bis(4-aminophenyl)-1-aminopyrene (APAP), and 4,4'-(hexafluoroisopropylidene)diphthalic anhydride (6FDA) (Scheme 5-1) were designed and synthesized for the purpose of tuning the electrical memory property form volatile to non-volatile by changing the stability of radical cations generated in the CT state through delocalization. The molar contents of APAP to AMTPA were set to be 0, 5, 10 and 100 mol% for PI(AMTPA), PI(AMTPA95-APAP5), PI(AMTPA90-APAP10), and PI(APAP), respectively. Typically, PI based resistance memories are fabricated on glass or silicon substrates to demonstrate the memory switching behavior. [4-22] Flexible electronic memory devices featuring good performance still have fundamental challenging problems for next-generation electronic devices. Therefore, since the coPIs showed high solubility to common organic solvents, they were used as a memory layer and fabricated on plastic poly(ethylene naphthalate) (PEN) substrates in a cross-point structure. Indeed, the reliable, reproducible, and tunable performance of sandwiched PEN/Al/coPI/Al memory devices was demonstrated. The memory parameters were analyzed statistically between all four coPIs and also under bending stress. Finally, the switching mechanism and discussion on the structural–memory property relationships are reported.

5-2. Results and discussion

5-2-1. Synthesis and characterization of coPIs

The coPIs, PI(AMTPA), PI(AMTPA95-APAP5), PI(AMTPA90-APAP10), and PI(APAP) were synthesized by a two-step polycondensation of aromatic dianhydride (6FDA) with aromatic diamines (AMTPA and APAP), followed by chemical imidization using acetic anhydride and pyridine as shown in Scheme 5-1. The molar ratios of APAP to AMTPA were controlled to be 0, 5, 10, and 100% for PI(AMTPA), PI(AMTPA95-APAP5), PI(AMTPA90-APAP10), and PI(APAP), respectively. All the coPIs were obtained in high yields (95-99%).

Scheme 5-1. Synthesis of the studied coPIs.

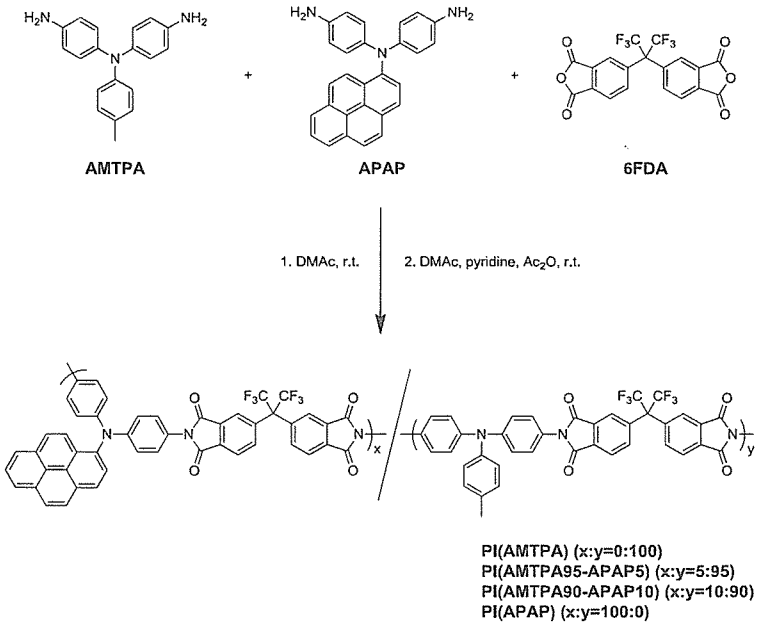

The chemical imidization of the poly(amic acid) (PAA) was characterized by FT-IR spectra, as shown in Figure 5-1. All the coPIs exhibits similar IR absorption peaks which originats from the imide moieties located around 1780 (ν_s, C=O), 1720 (ν_{as}, C=O), and 1370 (ν, C–N) cm^{-1}.

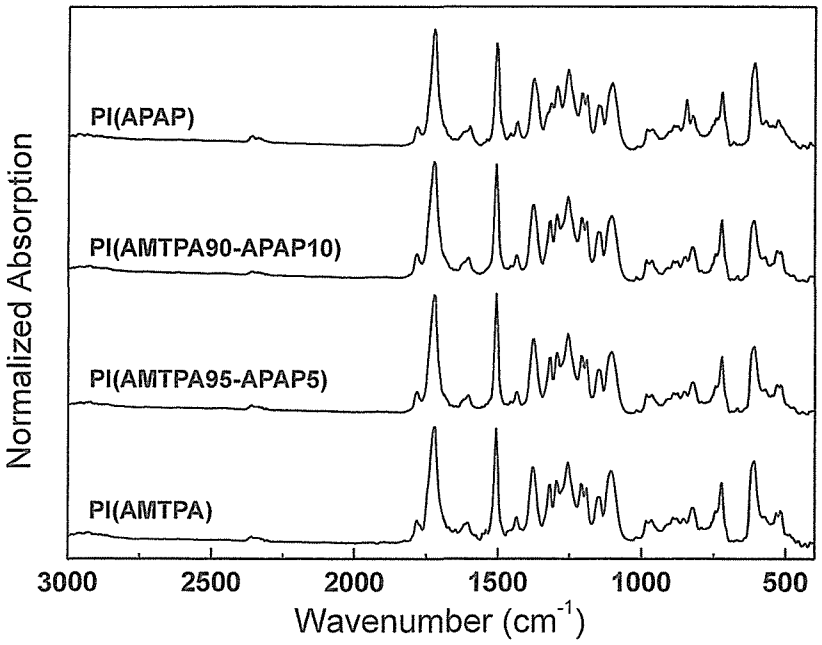

Figure 5-1. IR spectra of the studied coPIs.

The structures of all coPIs were also characterized by ^{1}H NMR (Figure 5-2). The aromatic signals for the protons (ArH) of the pyrene moiety and those for the imide ring are observed in the range of 7.9–8.5 ppm (#3' and #6'–14'). The structure and molar content of APAP in coPIs are determined by comparing the integral values of the spectra in the range of 7.9–8.5 ppm with that of tolyl ($ArCH_3$) signal (#8) of the AMTPA unit. The observed values of the ArH signals are 2.86 and 3.48 for PI(AMTPA95-APAP5) and PI(AMTPA90-APAP10) (compared to that of the tolyl signal set to be 3), which are close to the theoretical values of 2.65 and 3.30, respectively. The expected chemical structures of the coPIs were also confirmed by elemental analysis.

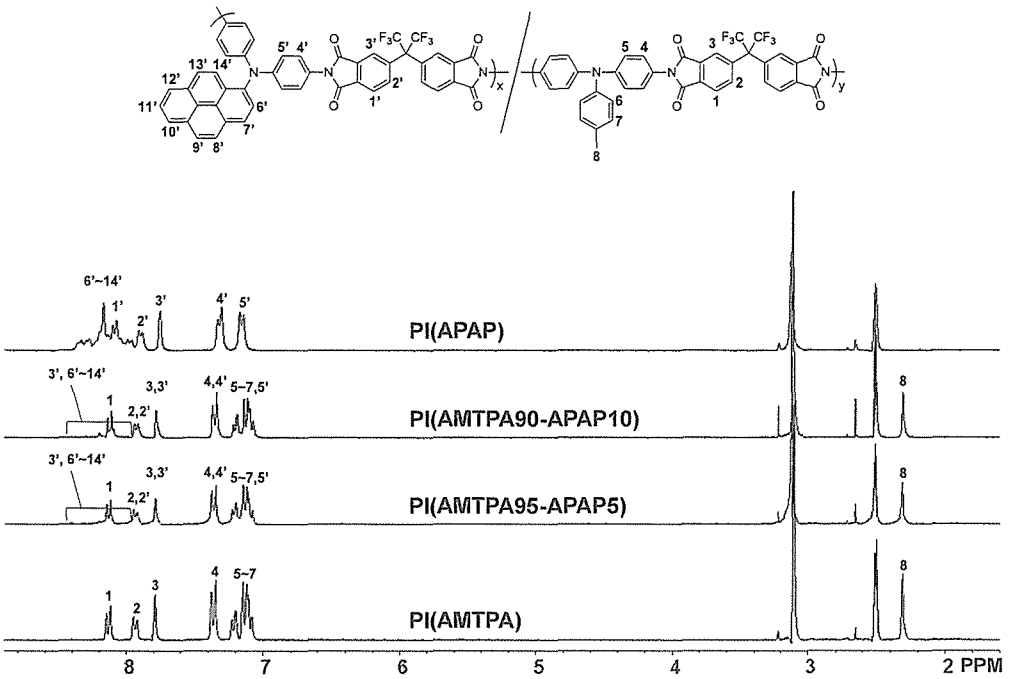

Figure 5-2. ^{1}H NMR spectra of the studied coPIs.

In addition, all the coPIs showed high number average molecular weight (M_n) and weight average molecular weight (M_w) of 42.5 and 112 kDa, respectively, with polydispersity indices (PDIs) ranging from 1.84 to 2.64 (see Table 5-1). Also, all the coPIs were readily soluble in common organic solvents such as chloroform, tetrahydrofuran (THF), *N*,*N*-dimethylformamide (DMF), *N*,*N*-dimethylacetamide (DMAc), and *N*-methylpyrrolidone (NMP), which is advantageous to develop various kinds of devices. The thermal decomposition temperatures T_ds (5% weight loss), evaluated by thermo gravimetric analysis (TGA) under flowing nitrogen, were in the range of 515–531 °C, inferring excellent thermal stability although a clear correlation between the molar ratio of APAP moieties and decomposition temperatures was not found. However, upon introduction of more thermally stable aromatic APAP, the coPIs exhibited higher T_d values than that of PI(AMTPA). Glass transition temperatures (T_gs)

of all the coPIs could not be observed up to 300 °C during the differential scanning calorimetry (DSC), indicating their high thermal stability. Here, the excellent thermal properties of all coPIs are expected to meet the requirement of heat resistance in electrical characteristics.

Table 5-1. Molecular weights and physical properties of the studied coPIs.

coPIs	M_n (g/mol)[a]	M_w (g/mol)[a]	PDI[a]	T_d (°C)[b]	T_g (°C)[c]	E_g^{opt} (eV)[d]	HOMO (eV)[e]	LUMO (eV)[f]
PI(AMTPA)	43,000	112,000	2.60	515	—	3.14	-5.31	-2.27
PI(AMTPA95-APAP5)	63,000	116,000	1.84	531	—	3.07	-5.28	-2.21
PI(AMTPA90-APAP10)	53,000	113,000	2.13	518	—	3.07	-5.26	-2.19
PI(APAP)	62,000	119,000	1.92	520	—	2.82	-5.25	-2.43

[a]Determined by SEC. [b]Determined by TGA measurement. [c]Determined by DSC measurement. The measurement was carried out in the range of -10-300 °C. [d]Estimated from the UV absorption spectra. [e]Estimated from CV. [f]LUMO = HOMO + band gap.

5-2-2. Optical and electrochemical properties

The UV-vis absorption spectra of all coPIs in solutions are shown in Figure 5-3a. The absorption peak at 302 nm and adjoining pronounced shoulder from PI(AMTPA) are assigned to the delocalized π–π* transitions of the AMTPA moieties and intermolecular π–π or CT interaction, respectively.[23] On the other hand, PI(APAP) exhibits two distinct absorption bands at 327 and 378 nm. The strong absorption peak maximum at 327 nm corresponds to the π–π* transitions of the pyrene heterocyclic ring,[24] while that around 378 nm is attributed to the intra- or inter-molecular charge transfer (CT) from the electron rich pyrene units to electron deficient phthalimide functionalities.[24] The absorption peak maximum and edge position of PI(AMTPA-95-APAP5) and PI(AMTPA90-APAP10) are almost equivalent to those of PI(AMTPA) except for a

slight increase at the longer absorption wavelength with an increased APAP content. Optical band gaps (E_g^{opt}s) were evaluated from the absorption onset of the copolymers films, as shown in Figure 5-3b. The obtained E_g^{opt}s of PI(AMTPA), PI(AMTPA95-APAP5), PI(AMTPA90-APAP10), and PI(APAP) were 3.14, 3.07, 3.07, and 2.82 eV, respectively.

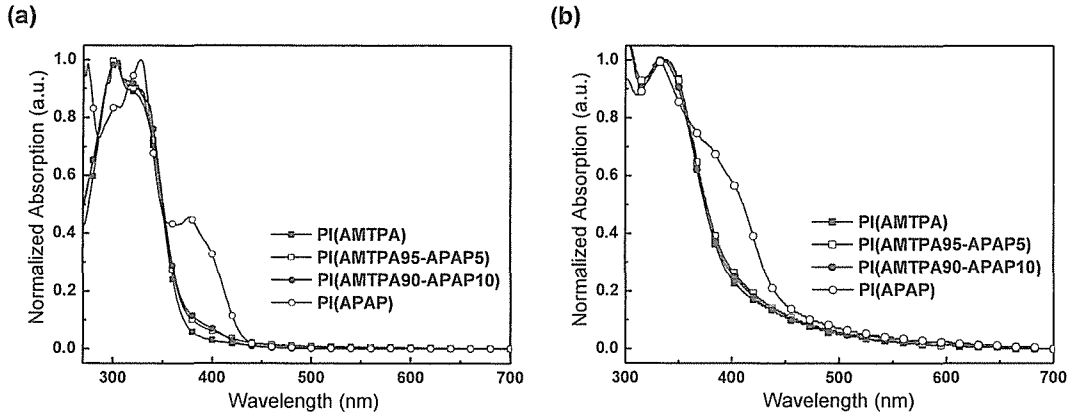

Figure 5-3. Optical absorption spectra of the studied coPIs (a) in DMAc solution and (b) film state.

Electrochemical properties measured by cyclic voltammetry (CV) using a three-electrode cell was utilized to investigate the oxidation behaviors to determine the highest occupied molecular orbital (HOMO) energy levels. As illustrated in Figure 5-4, cyclic voltammograms of all coPIs show a quasi-reversible *p*-doping process during the anodic scan and the HOMO energy levels were estimated from the onset of oxidation potential where the current differs from the baseline. The onset oxidation potentials are recorded to lie in the range from 0.99 to 0.93 V (*vs.* Ag/Ag^+); thus the corresponding HOMO energy levels of PI(AMTPA), PI(AMTPA95-APAP5), PI(AMTPA90-APAP10), and PI(APAP) are in the range from -5.31 to 5.25 eV (see Table 5-1). The HOMO energy levels are moved slightly towards higher positions with the incorporation of electron-rich pyrene moieties into the polymer backbones. In addition, the lowest

unoccupied molecular orbital (LUMO) energy levels of coPIs were evaluated by combining the HOMO energy levels of and E_g^{opt}s. The detailed HOMO and LUMO energy levels are listed in Table 5-1; they are comparable to those of previously reported functional PIs.[23-24] The high-lying HOMO and small band gap of the pyrene moiety contributed to the deep LUMO energy level (-2.43 eV) of PI(APAP), compared to -2.23 eV for PI(AMTPA). The differences in the coPI backbone structures lead to the differnces in HOMO–LUMO energy levels and band gaps.

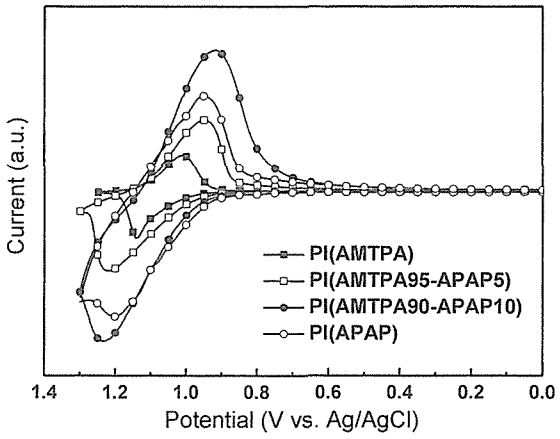

Figure 5-4. Cyclic voltammograms of the studied coPIs.

5-2-3. Memory properties

With the aim of elucidating the role of coPIs with specific AMTPA/APAP functionalities for electrical properties, the standard two terminal metal–insulator–metal (MIM) geometry of PEN/Al/PIs/Al cross-point devices structures were fabricated, consisting of planar Al electrodes sandwiching a 40 nm PIs memory layer (Figure 5-5). Instead of relying on an external diode or transistor as the selective device, the logical organization on the square of a single row (bit-line; utilized as the bottom electrode) and several columns (word-line; utilized as the top electrode) is obtained in the resistive

switches to break the sneak current paths from passing through the non-selected cells. The memory device was organized into memory cells, each storing one binary bit. This pattern significantly simplified the device fabrication process and enabled the selected device cells to be operated correctly.

Figure 5-5. Schematic and photographic memory device architecture.

The transitions in electrical resistance states of PI films were probed by direct voltage sweep measurements. A voltage bias was applied to the top Al electrode while the bottom Al electrode was grounded. A series of current density–voltage (*J–V*) characteristics of cross-point coPI systems with memory hysteresis behavior were measured in an inert atmosphere at room temperature. By increasing the APAP composition, the coPIs provided three types of switching properties that represent volatile dynamic random access memory (DRAM), non-volatile FLASH, and non-volatile write once read many (WORM) type behavior. Representative *J–V* characteristics plotted on a semilogarithmic scale of as-fabricated memory device based on PI(AMTPA) junction are nonlinear starting with a high zerobias resistance (see Figure 5-6a). Here the high resistance (OFF) state and low resistance (ON) state are defined for the low and high branches of the hysteretic *J–V* curve, respectively. For the backward (negative) bias (sweep 1), the state switches from the OFF to the ON state by a setting voltage (V_{set}) of -2.25 V, which corresponds to the writing process of the memory device with a resistance ON/OFF ratio larger than 10^4. The device remains in

the ON state during the subsequent negative scan (sweep 2). However, for the forward (positive) bias (sweep 3), it changes to the OFF state at the resetting voltage (V_{reset}) of 1.65 V. The device is kept in the OFF state after this erasing process as indicated by the subsequent 4th sweep. Although the memory device exhibits an interesting bistable resistance change from the OFF to the ON state, it could not maintain the ON state when the power was turned OFF. The device can be switched reversibly and repeatedly to the ON state (sweep 5 and sweep 7) or the OFF state by applying sufficiently large V_{set} or V_{reset}. Data is accessed by means of a binary address to the memory. Therefore, the PI(AMTPA) device is characterized as a volatile DRAM memory since it does not provide the bistable resistance states without an external voltage. The stability of the memory device against the switching time as function of the constant voltage bias was also evaluated under the same conditions with a pulse period of 1 ms and pulse width of 1 ms. Figure 5-6b and c show the retention times and stress tests of the ON and OFF states on the PI(AMTPA) device. Both OFF and ON states of the volatile PI(AMTPA) device can be maintained for a period of over 10^4 s at a read bias of -1 V (Figure 5-6b) and 10^8 continuous read pulse (Figure 5-6c).

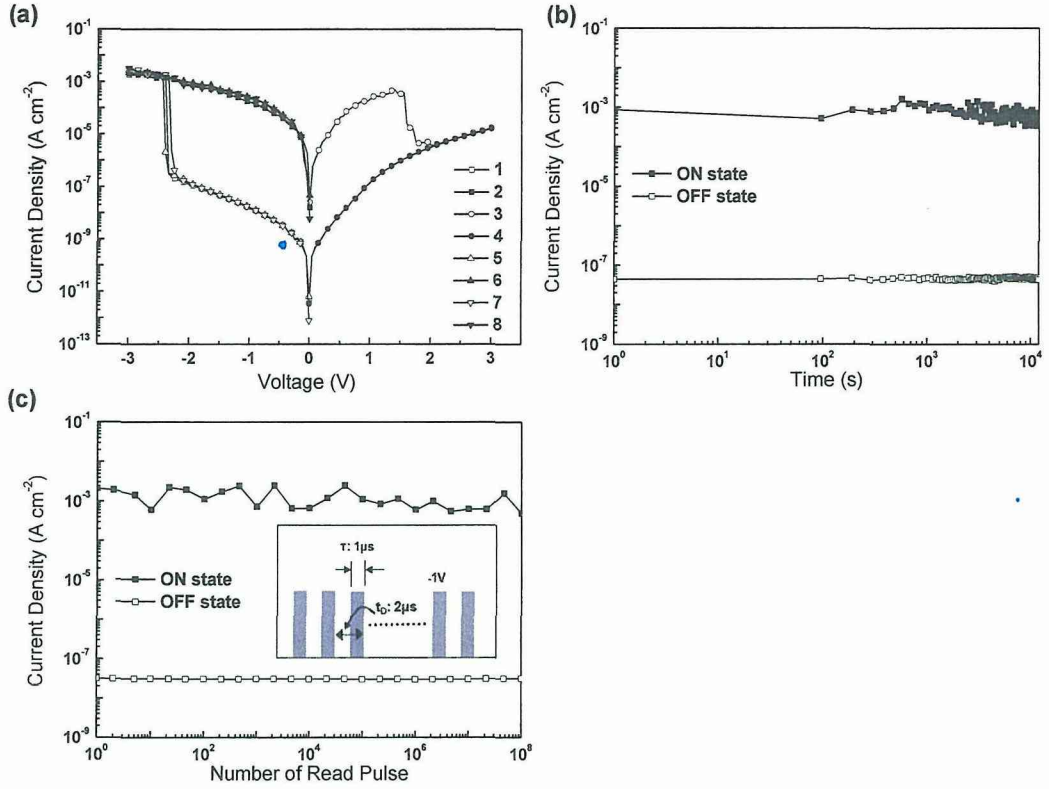

Figure 5-6. (a) *J-V* characteristics, (b) retention time test, and (c) stimulus effect of read pulse on the ON and OFF states of the PI(AMTPA) device. The inset of (c) shows the pulse shapes in the measurement.

Also, the bipolar resistance switching behaviors in the PI(AMTPA95-APAP5) (containing 5 mol% of APAP) device demonstrated a *J–V* hysteresis loop as a memristor (Figure 5-7a). On the 1st voltage sweep, the device starts in the OFF state until the bias is increased to approximately -2.2 V and the current abruptly increases to the ON state (an ON/OFF ratio of 10^4). This state remains until a reverse (positive) bias of around 1.60 V is applied. The writing process of the device can be achieved by applying an adequate negative bias through a negative scan; however, once the switching is performed, the opposite bias is required for an erasing procedure. This means that the ON state can be sustained even after turning off the power supply, indicating a

non-volatile behavior. Figure 5-7b reveals that the electrical measurements can be repeated for more than 10 cycles. The polarity of the SET (OFF to ON transition) and RESET (ON to OFF transition) voltage is always comparable in each case. The RESET voltages are located in the range of 1.5–2.3 V. Small vibrations inside the glovebox, thickness variations or conformational relaxations of polymer chains possibly contributes to the slight fluctuations in the switching threshold voltage.[9] All the *J–V* curves show quite stable memory switching behaviors with reasonable threshold voltage fluctuations and consistent OFF/ON resistance values. The high yield of the reproducible PI(AMTPA95-APAP5) device fulfills the criteria for non-volatile FLASH memory behavior, implying that stable switching requires voltage regulation, and SET or RESET are possibly dependent on the bias voltage polarity (bipolar switching). One can see that a retention time of at least 10^4 s had been demonstrated for both resistance states (see Figure 5-7c). To investigate the hysteresis nature of the PI(AMTPA95-APAP5) device as a memory operation, the fabricated device was biased with a negative voltage (-3.5 V) for writing and a positive bias (3 V) for erasing. Figure 5-7d shows the endurance test results of the reversible ON/OFF switching characteristics based on the Al/PI(AMTPA95-APAP5)/Al memory cell. After multiple applications of the writing and erasing voltages, the ON and OFF states are achieved similar to those of the original cycles at intermediate reading voltages of -1 and 1 V, respectively. The resistances of the two states are scattered to a certain extent for more than 200 repeated write–read–erase–read (WRER) cycles since such a high ON/OFF ratio of 10^4 can tolerate this scattering even through a few current fluctuations. The highly controllable resistance modulation of the PI(AMTPA95-APAP5) device implies that the conducting path repeatedly forms and ruptures under alternative bias polarity.

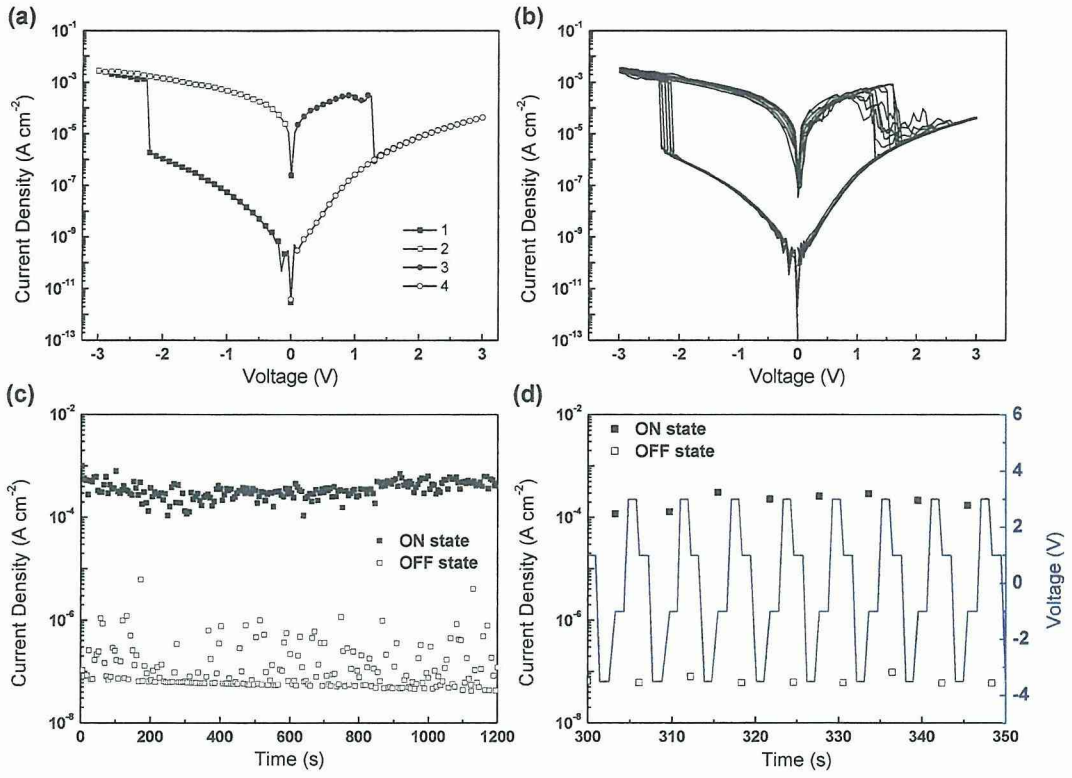

Figure 5-7. (a) *J-V* characteristics, (b) *J-V* characteristics during 10 cycles, (c) endurance, and (d) WRER cycles of PI(AMTPA95-APAP5) memory device.

However, for the device based on PI with 100 mol% APAP moieties, PI(APAP), the switching behavior conducted by applying a voltage cycle (±3.5 V) to a fixed memory cell indicates that resistance transition occurs at a specified polarity and the different branches of voltage sweep can be separately analyzed (Figure 5-8a). At a negative voltage value, the current density initially follows the OFF state and a sharp current injection drives the device to the ON state above the set bias of approximately -2.8 V where it remains until completing the voltage scan (sweep 1), subsequent negative scan (sweep 2), and after removing the power supply (at least 1 day; sweep 3). At a positive voltage value, the ON state does not return to the OFF state (sweep 4). The ON state is still retained steadily in the subsequent positive voltage scan (sweep 5). The irreversible

transition from the OFF to the ON state of the PI(APAP) device indicates a WORM type memory with an ON/OFF current ratio of more than 10^4 at -1.0 V where information cannot be modified once it has been written. The information storage of the PI(APAP) device is likely to persist permanently judging from the long-term trend of the data storage. Typical retention properties are shown in Figure 5-8b. The retention time of each ON and OFF state in the devices is sustained for a minimum of 10^4 s as a result of the stability of both states.

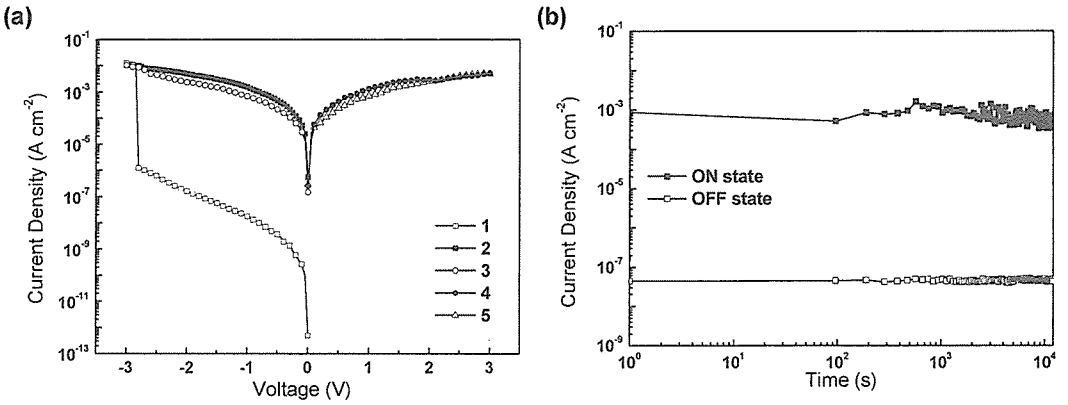

Figure 5-8. (a) *J-V* characteristics and (b) retention time test of PI(APAP) memory device.

For the case of the PI(AMTPA90-APAP10) device (Figure 5-9), the switching operation lies between bipolar FLASH PI(AMTPA95-APAP5) and bistable WORM-type PI(APAP). Of the 30 cells that were fabricated in the same device, 9 device cells (30%) exhibited bipolar non-volatile FLASH behavior while 21 (70%) cells showed electrical switching as WORM memory. These results suggest that the introduction of the pendent pyrene moiety to coPIs plays an important role in the volatility and switching behavior of memory behavior.

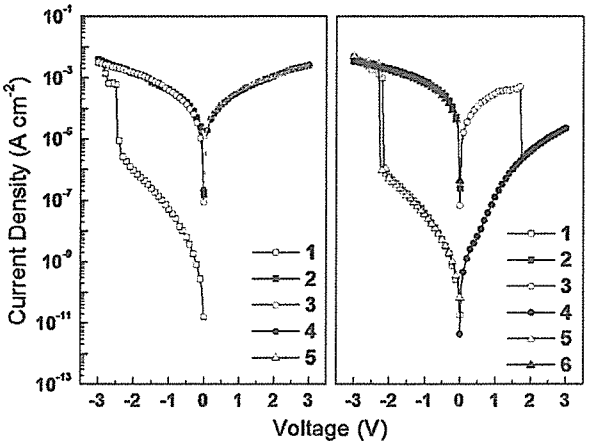

Figure 5-9. *J-V* characteristics of the PI(AMTPA90-APAP10) memory device. The left and right sides represents WORM (30% of the device) type and FLASH (70%) type memory properties, respectively.

Figure 5-10 shows the switching threshold voltage and current density of both OFF and ON states of the four coPIs obtained in different cells of the same memory device batch. The error bar at each point was evaluated by the standard deviation of ten sample measurements. With the selected word- and bit-line combination, the desired programming and reading process was applied to the selected cell only. When the Al/coPI/Al memory devices switches between the OFF and ON states, V_{set} of all PIs are distributed narrowly in a range of -2.8 to -2.1 V. The tight distribution is a condition for the operation of the resistive memory to avoid accidental misleading during the application of read voltages. The reliability of the memory array was illustrated by examining the current density of the OFF and ON states as plotted in Figure 5-10. Clear separation of the PI device between these two states reliably verifies the data storage. Note that the switching characteristics vary slightly from cell to cell and from device to device. This probably resulted from the thickness variation on the interfacial layer or conformation relaxation of the polymer chain.[7, 18] However, the memory elements based

on the newly synthesized coPI materials achieved a low operating voltage for the switching procedure and shows small fluctuations in the operation parameters for device scalability and stability.

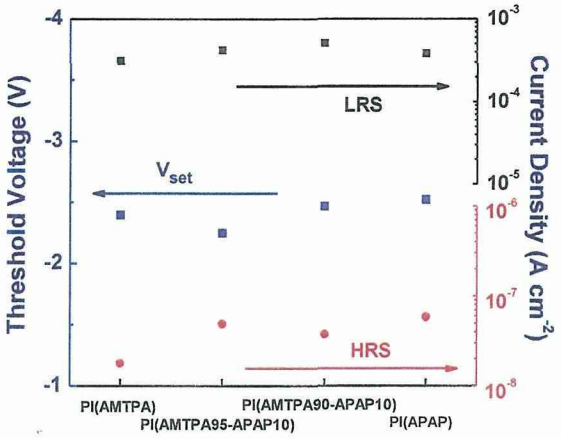

Figure 5-10. Variations of current density and threshold voltage of the PI(AMTPA), PI(AMTPA95-APAP5), PI(AMTPA90-APAP10) and PI(APAP) memory device.

As a next step, taking advantages of the high solubility, flexible coPI memory devices were fabricated to classify the feasibility of the switching performance. The devices were electrically characterized after being physically fixed with a vernier caliper from flat to bent conditions (see Figure 5-11).

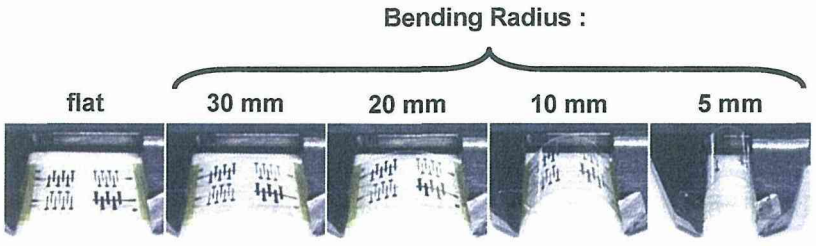

Figure 5-11. PI(AMTPA95-APAP5) memory device in flat and various bent states.

The statistical data on current response and threshold voltage extracted from the flexible PI(AMTPA95-APAP5) and PI(APAP) memory devices with various bending conditions

(radii or cycles) were analyzed in detail. The *J–V* characteristics of those memory devices under different bending conditions are shown in Figure 5-12, which suggest good flexibility and mechanical endurance.

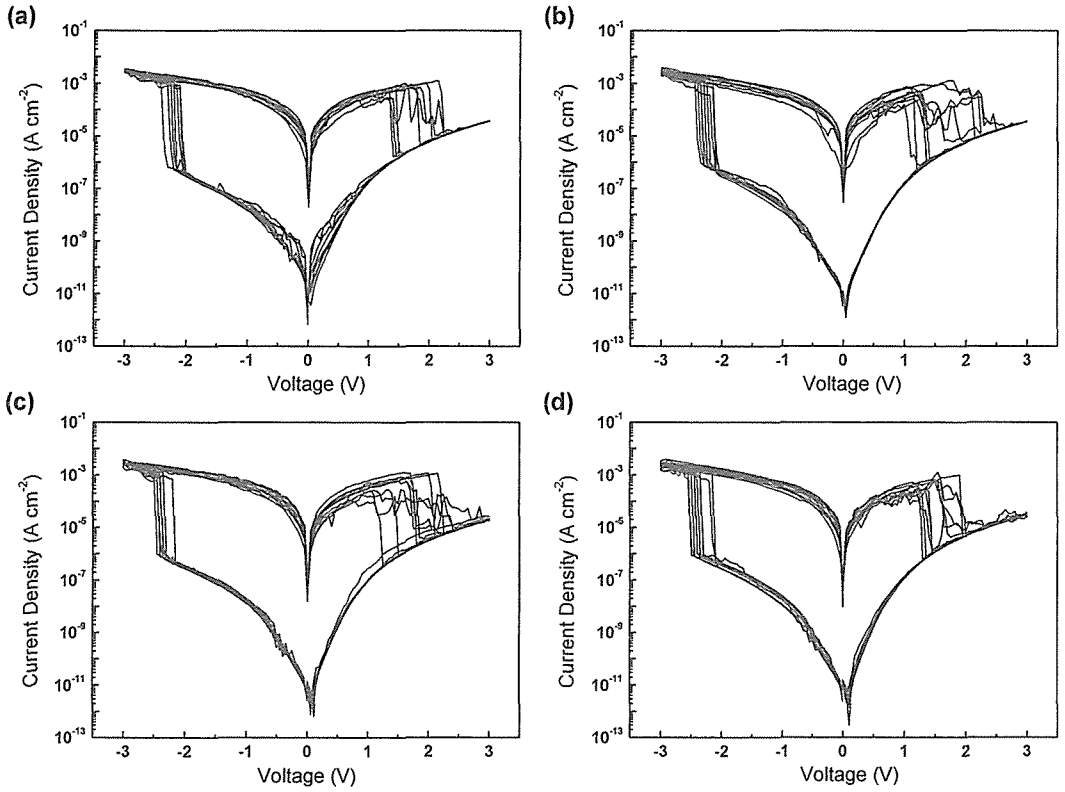

Figure 5-12. *J-V* characteristic of flexible PI(AMTPA95-APAP5) memory device under bending condition. The radius of curvatures are (a) 30 mm, (b) 20 mm, (c) 10 mm, and (d) 5 mm.

During the test, severe bending of the PI(AMTPA95-APAP5) device substrate at various curvature radii of 30, 20, 10 and 5 mm does not degrade the device characteristics, in particular the current density and threshold voltage (Figure 5-13a). The coPI film in the device was not cracked or deformed upon bending; therefore, reliable and reproducible switching behavior can be observed under mechanical bending stress. Retention characteristics of the PI(AMTPA95-APAP5) device were measured for up to 1.2×10^5 s while bent with a radius of curvature of 5 mm, which agreed with the device in the flat

state (Figure 5-13b). The current levels of the two resistance states were measured as a function of bending cycles during the spreading and bending at a radius of curvature as small as 5 mm (Figure 5-13c). The level of endurance was evaluated by means of repetitive bending tests at a rate of 2 bends per second. The PI(AMTPA95-APAP5) device retains the two well-separated resistance states without any noticeable electrical degradation during a 1000-bending cycle test. It reveals that our flexible PI devices are reliable even when the substrates are severely bent.

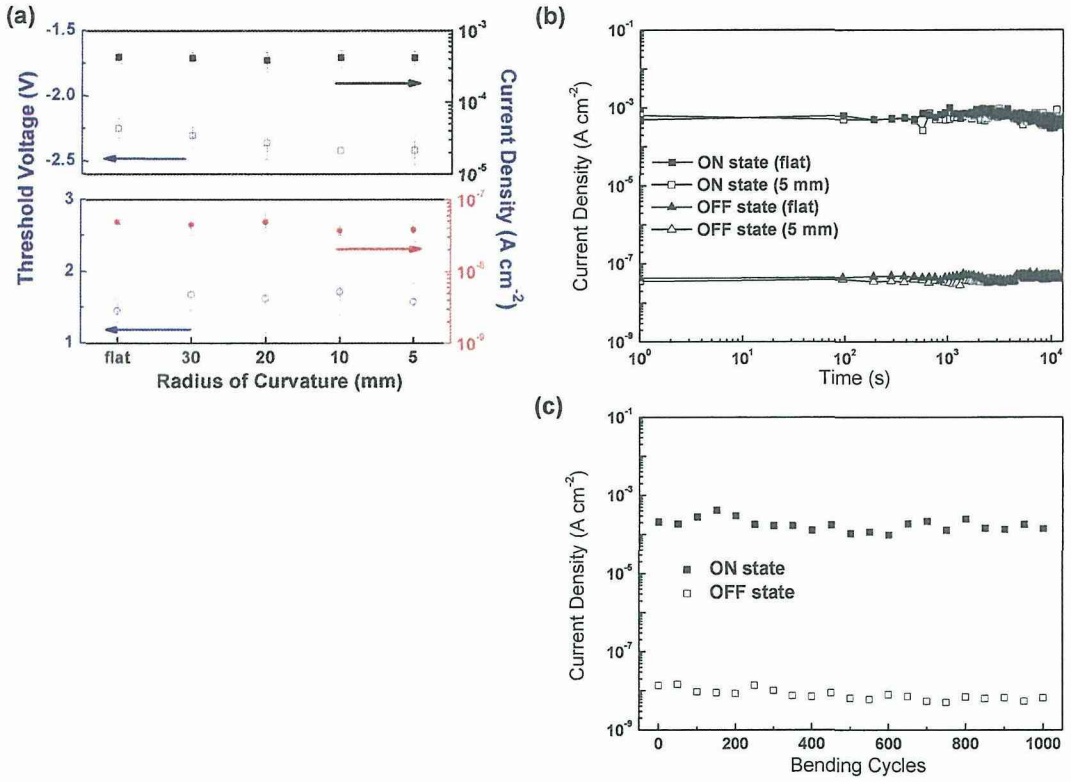

Figure 5-13. (a) Variation of current density and threshold voltage, (b) retention time test, and (c) mechanical endurance of the flexible PI(AMTPA95-APAP5) memory device.

5-2-4. Operation mechanism

The resistive memory exhibited two bistable resistances of the OFF and ON states, which can be switched by an external bias or preserved as information. Nowadays, the

resistance switching mechanisms of polymer memory devices reported in the literature include a conducting filamentary model, CT effect, and trap charge–discharging.[25-26] However, the conductance of the switching curves was linearly dependent on the pad area. The lack of need for an initial forming process (at pretty high voltage bias) or current compliance in the initial stage (to prevent permanent device breakdown) and evidence of structural-dependent electrical properties suggest that the observed resistive switching does not rely on the formation of a conductive metal filament at this stage. To investigate the transport region of the device, the experimental data of the OFF state undergoing a transition to the ON state were analyzed shown in Figure 5-14a. The fitted data for PI(AMTPA95-APAP5) devices reveal a transition at 0.75 V from linear (J–V) to non-linear quadratic (J–V^2). The current density scales linearly with voltage, characterized by ohmic conduction, and the higher voltage region may correspond to space charge limited conduction (SCLC).[27] The power-law region indicates that the switching is triggered by the carrier injection and hopping processes between the PI chains. Above the setting voltage, the numerous generated charges and CT process rapidly yield a conducting path and the J–V curve of the ON state behavior adapts to the Poole–Frenkel (PF) emission model in which the J–V relationship has characteristics of $\ln(J/V) - V^{1/2}$,[28] reflecting the change of the charge transport process. Herein, the ON and OFF switching of volatile PI(AMTPA) (Figure 5-14b) or non-volatile PI(APAP) (Figure 5-14c) can also be well fitted to the proper theoretical model.

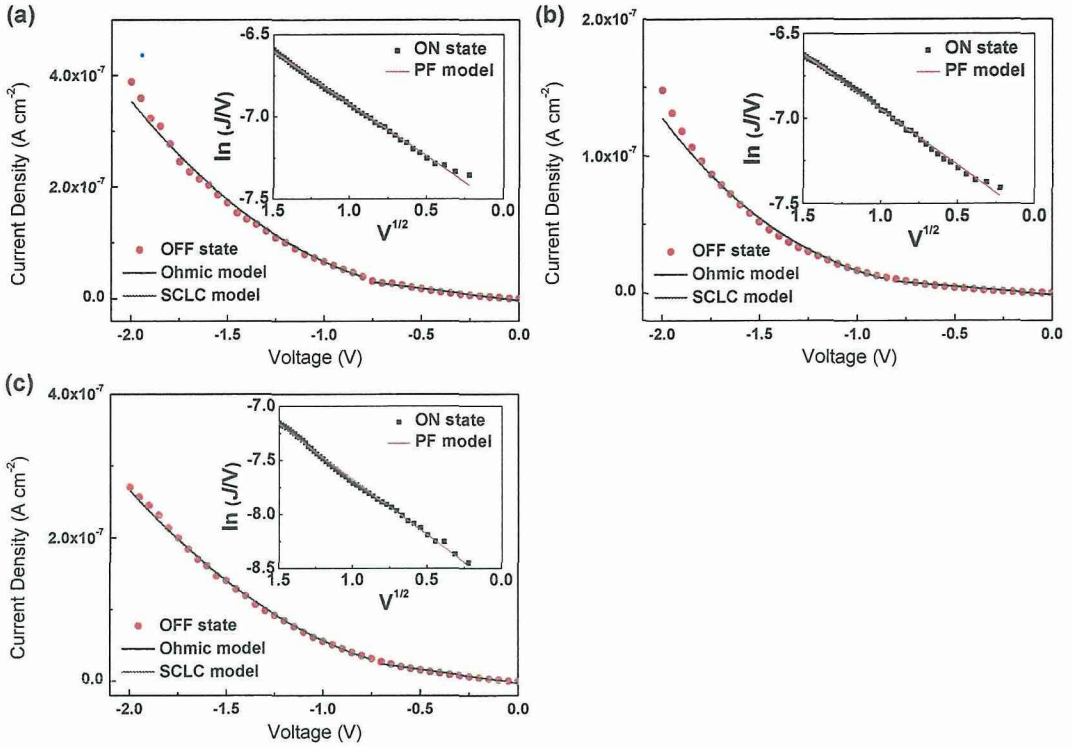

Figure 5-14. Experimental and fitted *J-V* characteristics of (a) PI(AMTPA95-APAP5), (b) PI(AMTPA), and (c) PI(APAP) device in the OFF and ON states.

To further confirm the recording mechanism of the coPI system, theoretical calculations were carried out at the B3LYP/6-31G(d) level with the Gaussian 03 program package.[29] Figure 5-15 shows the optimized geometry and molecular orbitals of the basic unit (BU) of PI(AMTPA) and PI(APAP). The mechanism of electronic transition of coPIs can be explained from the electric field induced CT effect between the donors and acceptors. It is obvious that phthalimide moieties contribute more to the LUMO while AMTPA or APAP contributes more to the HOMO. Similar molecular simulation of the BU of PI(AMTPA) relative to TP6F-PI (without a methyl group attached to triphenylamine) proposed by Kang's group[8] presents the plausible electronic transitions under excitation as follows: excitation from HOMO to HOMO+2; CT

indirectly from LUMO+2 to LUMO+1, then to LUMO or directly from HOMO to LUMO+1 and LUMO. In PI(APAP), the APAP with conjugated pyrene groups serves as electron donors and phthalimide moieties serve as electron acceptors. The excitation of the donors units leads to the intra- or intermolecular CT state. With the interaction between them, CT process gives rise to a conductive charge separation state.

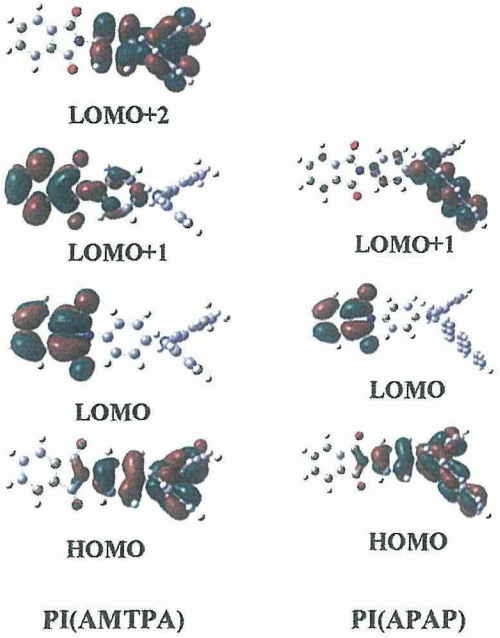

Figure 5-15. Optimized geometries and electronic density counters of molecular orbitals of PI(AMTPA) and PI(APAP) basic units.

During the voltage scan, holes would be easily transferred from the Al electrode to the coPI memory layer due to the lower hole injection barrier (1.05–1.11 eV) than electron injection (1.77–2.01 eV). The accumulation of holes near the anode and the related power law region (ohmic and SCLC process) can explain the OFF state. With the increase of the bias up to the threshold voltage, more and more charges continue to be generated with high electric field and the positive and negative charges are segregated from the CT state and localized in the donors and acceptors under the

voltage bias. The increasing numbers of migrating charges result in high conducting pathway inside the memory layer. The difference in the coPI structural compositions from 0 mol% of APAP (PI(AMTPA)) to 100 mol% of APAP (PI(APAP)) determines the switching behavior and recording volatility. Basically, the resistance decreases by the construction of conducting paths from the CT state and *vice versa*. When the power is turned off, the volatile PI(AMTPA) device undergoes charge recombination (*i.e.* back CT) directly through the donor–acceptor connection and the unstable CT state returns to the original OFF state. To suppress this recombination, trapping or delocalizing the radical anion or cation in the CT state by introducing high electron affinitive (such as fullerene derivatives or graphene oxide)[30-34] or large conjugated moieties is an effective strategy. The PI(APAP) device exhibits a very stable ON state once the device is written since the large conjugated resonance of the pyrene unit can stabilize the radical cation of the CT state.[1, 24] The stable CT environment from segregated cationic and anionic radicals restrains the charge recombination even after the application of a reverse bias. Meanwhile, difficult charge recombination can be observed through the incorporation of 5 mol% conjugated APAP moieties, indicating non-volatile behavior. After a reverse polarity bias, back CT in PI(AMTPA95-APAP5) occurs (reset to the OFF state) and this confirms the FLASH type switching behavior. For PI(AMTPA90-APAP10), the switching behavior follows partially the FLASH memory of PI(AMTPA95-APAP5) and partially the WORM memory of the PI(APAP) device. The matching molecular orbitals and corresponding memory behaviors make the following proposed mechanism reasonable: the CT conducting path under the application of an electric field switches the device and the contents of the largely conjugated pyrene moiety influence the charge recombination to control the volatility. The memory property can be modulated from

volatile DRAM to non-volatile WORM type by controlling the pyrene content in PIs. The clear correlation between resistive switching properties and structural control to the stability of CT state suggests a new design concept of functional polymers for advanced resistive switching devices.

5-3. Conclusion

In conclusion, coPIs with main chain AMTPA/APAP donors randomly copolymerized with 6FDA acceptors by chemical imidization were prepared and employed as the active layer for flexible resistance memory devices in a cross-point PEN/Al/coPIs/Al platform. The pyrene moiety, which is a well-known PCA, was introduced for the purpose of delocalizing the radical cation generated in the CT state and inducing non-volatile behavior. The memory behaviors varied with the APAP molar content starting from volatile DRAM to non-volatile FLASH, FLASH/WORM and WORM memory for PI(AMTPA), PI(AMTPA95-APAP5), PI(AMTPA90-APAP10) and PI(APAP), respectively. Electrical bistability was ascribed to the CT as suggested by theoretical simulation and the largely conjugated pyrene moiety benefits the stable CT state with excellent non-volatile electrical properties. The resistance switching characteristics have been successfully analyzed using a proper theoretical *J–V* dependence model. The fabricated coPIs exhibited superior memory performance and a high level of mechanical durability when operated under various bending conditions. The proposed structural design concept of polymers to modulate the memory behavior can be envisaged as a suitable approach towards future active memory elements in data storage applications.

5-4. Experimental section

Materials. All commercially available reagents or anhydrous solvents obtained from suppliers were used without further purification unless otherwise noted. Dehydrated DMAc, dehydrated pyridine, and acetic anhydride were purchased from Wako Pure Chemical Industries, Ltd. (Japan). Anhydrous chloroform was purchased from Aldrich (USA). 6FDA was purchased from TCI and purified by vacuum sublimation. APAP was prepared as reported.[35] AMTPA was kindly provided by JSR Corp.

Synthesis of poly[4,4'-diamino-4''-methyltriphenylamine-hexafluoroisopropylidenediphthalimide] PI(AMTPA). To a solution of AMTPA (0.289 g, 1.00 mmol) in DMAc (5.00 mL) was added 6FDA (0.444 g, 1.00 mmol) under nitrogen. The mixture was stirred for 2 h at room temperature to give a viscous poly(amic acid) (PAA) solution. Excess amounts of acetic anhydride (1.50 mL) and pyridine (1.50 mL) were then added to the above PAA solution and stirred for 24 h. The resulting solution was poured into methanol and the precipitate was collected by filtration. The final product was washed with methanol and dried at 200 °C for 5 h under vacuum to yield PI(AMTPA) (0.666 g, 95%). The M_n and M_w values of PI(AMTPA) estimated from size exclusion chromatography (SEC) were 4.25×10^4 and 11.2×10^4, respectively, with the PDI of 2.64. IR (KBr), ν (cm^{-1}): 1782, 1720 (C=O stretching), 1377 (C–N stretching). ^{1}H NMR (DMSO-d_6, δ, ppm, 40 °C): 8.13 (d, J = 7.8 Hz, ArH, 2H), 7.94 (d, J = 7.8 Hz, ArH, 2H), 7.79 (s, ArH, 2H), 7.36 (d, J = 9.0 Hz, ArH, 4H), 7.21 (d, J = 8.7 Hz, ArH, 2H), 7.15–7.08 (m, ArH, 6H), 2.30 (s, ArCH3, 3H). *Anal.* Calcd for $C_{38}H_{21}N_3$: C, 65.4; H, 3.03; N, 6.02. Found: C, 64.9; H, 3.21; N, 6.17.

Synthesis of poly[*N*,*N*-bis(4-aminophenyl)-1-aminopyrene-hexafluoroisopropylidenediphthalimide] PI(APAP). Using APAP as the diamine monomer, PI(APAP) was synthesized by a similar procedure to PI(AMTPA). The yield of PI(APAP) was 98%. Their M_n, M_w, and PDI values were 6.20×10^4, 11.9×10^4, and 1.92, respectively. IR (KBr), ν (cm^{-1}): 1782, 1724 (C=O stretching), 1377 (C–N stretching). ^1H NMR (DMSO-d_6, δ, ppm, 40 °C): 8.36–7.97 (m, ArH, 11H), 7.90 (d, J = 7.8 Hz, ArH, 2H), 7.76 (s, ArH, 2H), 7.32 (d, J = 8.4 Hz, ArH, 4H), 7.16 (d, J = 8.1 Hz, ArH, 4H). *Anal.* Calcd for $C_{47}H_{23}N_3$: C, 69.9; H, 2.87; N, 5.20. Found: C, 69.1; H, 3.08; N, 5.38.

General procedure for synthesis of random copolymers containing pyrene unit PI(AMTPA-APAP). 6FDA (0.444 g, 1.00 mmol) was added to a solution of AMTPA and APAP in DMAc (5.00 mL) and the mixture was stirred for 2 h at room temperature to afford a viscous PAA solution. The total amount of AMTPA and APAP was set to 1.00 mmol (the molar ratios of APAP to AMTPA were 5% and 10% for PI(AMTPA95-APAP5) and PI(AMTPA90-APAP10), respectively). A reaction mixture of acetic anhydride (1.50 mL) and pyridine (1.50 mL) was added to the above PAA solution. The reaction mixture was stirred at room temperature under a nitrogen atmosphere for 24 h. The resulting solution was poured into methanol, and the precipitate was collected by filtration and washed with methanol. The final product was dried at 200 °C for 5 h under vacuum. The yields of PI(AMTPA95-APAP5) and PI(AMTPA90-APAP10) were 98 and 99%, respectively. *Anal.* Calcd of PI(AMTPA95-APAP5): C, 65.6; H, 3.02; N, 5.98; found: C, 65.3; H, 3.28; N, 6.10. *Anal.* Calcd of PI(AMTPA90-APAP10): C, 65.9; H, 3.01; N, 5.94; found: C, 65.5; H, 3.20; N, 6.14.

Characterization. ^{1}H NMR spectra were obtained in DMSO-d_6 (tetramethylsilane as the reference) with a BRUKER DPX-300S at the resonant frequency of 300 MHz. FT-IR spectra were measured using a Horiba FT-120 Fourier transform spectrophotometer. M_n and M_w values were evaluated using a HITACHI SEC with two polystyrene gel columns (Shodex GPC KD-804, KD-805). DMF containing 0.01MLiBr was used as the eluent at a flow rate of 1.0 mL min^{-1} calibrated by polystyrene standard samples. Elemental analyses were performed with a Yanaco MT-6 CHN recorder elemental analysis instrument. Thermal properties were estimated from a Seiko TG/DTA 6300 TGA system and a DSCQ100 under a nitrogen atmosphere at heating rates of 10 and 6 °C min^{-1}, respectively. UV-Vis absorption spectral data were measured with a Hitachi U-4100 spectrophotometer. Thin film measurements were collected by spin-coating onto untreated quartz substrates. CV data were collected using a CHI 611B electrochemical analyzer. A three-electrode cell based on an ITO glass working electrode, an Ag–AgCl, KCl (sat.) reference electrode (calibrated *vs.* Fc/Fc+) and a Pt wire counter electrode was purged with nitrogen. The electrochemical properties of the polymer films were detected under 0.1 M anhydrous acetonitrile solution containing tetrabutylammonium perchlorate (TBAP) as the supporting electrolyte. The thickness of the polymer film was determined with a Microfig. Measuring Instrument (Surfcorder ET3000, Kosaka Laboratory Ltd.).

Device fabrication and measurement. PEN substrate was first pre-cleaned by an ultrasonic cleaning process with water, isopropanol, and acetone successively for 15 minutes each. 30 nm thick Al bottom electrode patterns were deposited by a thermal evaporator at a pressure of 10^{-5} Torr with a depositing rate of 1 Å s^{-1}. Then, 4 mgmL^{-1} of synthesized coPI in chloroform was filtered through a 0.45 μm pore size

poly(tetrafluoroethylene) (PTFE) membrane syringe filter, spin-coated onto the bottom Al electrode/PEN substrate at 1000 rpm for 60 s and baked at 100 °C on a hot plate in a N_2-filled glove box. Finally, the 30 nm Al top electrodes were deposited and patterned by a metal mask with a cross-point device joint area of 0.2×0.2, 0.4×0.4 and 0.6×0.6 mm^2. All the electrical characteristics of the fabricated flexible memory devices were measured using a Keithley 4200-SCS semiconductor parameter analyzer (with low noise pre-amplifier) and a probe station at room temperature in a N_2-filled glove box. The programming pulse signals were generated by a Keithley 4220-PGU pulse generator unit. The bottom electrode was grounded during all the electrical measurement with a swept step of 0.05 V.

Computational methodology. Molecular calculations studied in this work were performed through the Gaussian 03 program package.[29] Equilibrium ground state geometry and electronic properties were optimized by means of the density functional theory (DFT) method at the B3LYP level of theory (Becke-style three-parameter density functional theory using the Lee–Yang–Parr correlation functional) with the 6-31 G(d) basic set.

5-5. References

1. Laali, K. K., *Chem. Rev.* **1996,** *96*, 1873-1906.
2. LeBlanc, O. H., Jr., *J. Chem. Phys.* **1962,** *37*, 916-917.
3. Figueira-Duarte, T. M.; Mullen, K., *Chem. Rev.* **2011,** *111*, 7260-7314.
4. Park, S.; Kim, K.; Kim, D. M.; Kwon, W.; Choi, J.; Ree, M., *ACS Appl. Mater. Interfaces* **2011,** *3*, 765-773.
5. Hahm, S. G.; Choi, S.; Hong, S.-H.; Lee, T. J.; Park, S.; Kim, D. M.; Kwon, W.-S.; Kim, K.; Kim, O.; Ree, M., *Adv. Funct. Mater.* **2008,** *18*, 3276-3282.
6. Tian, G.; Qi, S.; Chen, F.; Shi, L.; Hu, W.; Wu, D., *Appl. Phys. Lett.* **2011,** *98*, 203302/1-203302/3.
7. Liu, Y.-L.; Wang, K.-L.; Huang, G.-S.; Zhu, C.-X.; Tok, E.-S.; Neoh, K.-G.; Kang, E.-T., *Chem. Mater.* **2009,** *21*, 3391-3399.
8. Ling, Q.-D.; Chang, F.-C.; Song, Y.; Zhu, C.-X.; Liaw, D.-J.; Chan, D. S.-H.; Kang, E.-T.; Neoh, K.-G., *J. Am. Chem. Soc.* **2006,** *128*, 8732-8733.
9. Liu, Y.-L.; Ling, Q.-D.; Kang, E.-T.; Neoh, K.-G.; Liaw, D.-J.; Wang, K.-L.; Liou, W.-T.; Zhu, C.-X.; Chan, D. S.-H., *J. Appl. Phys.* **2009,** *105*, 044501/1-044501/9.
10. Hu, B.; Zhuge, F.; Zhu, X.; Peng, S.; Chen, X.; Pan, L.; Yan, Q.; Li, R.-W., *J. Mater. Chem.* **2012,** *22*, 520-526.
11. Li, Y.; Xu, H.; Tao, X.; Qian, K.; Fu, S.; Shen, Y.; Ding, S., *J. Mater. Chem.* **2011,** *21*, 1810-1821.
12. Li, Y.-Q.; Fang, R.-C.; Zheng, A.-M.; Chu, Y.-Y.; Tao, X.; Xu, H.-H.; Ding, S.-J.; Shen, Y.-Z., *J. Mater. Chem.* **2011,** *21*, 15643-15654.
13. Kim, K.; Park, S.; Hahm, S. G.; Lee, T. J.; Kim, D. M.; Kim, J. C.; Kwon, W.; Ko, Y.-G.; Ree, M., *J. Phys. Chem. B* **2009,** *113*, 9143-9150.
14. Liu, C.-L.; Kurosawa, T.; Yu, A.-D.; Higashihara, T.; Ueda, M.; Chen, W.-C., *J. Phys. Chem. C* **2011,** *115*, 5930-5939.
15. Wang, K.-L.; Liu, Y.-L.; Shih, I. H.; Neoh, K.-G.; Kang, E.-T., *J. Polym. Sci., Part A: Polym. Chem.* **2010,** *48*, 5790-5800.
16. Li, Y.; Fang, R.; Ding, S.; Shen, Y., *Macromol. Chem. Phys.* **2011,** *212*, 2360-2370.
17. Tian, G.; Wu, D.; Qi, S.; Wu, Z.; Wang, X., *Macromol. Rapid Commun.* **2011,** *32*, 384-389.
18. Kuorosawa, T.; Chueh, C.-C.; Liu, C.-L.; Higashihara, T.; Ueda, M.; Chen, W.-C., *Macromolecules* **2010,** *43*, 1236-1244.
19. You, N.-H.; Chueh, C.-C.; Liu, C.-L.; Ueda, M.; Chen, W.-C., *Macromolecules*

2009, *42*, 4456-4463.

20. Lee, T. J.; Chang, C.-W.; Hahm, S. G.; Kim, K.; Park, S.; Kim, D. M.; Kim, J.; Kwon, W.-S.; Liou, G.-S.; Ree, M., *Nanotechnology* **2009,** *20*, 135204/1-135204/7.
21. Li, Y.; Chu, Y.; Fang, R.; Ding, S.; Wang, Y.; Shen, Y.; Zheng, A., *Polymer* **2012,** *53*, 229-240.
22. Park, S.; Kim, K.; Kim, J. C.; Kwon, W.; Kim, D. M.; Ree, M., *Polymer* **2011,** *52*, 2170-2179.
23. Yen, H.-j.; Guo, S.-m.; Yeh, J.-m.; Liou, G.-S., *J. Polym. Sci., Part A: Polym. Chem.* **2011,** *49*, 3637-3646.
24. Kung, Y.-C.; Lee, W.-F.; Hsiao, S.-H.; Liou, G.-S., *J. Polym. Sci., Part A: Polym. Chem.* **2011,** *49*, 2210-2221.
25. Heremans, P.; Gelinck, G. H.; Muller, R.; Baeg, K.-J.; Kim, D.-Y.; Noh, Y.-Y., *Chem. Mater.* **2011,** *23*, 341-358.
26. Ling, Q.-D.; Liaw, D.-J.; Zhu, C.; Chan, D. S.-H.; Kang, E.-T.; Neoh, K.-G., *Prog. Polym. Sci.* **2008,** *33*, 917-978.
27. Shang, D. S.; Wang, Q.; Chen, L. D.; Dong, R.; Li, X. M.; Zhang, W. Q., *Phys. Rev. B Condens. Matter Mater. Phys.* **2006,** *73*, 245427/1-245427/7.
28. Sze, S. M.; Editor, *Modern Semiconductor Device Physics*. 1998; p 556 pp.
29. Frisch, M. J. T., G. W.; Schlegel, H. B.; Scuseria, G. E.; Robb, M. A.; Cheeseman, J. R.; Montgomery, Jr., J. A.; Vreven, T.; Kudin, K. N.; Burant, J. C.; Millam, J. M.; Iyengar, S. S.; Tomasi, J.; Barone, V.; Mennucci, B.; Cossi, M.; Scalmani, G.; Rega, N.; Petersson, G. A.; Nakatsuji, H.; Hada, M.; Ehara, M.; Toyota, K.; Fukuda, R.; Hasegawa, J.; Ishida, M.; Nakajima, T.; Honda, Y.; Kitao, O.; Nakai, H.; Klene, M.; Li, X.; Knox, J. E.; Hratchian, H. P.; Cross, J. B.; Bakken, V.; Adamo, C.; Jaramillo, J.; Gomperts, R.; Stratmann, R. E.; Yazyev, O.; Austin, A. J.; Cammi, R.; Pomelli, C.; Ochterski, J. W.; Ayala, P. Y.; Morokuma, K.; Voth, G. A.; Salvador, P.; Dannenberg, J. J.; Zakrzewski, V. G.; Dapprich, S.; Daniels, A. D.; Strain, M. C.; Farkas, O.; Malick, D. K.; Rabuck, A. D.; Raghavachari, K.; Foresman, J. B.; Ortiz, J. V.; Cui, Q.; Baboul, A. G.; Clifford, S.; Cioslowski, J.; Stefanov, B. B.; Liu, G.; Liashenko, A.; Piskorz, P.; Komaromi, I.; Martin, R. L.; Fox, D. J.; Keith, T.; Al-Laham, M. A.; Peng, C. Y.; Nanayakkara, A.; Challacombe, M.; Gill, P. M. W.; Johnson, B.; Chen, W.; Wong, M. W.; Gonzalez, C.; and Pople, J. A., *Gaussian, Inc., Wallingford CT* **2004.**
30. Hahm, S. G.; Kang, N.-G.; Kwon, W.; Kim, K.; Ko, Y.-K.; Ahn, S.; Kang,

B.-G.; Chang, T.; Lee, J.-S.; Ree, M., *Adv. Mater.* **2012,** *24*, 1062-1066.

31. Yu, A.-D.; Liu, C.-L.; Chen, W.-C., *Chem. Commun.* **2012,** *48*, 383-385.
32. Lai, Y.-C.; Ohshimizu, K.; Lee, W.-Y.; Hsu, J.-C.; Higashihara, T.; Ueda, M.; Chen, W.-C., *J. Mater. Chem.* **2011,** *21*, 14502-14508.
33. Ling, Q.-D.; Lim, S.-L.; Song, Y.; Zhu, C.-X.; Chan, D. S.-H.; Kang, E.-T.; Neoh, K.-G., *Langmuir* **2007,** *23*, 312-319.
34. Chen, J.-C.; Liu, C.-L.; Sun, Y.-S.; Tung, S.-H.; Chen, W.-C., *Soft Matter* **2012,** *8*, 526-535.
35. Kung, Y.-C.; Hsiao, S.-H., *J. Mater. Chem.* **2010,** *20*, 5481-5492.

Chapter 6. General Conclusion

Conclusions of each chapter and further prospect for the development of polyimide (PI) memory materials are summarized in this chapter.

In Chapter 1, the general introduction regarding the background of this study is described.

In Chapter 2, two triphenylamine (TPA) based PIs containing mono- or dual-mediated phenoxy linkages were designed and synthesized for the purpose of verifying the effect of the number of mediators on the resulting memory properties. The mono-mediated linkage led to volatile dynamic random access memory (DRAM) property while the dual-mediated linkages induced a twisted conformation, resulting in a "remnant", yet volatile static random access memory (SRAM) behavior.

In Chapter 3, extending the concept discussed in Chapter 2, two PIs having bulky donor (D) units in the pendant position to induce highly twisted conformation were designed and synthesized in order to suppress the back charge transfer (CT) and induce non-volatile memory characteristic. The PI having TPA as the D unit showed distinct charge separation and large dihedral angle in the CT state compared to the PI having diphenylamine as the D unit, which contributed to the highly stable and non-volatile

memory characteristic.

In Chapter 4, three series of random copolyimides (coPIs) containing perylene, naphthalene, and benzene diimides were designed and synthesized with the view of modulating the volatility and clarifying the effects of the ring size effect of the diimide moieties on the resulting memory properties. Comparative studies of the energy levels of the components revealed that the stable CT state was obtained through stabilization of the radical anion by means of long conjugation and high electron affinity of the diimide moieties, leading to non-volatile memory characteristics.

In Chapter 5, a series of random coPIs with pyrene containing D unit were prepared and employed as the active layer for flexible memory devices. The pyrene moiety was introduced for the purpose of delocalizing the radical cation generated in the CT state and inducing non-volatile behavior. By controlling the composition of the pyrene containing D unit, the memory characteristics were successfully tuned form volatile to non-volatile. Moreover, the fabricated flexible memory device showed excellent mechanical durability when operated under various bending conditions.

The development of polymer materials for application to low processing cost, flexible, and high density data storage devices is an emerging area. It is believed that one of the best candidates for such a material is PI. Energetic researches around the world have shown great possibilities for the future application of PI as a memory device material. Although the structure and operating mechanism of the memory device is quite simple, that is, the sandwich device structure and using the conductivity response, the mechanism underlying the switching behavior of the functional material is extremely complicated. So far, the field induced CT theory has been used to explain such phenomena and have been working well to a great extent. As been clarified in this

dissertation, by carefully designing the polymer structure based on this theory, the control through the volatility (from volatile to non-volatile) can certainly be achieved. Also, almost without exception, these memory properties show extremely high endurance during long term operation, which again makes PI a very suitable material for memory applications. However, there still remain a number of issues to be solved. One of the big problems is that the considerations of the resulting memory properties and their mechanism include many speculations. No conclusive evidence for the key factors of the switching behavior such as the formation of the CT state has been obtained. One way to gain insight into this formation is to observe them indirectly through spectroscopic measurements. Since the CT state exhibits characteristic UV-vis absorption behavior, measuring the absorption spectrum before and after or during the application of electric field higher than the threshold value should provide the evidence for the formation of CT state. When the active PI possesses a volatile nature, the characteristic absorption of the CT state would disappear after turning off the power supply and *vice versa*. Now that we have the appropriate materials that show distinct memory behaviors or concrete design concept to prepare these materials, the observation of clear and accurate evidence supporting the switching mechanism which will accelerate the further development of PI memory materials can be achieved in the near future. Also, in the not very distant future, it can be predicted that the polymer memory device might be driven by alternative media to electricity. Since the underlying mechanism of the switching behavior of polymer memory device is based on the formation of CT state, the switching from the OFF state to the ON state might also be done by means of photoexcitation. Using the light as a media, numerous achievements, which can never be attained in the current memory devices, can be adduced. For

example, one can easily imagine that the mobility of electrons or holes in any conducting materials is no match for the speed of light. Hence, unimaginable writing and read out speed of the data can be achieved if the memory device is driven by light. Taking the fact that enormous researches have been carried out for the development of optical waveguide into consideration, the future prospect described above will not be just a fancy imagination but an attainable objective.

The author hopes that this study will be of great help for the development of polyimide memory for the near and also distant future application.

Appendix

List of publications (concerning this dissertation)

1. "High performance volatile polymeric memory devices based on novel triphenylamine-based polyimides containing mono- or dual-mediated phenoxy linkages" Kuorosawa, T.; Chueh, C.-C.; Liu, C.-L.; Higashihara, T.; Ueda, M.; Chen, W.-C., *Macromolecules* **2010,** *43*, 1236-1244.
2. "Tuning the electrical memory characteristics from volatile to nonvolatile by perylene imide composition in random copolyimides" Kurosawa, T.; Lai, Y. C.; Higashihara, T.; Ueda, M.; Liu, C. L.; Chen, W. C., *Macromolecules* **2012,** *45*, 4556-4563.
3. "Flexible Polymer Memory Devices Derived from Triphenylamine-Pyrene Containing Donor-Acceptor Polyimides" Yu, A.-D.; Kurosawa, T. (co-first author); Lai, Y.-C.; Higashihara, T.; Ueda, M.; Liu, C.-L.; Chen, W.-C., *J. Mater. Chem.* **2012,** *22*, 20754-20763.
4. "Polyimide memory: a pithy guideline for future applications" Kurosawa, T.; Higashihara, T.; Ueda, M., *Polym. Chem.* **2013,** *4*, 16-30.
5. "Effects of the acceptor conjugation length and composition on the electrical memory characteristics of random copolyimides" Kurosawa, T.; Lai, Y. C.; Yu, A.-D.; Wu, H.-C.; Higashihara, T.; Ueda, M.; Liu, C.-L.; Chen, W.-C., *J. Polym. Sci., Part A: Polym. Chem.* DOI: 10.1002/pola.26502.
6. "Inducing a high twisted conformation in the Polyimide Structure by bulky donor moieies for the development of non-volatile memory" Kurosawa, T.; Yu, A.-D.; Higashihara, T.; Chen, W.-C.; Ueda, M., submitted article.

List of other publications

7. "New dibenzothiophene-containing donor-acceptor polyimides for high-performance memory device applications" Liu, C.-L.; Kurosawa, T. (co-first author); Yu, A.-D.; Higashihara, T.; Ueda, M.; Chen, W.-C., *J. Phys. Chem. C* **2011,** *115*, 5930-5939.
8. "New donor-acceptor oligoimides for high-performance nonvolatile memory devices" Lee, W.-Y.; Kurosawa, T. (co-first author); Lin, S.-T.; Higashihara, T.; Ueda, M.; Chen, W.-C., *Chem. Mater.* **2011,** *23*, 4487-4497.
9. "Thiophene and selenophene donor-acceptor polyimides as polymer electrets for nonvolatile transistor memory devices" Chou, Y. H.; You, N. H.; Kurosawa, T.; Lee, W. Y.; Higashihara, T.; Ueda, M.; Chen, W. C., *Macromolecules* **2012,** *45*, 6946-6956.

List of presentations (concerning this dissertation)

1. "Synthesis of polyimide containing triphenylamine units and its application to polymer memory" Kurosawa, T.; Chueh, C.-C.; Liu, C.-L.; Higashihara, T.; Chen, W.-C.; Ueda, M., *58th SPSJ Annual Meeting* Kobe (Japan), May **2009** (poster).
2. "Synthesis and characterization of new polyimides derived from 4,4'-bis(*p*-aminophenoxy)triphenylamine and *N,N*-bis[4-(4'-aminophenoxy)phenyl]aminopyrene." Kurosawa, T.; You, N.-H.; Higashihara, T.; Ueda, M., *238th ACS National Meeting* Washington, D.C. (USA), August **2009** (poster).
3. "Synthesis of polyimide containing triphenylamine units and its application to polymer memory" Kurosawa,T.; Chueh, C.-C.; Liu, C.-L.; Higashihara, T.; Chen, W.-C.; Ueda, M., *59th SPSJ Annual Meeting* Yokohama (Japan), May **2010** (oral).
4. "High performance volatile polymeric memory devices based on novel triphenylamine-based polyimides" Kurosawa, T.; Chueh, C.-C.; Liu, C.-L.; Higashihara, T.; Chen, W.-C.; Ueda, M., *Polycondensation 2010 Meeting* Kerkrade (The Netherlands), September **2010** (poster).
5. "Synthesis of copolyimides containing perylenebisimide and their application to polymer memory device" Kurosawa, T.; Yu, A.-D.; Liu, C.-L.; Higashihara, T.; Chen, W.-C.; Ueda, M., *61th SPSJ Annual Meeting* Yokohama (Japan), May **2012** (oral).
6. "Synthesis of copolyimides containing perylenebisimide and their application to polymer memory" Kurosawa, T.; Lai, Y.-C.; Higashihara, T.; Liu, C.-L.; Chen, W.-C.; Ueda, M., *244th ACS National Meeting & Exposition* Philadelphia (USA),

W.-C.; Ueda, M., *244th ACS National Meeting & Exposition* Philadelphia (USA), August **2012** (oral).

7. "Synthesis of copolyimides containing pyrene structure and their application to polymer memory device" Kurosawa, T.; Yu, A.-D.; Liu, C.-L.; Higashihara, T.; Chen, W.-C.; Ueda, M., *61st SPSJ Symposium on Macromolecules* Nagoya (Japan), September **2012** (oral).
8. "Synthesis of copolyimides containing pyrene structure and their application to polymer memory device" Kurosawa, T.; Yu, A.-D.; Liu, C.-L.; Higashihara, T.; Chen, W.-C.; Ueda, M., *The 9th SPSJ International Polymer Conference* Kobe (Japan), December **2012** (oral).

List of other presentations

9. "Synthesis of polyimide containing dibenzothiophene units and its application to polymer memory" Kurosawa, T.; Yu, A.-D.; Liu, C.-L.; Higashihara, T.; Chen, W.-C.; Ueda, M., *60th SPSJ Annual Meeting* Osaka (Japan), May **2011** (poster).
10. "Synthesis of Novel Oligoimides and Their Applications to Non-volatile Memory" Kurosawa, T.; Lee, W.-Y.; Higashihara, T.; Chen, W.-C.; Ueda, M., *European Polymer Congress 2011* Granada (Spain), June-July **2011** (poster).
11. "Synthesis of Novel Oligoimides and Their Applications to Non-volatile Memory" Kurosawa, T.; Lee, W.-Y.; Higashihara, T.; Chen, W.-C.; Ueda, M., *19th Japan Polyimide & Aromatic Polymer Conference* Tokyo (Japan), November **2011** (poster).

Acknowledgements

The studies described in this dissertation have been carried out under the direction of Prof. Mitsuru Ueda at Department of Organic and Polymeric Materials, Graduate School of Science and Engineering, Tokyo Institute of Technology during 2011 to 2013. The studies are concerned with development of polyimide memory.

The author's deepest appreciation goes to Prof. Mitsuru Ueda. His enthusiastic guidance and encouragements have guided the author to take the first step into the world of polymer chemistry and materials science. Now that the author has decided to move on to the academe, a lesson of what can be done and what cannot be done with and without passion, respectively, from Prof. Ueda will always be the instruction of his future performance.

The author also wishes to express his gratitude to Prof. Wen-Chang Chen at National Taiwan University for his amazing collaboration throughout the studies described in this dissertation. The author is sincerely grateful to Assistant Prof. Tomoya Higashihara for his innumerable suggestion and teachings during the author's laboratory life.

Special thanks will be expressed to Mr. Yu Shoji and Ms. Yukari Segawa for their mental and physical supports to accomplish the author's whole work. During the past two years, the author found out them to be not only his senior associates but also his best friends. The author also gives his thanks to all members in Ueda and Chen group for their collaboration.

Finally, the author wishes to express his deep appreciation to his parents, grandparents, sister, and brother; Daisuke Kurosawa, Terumi Kurosawa, Chuji Kurosawa, Kazuko Kurosawa, Fujiko Kurosawa, and Eisuke Kurosawa for their constant supports. The gratefulness is beyond expression.

Tadamori Kurosawa